



BEHAVIOR AND DSM DESIGN OF COLD-FORMED STEEL “S” TYPE BEAMS
EXPERIENCING DISTORTIONAL FAILURE

Carolina Barichello

Dissertação de Mestrado apresentada ao Programa de Pós-graduação em Engenharia Civil, COPPE, da Universidade Federal do Rio de Janeiro, como parte dos requisitos necessários à obtenção do título de Mestre em Engenharia Civil.

Orientadores: Alexandre Landesmann
Dinar Reis Zamith Camotim

Rio de Janeiro
Março de 2016

BEHAVIOR AND DSM DESIGN OF COLD-FORMED STEEL “S” TYPE BEAMS
EXPERIENCING DISTORTIONAL FAILURE

Carolina Barichello

DISSERTAÇÃO SUBMETIDA AO CORPO DOCENTE DO INSTITUTO ALBERTO LUIZ COIMBRA DE PÓS-GRADUAÇÃO E PESQUISA DE ENGENHARIA (COPPE) DA UNIVERSIDADE FEDERAL DO RIO DE JANEIRO COMO PARTE DOS REQUISITOS NECESSÁRIOS PARA A OBTENÇÃO DO GRAU DE MESTRE EM CIÊNCIAS EM ENGENHARIA CIVIL.

Examinada por:

Prof. Alexandre Landesmann, D.Sc.

Prof. Luiz Fernando Lomba Rosa, D.Sc.

Prof. Daniel Carlos Taissum Cardoso, D.Sc.

RIO DE JANEIRO, RJ – BRASIL

MARÇO DE 2016

Barichello, Carolina

Behavior and DSM design of cold-formed steel “S” type beams experiencing distortional failure / Carolina Barichello. – Rio de Janeiro: UFRJ/COPPE, 2016.

VIII, 76 p.: il.; 29,7 cm.

Orientadores: Alexandre Landesmann

Dinar Reis Zamith Camotim

Dissertação (mestrado) – UFRJ/ COPPE/ Programa de Engenharia Civil, 2016.

Referências Bibliográficas: p. 57-58.

1. Distortional failure. 2. Cold-formed steel beams. 3. Numerical analysis. I. Landesmann, Alexandre *et al.* II. Universidade Federal do Rio de Janeiro, COPPE, Programa de Engenharia Civil. III. Título.

Acknowledgements

Firstly, I would like to express my gratitude to my advisors Prof. Alexandre Landesmann and Prof. Dinar Camotim for their continuous support and for providing me with all the necessary facilities for this research. Their guidance helped me in all the time of research and writing of this thesis.

I would also like to acknowledge COPPE, for made possible my graduate experience.

My thanks also go to METALSHOP, who provided me access to the “S” types cross-section data.

I am also grateful to my fellows from work and from COPPE for the encouragement and everyday help to make this thesis possible.

Last but not the least, I would like to thank my partner Isac, my family and closer friends for supporting me throughout this journey and incited me to strive towards my goal.

Resumo da Dissertação apresentada à COPPE/UFRJ como parte dos requisitos necessários para a obtenção do grau de Mestre em Ciências (M.Sc.)

COMPORTAMENTO E DIMENSIONAMENTO VIA MRD DE VIGAS DE AÇO EM
PERFIL FORMADO A FRIO DO TIPO “S” SOB O MODO DE FALHA
DISTORCIONAL

Carolina Barichello

Março/2016

Orientadores: Alexandre Landesmann

Dinar Reis Zamith Camotim

Programa: Engenharia Civil

Este trabalho apresenta resultados de uma investigação numérica sobre o comportamento na flambagem, pós-flambagem, resistência última e dimensionamento através do Método da Resistência Direta (MRD) de vigas de perfil formados a frio com seções transversais do tipo “S” e U enrijecido (com e sem enrijecedores intermediários) sob modo de flambagem distorcional. As vigas analisadas (i) são compostas por um único vão, (ii) são simplesmente apoiadas, porém com condições de apoio distintas no que se refere à restrição do empenamento e rotação em torno do eixo de menor inércia em suas extremidades, (iii) têm dimensões de seção transversal e comprimentos de flambagem diversos, que proporcionam uma vasta gama de relações geométricas que auxiliam no entendimento de seu comportamento. Garantiu-se que todas as vigas analisadas (i) apresentassem modo de flambagem “puramente” distorcionais e (ii) abrangessem uma vasta gama de tensões de escoamento, possibilitando a investigação em um grande número de esbeltezes distorcionais. As trajetórias de equilíbrio de pós-flambagem e momentos últimos apresentados neste trabalho são obtidos através de análises não lineares elásticas e elasto-plásticas com emprego de elementos finitos de casca através do programa ANSYS. Os resultados numéricos obtidos neste trabalho indicam, com relação a segurança e precisão, que a atual curva de resistência distorcional do MRD não é capaz de prever adequadamente os momentos últimos das vigas estudadas.

Abstract of Dissertation presented to COPPE/UFRJ as a partial fulfillment of the requirements for the degree of Master of Science (M.Sc.)

BEHAVIOR AND DSM DESIGN OF COLD-FORMED “S” TYPE BEAMS
EXPERIENCING DISTORTIONAL FAILURE

Carolina Barichello

March/2016

Advisors: Alexandre Landesmann

Dinar Reis Zamith Camotim

Department: Civil Engineering

The present work reports a numerical analysis investigation about the buckling and post-buckling behavior, ultimate strength and Direct Strength Method (DSM) design predictions applied to cold formed steel beams with “S” type and lipped channels (plane and stiffened) sections experiencing distortional buckling. The analyzed beams (i) are single-span members, (ii) are simply supported but they exhibit different end support conditions regarding warping and minor-axis flexural rotations and (iii) present different cross-section dimensions and buckling lengths, which provide a wide range of geometrical relations that help understanding their behavior. It is assured that all analyzed beams (i) present “purely” distortional buckling modes and (ii) cover a wide range of yielding stresses, enabling the investigation on a great amount of distortional slenderness. The post-buckling equilibrium paths and ultimate bending moments exhibited in this work are extracted from shell finite element non-linear elastic and elastic-plastic analysis through the software ANSYS. The results obtained in this work evidence that current codified DSM distortional curve is unable to estimate safely and accurately the ultimate bending moments for the selected beams.

Index

Acknowledgements	iv
Index	vii
Symbols.....	viii
1 Introduction	1
1.1 Historic.....	3
1.2 Motivation.....	4
1.3 Objective.....	4
1.4 Outline	5
2 Bibliography Review	6
2.1 Structural stability and buckling	6
2.2 Buckling modes	8
2.3 Post-buckling and ultimate strength	12
2.4 Distortional buckling	14
2.5 Design methods for cold formed shapes	19
2.5.1 Effective Width Method (EWM)	20
2.5.2 Effective Section Method (ESM).....	20
2.5.3 Direct Strength Method (DSM)	21
3 Beam Selection and Buckling Behavior	26
3.1 Beam geometry selection and buckling analysis	26
4 Post-buckling, Ultimate Strength and DSM.....	37
4.1 Finite Element Analysis (FEA).....	37
4.2 Elastic post-buckling behavior.....	40
4.3 Elastic-plastic post-buckling behavior and ultimate strength	43
4.4 Direct Strength Method	50
5 Concluding Remarks	54
5.1 Suggestions for future works	56
6 Bibliography.....	57
APPENDIX A.....	59
APPENDIX B.....	68

Symbols

Roman letters

A	cross-section area
b_f	cross-section flange length
b_{f1}	cross-section flange stiffener length
b_{f2}	cross-section flange stiffener height
b_l	cross-section lip length
b_w	cross-section web length
b_{w1}	cross-section web stiffener length
b_{w2}	cross-section web stiffener height
E	elastic modulus
f_y	yield stress
f_{VM}	von Mises stress
L	member length
L_D	member length associated to distortional buckling
M	acting bending moment
M_{bL}	lowest local bifurcation bending moment
M_{bG}	lowest global bifurcation bending moment
M_{cr}	critical bending moment (or bifurcation bending moment)
M_{crD}	distortional buckling critical bending moment
M_{nD}	nominal member capacity in distortional buckling
M_u	ultimate strength
M_y	yielding bending moment
p	GBT modal participation
S	elastic modulus
t	cross-section thickness

Greek letters

δ	maximum absolute transversal displacement along the flange-lip edges
λ	slenderness
λ_D	slenderness associated to distortional buckling
ν	Poisson's ratio

1 Introduction

There are basically two common types of structural members in steel construction: hot-rolled and cold-formed. The hot-rolled steel members are conformed at elevated temperatures and are built up of an assembly of plates, whilst the cold-formed are shaped at room temperature. The cold-formed member production is made with structural quality steel sheet, strip, plate or flat bar which is formed into shape by processes of (i) roll-forming, (ii) press braking or (iii) bending brake operations. The most commonly used sheet thicknesses range up to 6.35 mm.

The nature of the fabrication of the cold-formed steel members allows different configurations to be produced, which might stimulate the design optimization of the cross-sections shapes for structural and economical purposes. The key idea for cold-formed members is to exploit the shape to support the loads instead of the thickness. Common cold-formed steel shapes are illustrated in Figure 1.1.

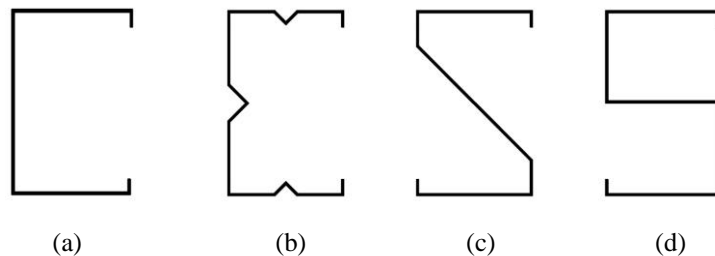


Figure 1.1 - Cold-formed cross-section shapes: (a) plane lipped channel – PLC, (b) stiffened lipped channel (SLC), (c) S-section with sloped web (S45) and (d) S-section with straight web (S90)

Besides the flexibility in fabricating different cross-section shapes, cold-formed members present other advantages in comparison to the hot-rolled members such as: (i) can be manufactured for relatively light loads and short spans, (ii) cold-formed panels and decks can provide useful surfaces for roof, wall and floor construction, (iii) panels and decks, besides withstanding loads normal to their surfaces, might act as shear diaphragms, (iv) the installation is faster and easier and (v) they allow compact packaging resulting in economy during transportation and handling.

Cold-formed member's behavior is substantially different from the hot-rolled's. The former has the cross-section thickness thinner than the latter, resulting in peculiar failure modes – such as local and distortional buckling, which are not common in hot-rolled members. Besides, the hot-rolled industries require great investments in equipment

leading to a standardization of the cross-sections, while cold-formed industries are simpler and enable the fabrication of distinct cross-section shapes along with the need. The fastening methods also contribute to the differences between hot-rolled and cold-formed members, since the former involves basically welding and bolting, while the latter might present several connection practices, such as bolts, screws, rivets and puddle welds. The presented differences turned into impossible the adoption of hot-rolled building and design codes to CFS profiles and made necessary the elaboration of codes which were sensitive to these member's particularities.

The structural use of cold-formed steel members started with secondary structures, including roof and wall systems, in place of typical timber structural framing, but now, they are also present in primary structures like residential, agricultural, light commercial and light industrial applications – especially racking. The use of the steel frame and drywall systems for housing and industrial purposes had certainly helped the growth in the usage of cold-formed steel members. Figure 1.2 illustrates some of the purposes discussed here mentioned.



(a)



(b)

Figure 1.2 - Cold-formed members applied for a (a) pallet racking system and (b) residential building (METALSHOP, 2015)

1.1 Historic

According to YU & LABOUBE (2010), cold-formed steel (CFS) members started to be used in building construction about the 1850s in the United States and Great Britain. At that time, building codes had no provisions for thin-walled CFS members, thus, there were no acceptance of these by the construction industry.

The use of thin-walled cold-formed members became more expressive in buildings from 1940 onwards. This accomplishment might be attributed by the development of the AISI specifications directed to cold-formed members design, namely “Specification for the Design of Cold-Formed Steel Structural Members”. The first edition of the AISI specification date 1946 and relied on the research carried out at Cornell University by George Winter. This research comprised the study of the performance and experimental results for cold-formed beams, studs, roof decks and connections and led to the development of the Effective Width Method (EWM) for the CFS member design. Since the first edition, the AISI code has been revised to reproduce the technical developments and the results of the newest researches. One of the most remarkable revisions of the AISI was the publication of the Appendix 1 in 2004, which presented an alternative approach for the thin-walled cold-formed members design, namely Direct Strength Method (DSM).

According to CHODRAUI (2003), the use of cold-formed members in the Brazilian building started in 1960, when manufacturers acquired their first folding equipment. The first Brazilian structural design code directed to thin-walled cold-formed profiles was presented in 1967 by ABNT and it was based on current AISI specifications. Nowadays, the current Brazilian standard is the ABNT (2010) and, as well as the AISI, presents the DSM as an alternative method. ABNT (2010) main recommended design methods are the EWM and its analogous method – the effective section method (ESM).

The popularity of the cold-formed profiles has increased in recent years due to their wide range of application and advantages. The research challenges associated also increased along with this growth. The discussion about some cold-formed member’s issues, such as distortional buckling and DSM, are still open and motivate series of research works.

1.2 Motivation

The DSM has gained international recognition since its publication in AISI. It has been well accepted as a design method for thin-walled CFS structural member by the community, specially due to characteristics such as integration of computational stability analysis into the design process and coverage of distortional buckling with a proper design curve.

DSM was developed through experimental tests and its data base consisted basically of PLC and Z cross-sections specimens. Due to this fact, AISI (2012) presents geometrical and material restrictions to the application of the DSM design curves and the sections that fulfill these requirements are called “pre-qualified”. This pre-qualification reduces to a limited range the application of the DSM. Recent studies have been developed in the sense of compare experimental results of cold-formed member’s ultimate loads with the predictions of the DSM distortional curve. Special attention is given to LANDESMANN & CAMOTIM (2015), which reports a shell finite element (SFE) investigation on the distortional post-buckling behavior, ultimate strength and DSM design of CFS single-span lipped channel (PLC) beams. In this work, numerical evidence is presented that the current DSM distortional strength curve is not completely appropriate to predict beam failure moments at room temperature. The authors found unsafe DSM estimates obtained for the beams within moderate-to-high slenderness range.

Moreover, although the remarkable commercial use of CFS “S” type sections (namely, S45 and S90 cross-section shapes), there is a lack of information if the current codified DSM design is able to predict, safely and accurately, their ultimate strength.

1.3 Objective

The aim of this work is to report a SFE investigation on the distortional post-buckling behavior, ultimate strength and DSM design of CFS single-span beams. This work is conceived to extend LANDESMANN & CAMOTIM (2015) numerical investigation to beams with other PLC cross-sections, in addition to SLC, S45 and S90 cross-sections shapes – where all analyzed beams are not pre-qualified and fail in “pure” distortional modes.

To achieve the main objective, this work proposes to: (i) perform GBT buckling analysis aiming at studying the buckling modes nature involved in the selected beams

failures, (ii) perform non-linear analysis in ANSYS (2009) to acquire numerical data for the post-buckling behavior study and (iii) apply the DSM codified method to enable comparison with the numerical data of the ultimate beams bending moments.

1.4 Outline

This work starts with the bibliography review, presented in Chapter 2, summarizing previous works about post-buckling behavior of CFS beams under distortional buckling and the applicable design methods codified up to now.

In Chapter 3, the methods employed to select the beams analyzed are outlined including (i) the description of the end support conditions, (ii) the main conditions imposed to the beams to be selected, which basically comprises buckling occurring in “pure” distortional modes and having different geometrical ratios, (iii) the analysis of the buckling modes of the studied cross-sections, since this step is necessary to extract the results from the code GBTUL (BEBIANO *et al.* 2010a,b), (iv) the critical moments evolution for a range of lengths – which are results of GBTUL analyzes and helped with single-span member’s length choice, and, finally (v) the results of the selection: the cross-sections dimensions and geometrical properties of the selected beams. This chapter also exhibits an investigation about the relation between modal participation and the cross-sections geometrical ratios.

Finally, Chapter 4 presents and discusses the methods and results of the numerical analyzes. The section 4.1 is dedicated to the numerical methodology, more specifically, exploring the parameters involved in the numerical analyzes such as the finite element types and mesh employed, simulation of end support conditions and applied loads, analyzes types and its inputs. While the section 4.2 addresses the elastic post-buckling distortional response of the analyzed beams and examine the relevance of the inward and outward compressed flange-lip motions for the results. Next, on section 4.3, the elastic-plastic post-buckling distortional behavior is shown and important discussions about the beams ultimate strength are raised. On section 4.4 the numerical results obtained are compared with the DSM predictions, which is the current design method applicable to CFS beams failing in distortional modes.

This work closes providing, in Chapter 5, the remarkable conclusions about the results obtained and suggestion for future works to continue the investigation initiated.

2 Bibliography Review

This section presents some fundamental concepts about structural stability and buckling, with a special focus in recent studies about distortional buckling and post-buckling behavior in cold formed cross-sections. It is also discussed the ultimate strength determination and the current design methods related to the application of cold-formed profiles.

2.1 Structural stability and buckling

The static equilibrium of an elastic structure is reached when external causes are applied on it statically and the structure responds with a deformation. If small disturbances are applied and the structure responds with small oscillations around the equilibrium state, it would be still considered in equilibrium – in this case is said the structure is stable. Otherwise, if the structure exhibits a different configuration from the former state in the presence of the disturbances, its equilibrium is called unstable and this new equilibrium configuration is the buckled configuration (SIMITSES & HODGES, 2006).

An example of instability is the lateral-torsional buckling, which occurs in beams when they are loaded with major-axis bending. At the beginning of the load application, an in-plane bending occurs, but when the beam reaches a certain limit load, if it is not properly laterally restrained, it will occur out-of-plane bending and cross-section twisting. This limit load is the elastic lateral-torsional buckling load for geometrically perfect elastic beams. CFS beams with open cross-sections, such as PLC and Z, composed by thin plates, are usually prone to this kind of instability due to its low torsional rigidity (CHEN & LUI, 1987).

GALAMBOS & SUROVEK (2008) present a case of a simply supported beam loaded with major-axis bending moments (M_0) in both ends, considering that the beam is elastic and its cross-section is doubly-symmetric. According to Figure 2.1, the action of M_0 causes the in-plane deflection, v , up to the moment when the critical moment is reached (M_{0cr}) and the out-of-plane deflection u and twisting angle Φ take place. At this moment, the equilibrium exists in both buckled and unbuckled configurations. In this

case, the expression for this critical lateral-torsional buckling moment is given by Equation 2.1, where L is the beam length, E is the elastic modulus, I_y is the major-axis moment of inertia (about y-axis), G is the shear modulus, C_w is the warping constant and J is the St. Venant's torsion constant. The achievement of Equation 2.1 admits that the (i) twisting angle is sufficiently small, (ii) beam material is elastic, homogeneous and isotropic, (iii) there is no plate or cross-section deformations during the process – the cross-section geometry remains the same and (iv) the warping is free in both ends.

$$M_{0cr} = \frac{\pi}{L} \sqrt{EI_y GJ} \sqrt{1 + \frac{\pi^2 EC_w}{GJL^2}} \quad (\text{Eq. 2.1})$$

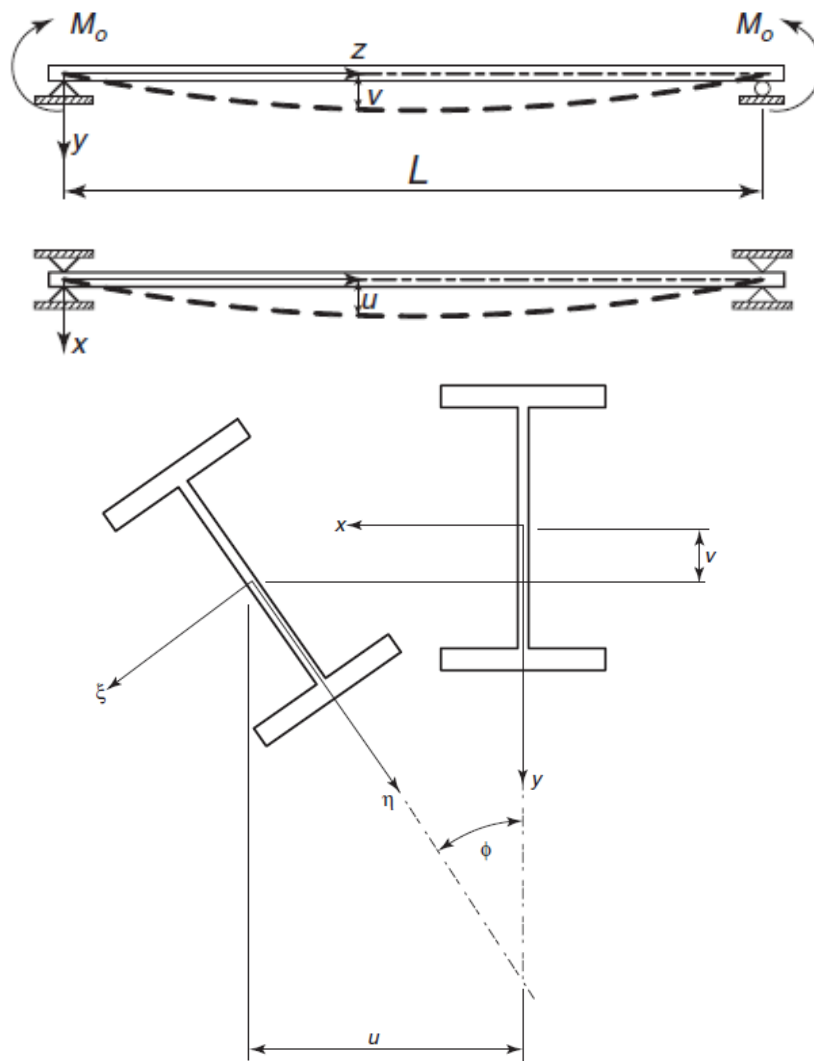


Figure 2.1 - Lateral-torsional buckling in simply supported beams (GALAMBOS & SUROVEK, 2008)

According to CHEN & LUI (1987), the effects of the (i) beam unbraced length, (ii) cross-section geometry, (iii) material behavior, (iv) load type and location and (v) end support conditions might affect the beam buckling behavior and the equations related to

the critical load. Other buckling modes that might affect beams are presented in the next section.

2.2 Buckling modes

For cold-formed profiles open cross-section members, due to its thin walls and consequent low torsional rigidity, the buckling mechanisms are usually different from common hot-rolled sections. Cold-formed profiles beams could buckle in three distinct modes: global (namely, lateral-torsional), local and distortional (YU & SCHAFER, 2006).

The lateral-torsional buckling mode comprises a translation and rotation of the cross-section in a rigid-body movement, so that the cross-section shape remains unchanged. Usually occurs in longest wavelengths than the other two beam buckling modes. In the other hand, the local buckling mode normally occurs with the shortest wavelengths between the three modes. It is characterized by the plate elements (*i.e.*; web, stiffeners and compression flange) rotation around the corners of the cross-section, which do not move. Finally, the distortional mode comprises a distortion of the cross-section. According to ROGERS & SCHUSTER (1997), there are two possible configurations for this distortion, as illustrated in Figure 2.2: (i) the compressed lip-flange assembly rotates around the web-flange corner and (ii) the same described before along with a translation of the web-flange corner in a direction perpendicular to the web.

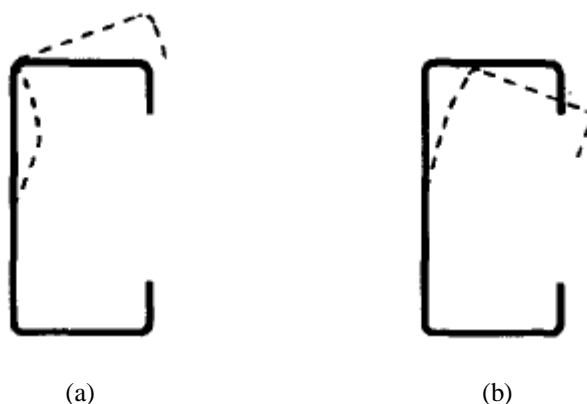


Figure 2.2 – Flexural member distortional mode shapes: (a) lip-flange and (b) web-flange (ROGERS & SCHUSTER, 1997)

According to YU & SCHAFER (2005), the distortional mode is usually induced by the compression of the flange-lip set, but might be caused by the buckling of the web too. This mode commonly occurs in members where the lateral deformations are

restrained – which prevents lateral-torsional buckling to occur – but the compressed flange is not properly restrained. Figure 2.3 shows a relation between the ratio of the critical buckling bending moment divided by the yielding bending moment (M_{cr}/M_y) and the half wavelengths, where every minimum local correspond to a buckling mode, clearly identified.

Identifying the three buckling modes occurring is not an easy task. It cannot be achieved in a finite element investigation, for example. Hence, there is an approach, denoted by GBT (Generalized Beam Theory) through which is possible to decompose a member buckling mode into a linear combination of longitudinally varying cross-section deformation modes – such modal decomposition requires the identification of cross-section deformation modes, which is achieved through the performance of a special discretization-and-orthogonalization procedure designated as “cross-section analysis” (BEBIANO *et al.*, 2010a).

GBTUL, a software which comprises the GBT method, presents three types of deformation modes in its analyzes, described as follows:

- (i) The first 4 correspond to rigid-body global modes – namely axial extension (mode **1**), major and minor axis bending (modes **2** and **3**) and torsion (mode **4**).
- (ii) Once n is the number of natural nodes – the ones placed in walls ends, and d is the number of dependent natural nodes – which can be neglected for unbranched sections, modes **5** to $n+1-d$ are distortional and related with fold-line motions. Thus, distortional modes occur only for cross-section presenting 4 walls or more.
- (iii) The remaining modes are local-plate, comprising wall bending, and its number is given by m , which is the number of intermediate nodes.

Regarding the GBTUL outputs, since the deformation modes contribute individually to the member overall deformed configuration (or buckling mode), the code offers the modal participation factor results for each member length given. This enables to assess the influence of each deformation mode for the interest length. GARCIA (2015) presents results of GBTUL modal participation factors for cold formed steel SLC columns cross-sections, which are illustrated in Figure 2.4.

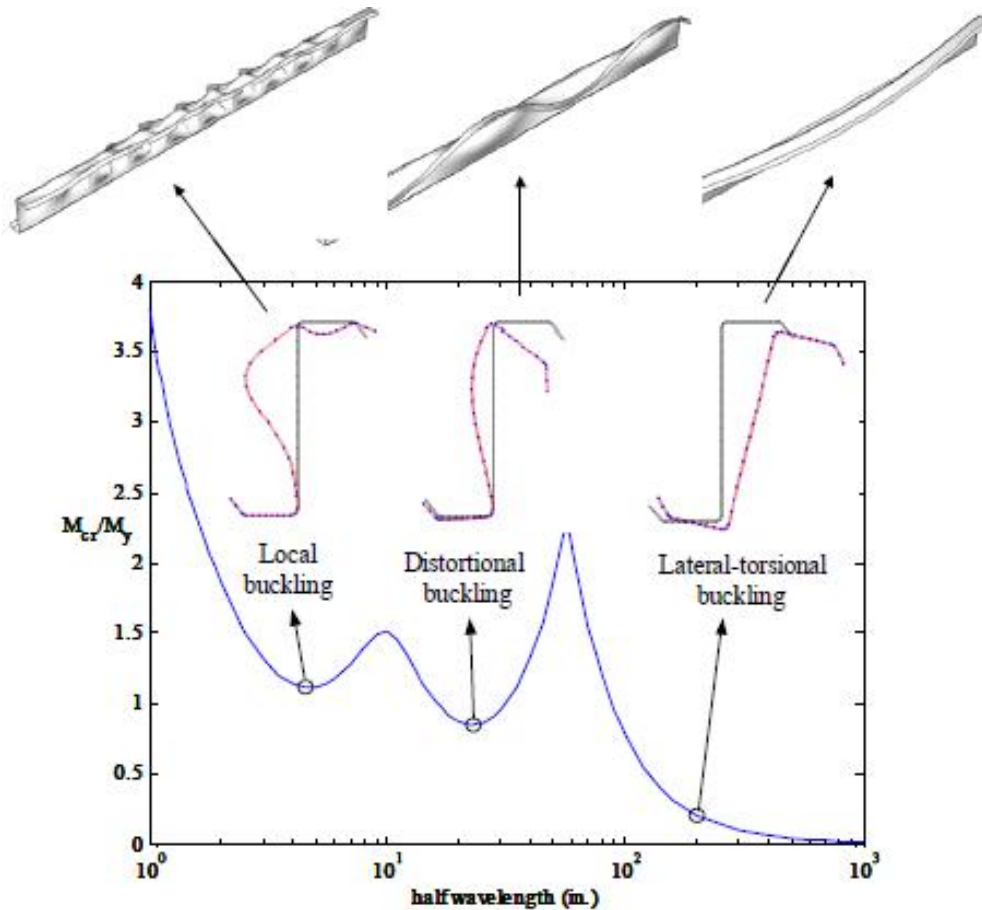


Figure 2.3 - Buckling modes of a CFS Z-section in bending (YU & SCHAFER, 2005)

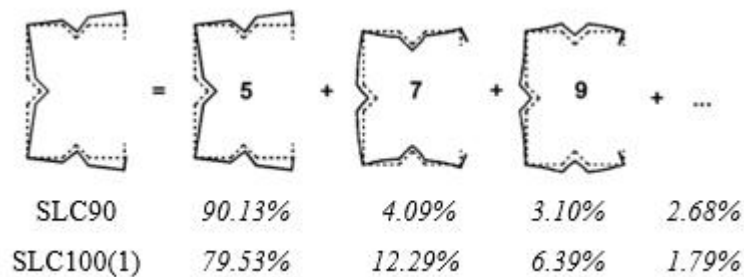


Figure 2.4 GBT modal decomposition: distortionally buckled mid-span cross-section of the (a) SLC90, SLC100(1) and (b) PLC60 columns (GARCIA, 2015)

GARCIA (2015) also establishes correlations between the modal participation of the most relevant modes and some cross-section geometrical ratios. Figure 2.5 presents the relation between the SLC modal participation of distortional mode **5** (p_5), local modes **7** and **9** (p_{7+9}) and other local modes (p_{other}). In this figure, it can be observed that the participation of mode **5** increases with the lip dimension (d) – in other words, lower h/d ratios, where h is the web dimension, and, an opposite trend is noticed in the participation of modes **7** and **9** – which decreased for lower h/d ratios.

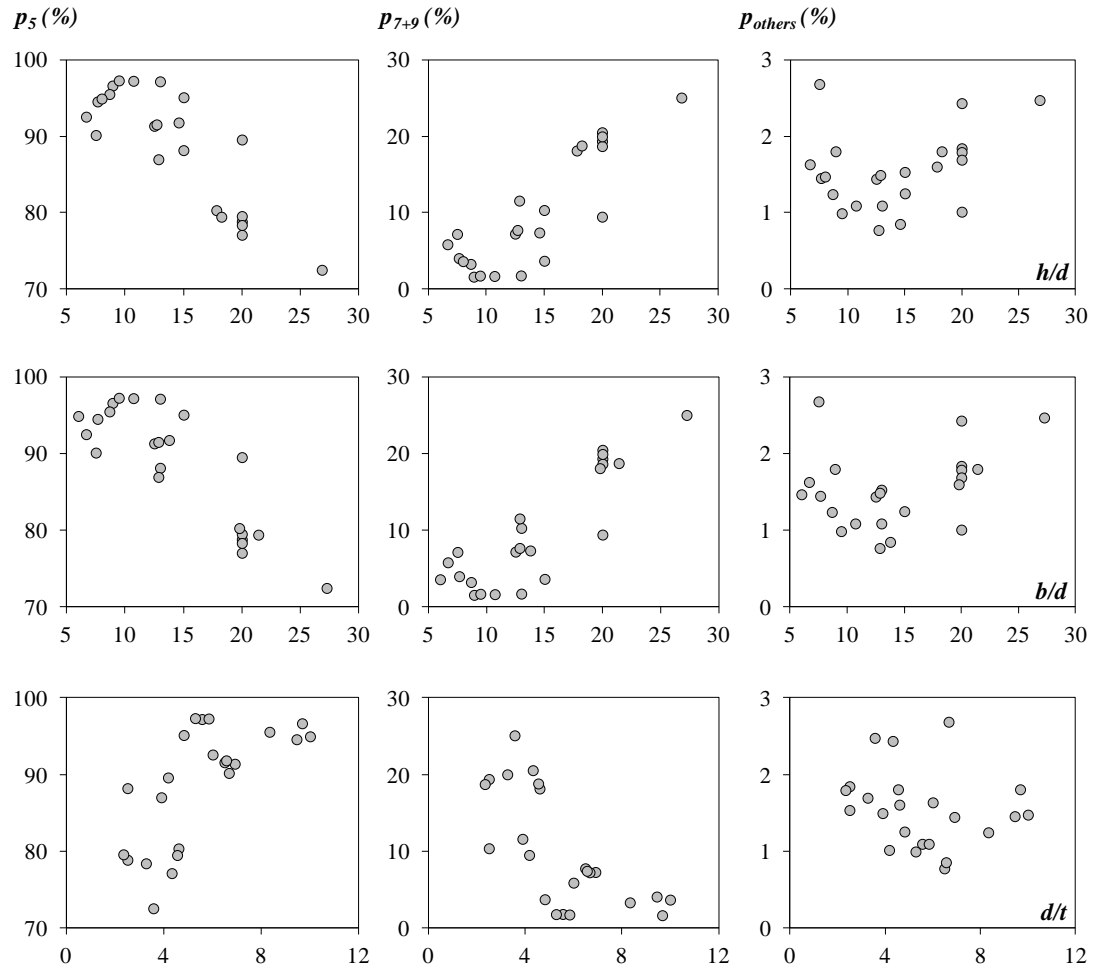


Figure 2.5 - Variation of p_5 , p_{7+9} and p_{others} with h/d , b/d and d/t ratios (GARCIA, 2015)

LANDESMANN & CAMOTIM (2015) report an investigation on the distortional behavior of cold formed steel PLC beams subjected to room and elevated temperatures. In the work, a beam geometry selection is carried out with GBTUL and the relation between the elastic critical buckling moments in a certain temperature T ($M_{cr,T}$) and the member's length (L) – in logarithmic scale – for three distinct end support conditions is studied: the free warping and rotations (F), the prevented warping and free rotations (PF) and the prevented warping and rotations (P) – see Figure 2.6.

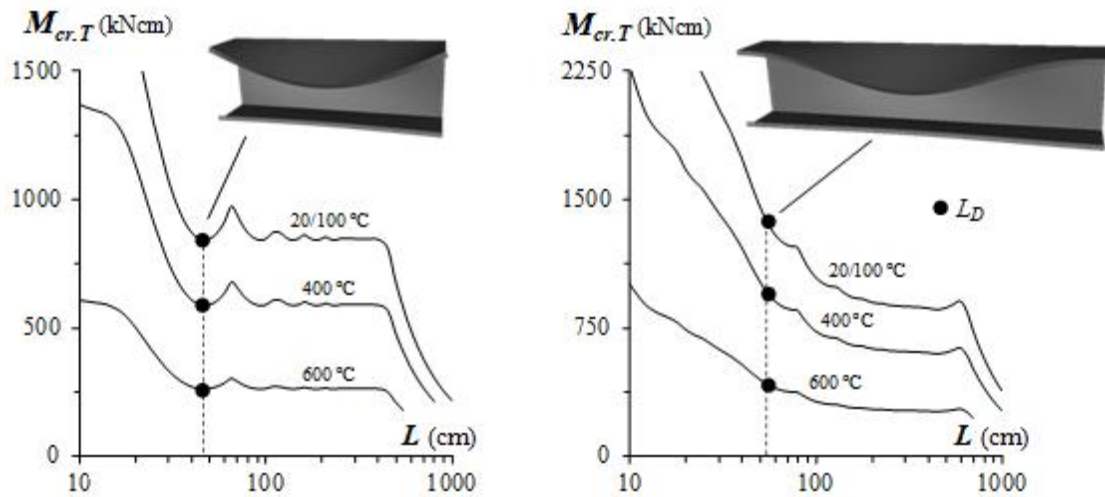


Figure 2.6 - Variation of $M_{cr,T}$ with L and T for (a) F and (b) PF-P PLC-160 beams (LANDESMANN & CAMOTIM, 2015)

Thus, with the relation between the member's buckling critical moments along the member's length associated with the modal participation, it is possible to assess the variation and the magnitude of the influence of the deformation modes in every member length. It is worth to mention that the elastic results provided by the buckling analyzes, carried out with GBTUL code, for example, offer a good indication of the controlling modes. However, to confirm the member's ultimate strength an examination of the post-buckling behavior is required.

2.3 Post-buckling and ultimate strength

The determination of the ultimate bending strength, important for design purposes, demands verification of three buckling modes and their respective post-buckling characteristics.

According to SIMITSES & HODGES (2006), considerable attention has been given to the stability of systems which comprise initial imperfections, which is due to the attempt to associate critical load conditions to load carrying capacity of the system. The large deflection method should be applied for an imperfect structure to obtain information about its post-buckling behavior, since this method provides the whole deformation history, as much as the stiffness reduction closer to the critical load (GALAMBOS & SUROVEK, 2008).

SIMITSES & HODGES (2006) addresses that a usual method to perform a non-linear analysis considering large deflections imply in establishing the maximum load

versus displacement curve. This is reached by initiating with a low load level and acquiring the corresponding displacement through the solution of nonlinear equilibrium equations. This method is repeated after increasing the applied load successively in incremental steps. The criterion for achieve the collapse load is that the convergence cannot be obtained even for small load increments. The finite element analyzes softwares, such as ANSYS, are good tools to perform this kind of analysis. For instance, in ANSYS, it is possible to easily input informations about non-linear materials, to give information about geometrical imperfections, to control non-linear options and to specify analysis failure criteria.

Three post-buckling conditions might occur in real structures: (i) hardening post-buckling behavior, (ii) softening post-buckling behavior and (iii) the transitional case – where the post-buckling curve is flat for all practical purposes (GALAMBOS & SUROVEK, 2008). Figure 2.7 illustrates these three post-buckling situations. This hardening behavior can be observed in cold formed steel members failing in local and distortional modes, where they might present a post-buckling strength reserve beyond the first yielding. This property has been the focus of investigations once is obviously desirable from the standpoint of safety.

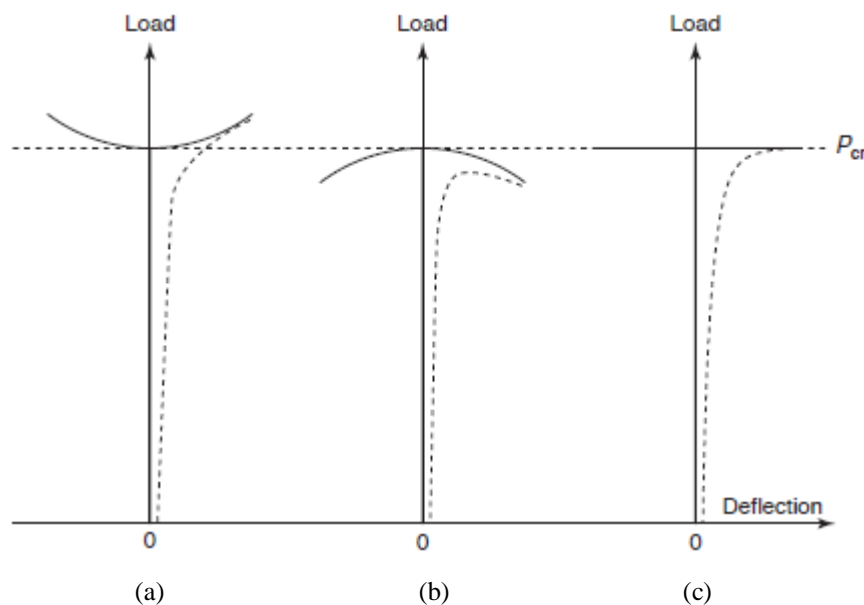


Figure 2.7 - Post-buckling behavior in real structures: (a) hardening, (b) softening and (c) transitional case (GALAMBOS & SUROVEK, 2008)

2.4 Distortional buckling

According to YU & SCHAFER (2005), laterally braced CFS beams usually fail because of local and distortional buckling in addition to yielding. For CFS members such as studs, joists, purlins or girts, the distortional buckling might be the dominant failure mode. One of the first relevant works to describe the distortional behavior in cold formed steel beams was conducted by HANCOCK *et al.* (1994). These authors attributed the occurrence of distortional buckling to members composed of high-strength steel and edge-stiffened flange cross-sections and reported that the current design methods at that time were not capable of account for a properly distortional strength. Moreover, HANCOCK *et al.* (1994) conducted tests with PLC, hat and rack cross-sections, with fixed ends members, undergoing to distortional failure and compared the experimental results with two sets of design curves proposed by themselves – one based in the Effective Section Method and the other predicting the maximum stress in the distortional buckling mode including the post-buckling reserve of slender sections. Both design curves presented adequate prediction of the results for sections with distortional buckling occurring before or at the same time as local buckling.

Later on, HANCOCK *et al.* (1996) recognized the influence of certain geometric proportions in the occurrence of distortional buckling. The authors proposed a new curve – modified regarding the one presented in HANCOCK *et al.* (1994) – for distortional buckling which reproduced more accurately their test data for flexural sections with edge stiffened flanges. The results of this work were included in the Australian standards directed to the design of CFS members.

According to ROGERS & SCHUSTER (1997), cross-sections designed with narrow flanges and web slenderness ratios of up to 200 are prone to fail by web-flange distortional buckling. These authors investigated the current available analytical distortional buckling methods by comparison with tests results. They concluded that the formulation proposed by HANCOCK *et al.* (1996) was a reasonable design method and could provide the bending moment resistance for CFS members prone to web-flange distortional buckling.

SCHAFER & PEKÖZ (1998) summarized experimental data of 574 flexural members, between PLC, Z, hats and decks, comprising distortional buckling. These authors also compared three options of direct strength approach curves – including the one reported in HANCOCK *et al.* (1996) – with the results and they concluded that the

direct strength approaches could provide the same overall average predictive capabilities and lower variation in the results than the EWM.

In SCHAFER & PEKÖZ (1999) it was conducted a numerical investigation to study the post-buckling behavior characteristic of the distortional mode. They emphasized that the distortional mode has less post-buckling capacity than the local mode – confirming HANCOCK *et al.* (1994) results – and that the distortional mode is capable of dominating the failure mechanism even when the elastic buckling stress in the local mode is lower than the distortional one. These authors also presented a hand design method that aimed an assimilation of the distortional buckling by the EWM. This method involved a new approach to define the web effective width and, compared to the current design method, presented more consistent and conservative predictions for cold formed members strength.

PROLA & CAMOTIM (2002) conducted an investigation on the elastic distortional post-buckling behavior of CFS PLC beams subjected to pure bending, accounting for initial geometrical imperfections. They found that the beam distortional post-buckling behavior exhibited a dependence on the cross-section distortion “sign” – where positive indicated a compressed flange-lip inward motion and the negative, outward. For the same applied stress level, the outward distortion led to higher post-buckling strength or to a larger warping restraint than the inward. These results were also verified later in LANDESMANN & CAMOTIM (2015) and MARTINS *et al.* (2016).

YU & SCHAFER (2005, 2006) addressed the first experimental results for industry standard CFS, PLC and Z cross-sections in bending with unrestricted compression flanges in order to determine the capacity in distortional buckling failures. Finite element models were checked by the results of the tests and extended to other non-tested beams (with yield stress varying from 228 to 506 MPa). They concluded that the two methods which comprised explicit procedures for distortional buckling – the Australian standard and DSM – offered simpler and more accurate predictions for distortional buckling failures than the current American standards – comprising the EWM.

A parametric investigation of cold formed steel PLC members under bending was executed by CHODRAUI *et al.* (2006), aiming a verification about the conformity and the range of validity of the current Brazilian Standard simplified model for distortional buckling. When compared with results obtained in the analysis of elastic buckling through the finite strip method, differences obtained were pronounced, even for members within

the range indicated by the Brazilian standard, implying that the model needed adjustments.

LANDESMANN & CAMOTIM (2015) reported a SFE investigation on the distortional post-buckling behavior and ultimate strength of CFS PLC beams subjected to room and elevated temperatures, carried out with ANSYS. These authors employed a steady-state loading strategy which consisted of applying an increasing major-axis uniform bending moment to a beam, in order to obtain the corresponding failure moments. The SFE analyzes incorporated critical-mode initial geometrical imperfections. One of the results of their work is displayed in Figure 2.8, for the three analyzed end support conditions – F, PF and P, concerning PLC-120 beams with room temperature and distortional slenderness $\lambda_{D,20}$ varying between 0.25 and 2.0, it is a sample of the non-linear (geometrically and materially) elastic and elastic-plastic equilibrium path $M/M_{cr,D,20}$ versus $|\delta|/t$, determined to obtain the ultimate moments $M_{u,20}$ (identified by white circles) – where M is the applied bending moment, δ is the displacement and t is the cross-section thickness. About Figure 2.8, the authors made some observations, as follows:

- (i) The F beam elastic and elastic-plastic post-buckling behavior and ultimate strength were different from their PF/P beams counterparts, both qualitatively and quantitatively.
- (ii) The ultimate bending moment ratios $M_{u,20}/M_{cr,D,20}$ and associated $(|\delta|/t)_{lim}$ values increased with the yield stresses $\sigma_{y,20}$, regardless of the end support condition and cross-section dimensions.

Figure 2.9 plots the ultimate bending moment ratios $M_{u,20}/M_{y,20}$ and $M_{u,20}/M_{cr,D,20}$ against the distortional slenderness $\lambda_{D,20}$ for the 110 beams considered by LANDESMANN & CAMOTIM (2015). The observation of these two figures led these authors to the following conclusions:

- (i) All beam failing below the critical bending moment level (*i.e.*; $M_{u,20}/M_{cr,D,20} \leq 1$) exhibited a rather small elastic-plastic strength reserve and very little ductility prior to failure. This assertion did not remain valid when $M_{u,20}/M_{cr,D,20} > 1$: while the F beams collapsed almost immediately after the onset of yielding, the PF/P beams exhibited a considerably higher elastic-plastic strength reserve.
- (ii) The $M_{u,20}/M_{y,20}$ versus $\lambda_{D,20}$ “cloud” followed the trend of a the elastic buckling strength curve $1/(\lambda_{D,20})^2$, with some “vertical dispersion” for all the PF and F beams (it was minute in the F beams), due to the differences in elastic-plastic

strength reserve. This dispersion grew with the slenderness increase and were more pronounced for $\lambda_{D,20} > 1.5$.

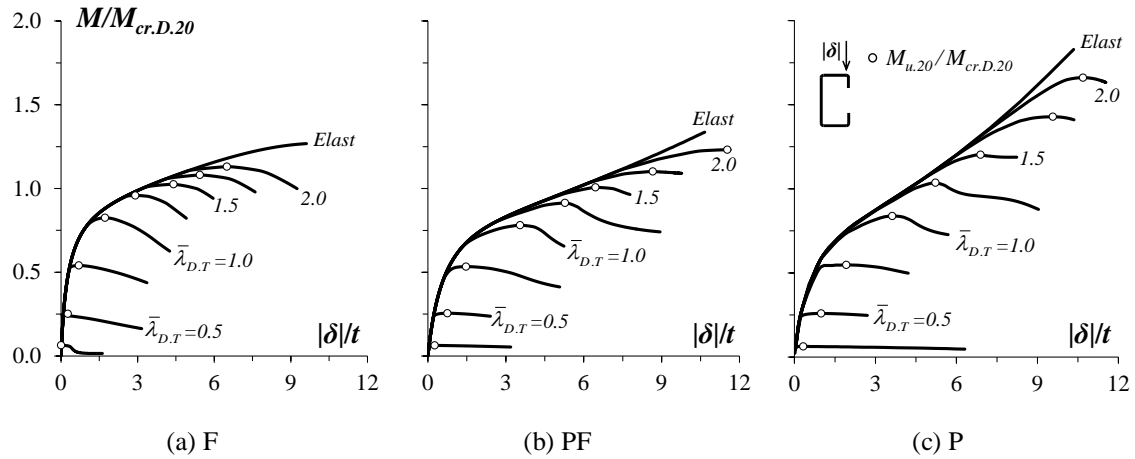


Figure 2.8 - Room temperature elastic-plastic distortional equilibrium paths ($M/M_{cr,D,20}$ vs. $|\delta|/t$) concerning the (a) F, (b) PF and (c) P PLC-120 beams with distortional slenderness $\lambda_{D,20}$ varying between 0.25 and 2.0 (LANDESMANN & CAMOTIM, 2015)

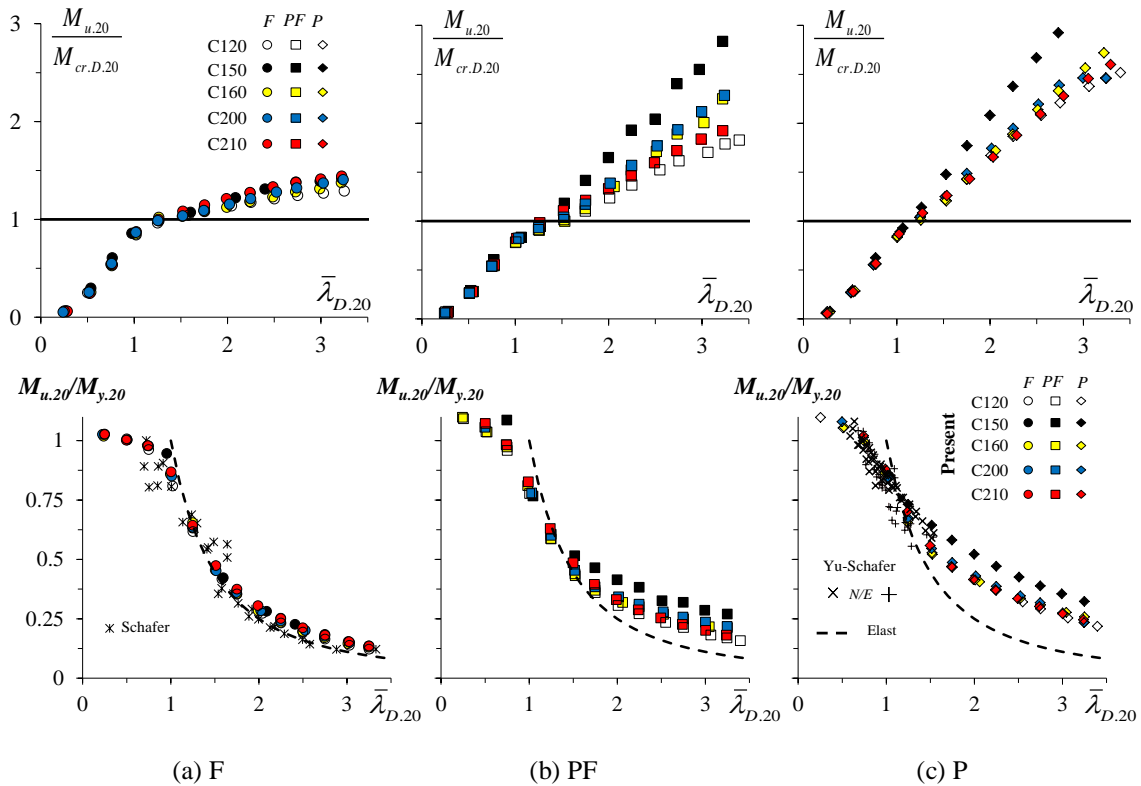


Figure 2.9 - Plots of the (a) F, (b) PF and (c) P beams ultimate bending moment ratios (a) $M_{u,20}/M_{cr,D,20}$ and (b) $M_{u,20}/M_{y,20}$ against the distortional slenderness $\lambda_{D,20}$ (LANDESMANN & CAMOTIM, 2015)

Similar numerical investigation was reported in MARTINS *et al.* (2016), which comprised CFS simply supported beams failing in distortional modes under uniform

bending and exhibiting three cross-section shapes, namely (i) lipped channels – C – bent about the major-axis, (ii) zed-sections – Z – under skew bending causing uniform flange compression (worst case) and (iii) hat-sections subjected to either major-axis – H_M – or minor-axis bending (compressed lips in the latter case) – H_m . Two end support conditions were considered in their work: SCA and SCB – respectively analogous to F and P described in LANDESMANN & CAMOTIM (2015). These authors conclude that:

- (i) The end support conditions, flange-lip width ratio (b_f/b_l) and the critical buckling mode half-wave number (n_D) affected considerably the distortional post-buckling ultimate strength of all the beams analyzed, especially on P beams. Figure 2.10 illustrates that the SCB beams exhibited a more pronounced distortional post-buckling strength than their SCA counterparts, which stemmed essentially from the end support warping fixity. In Figure 2.11 it is possible to observe that, for beams bent in the major-axis, b_f/b_l decrease caused a drastic M_U/M_{crD} reduction. Figure 2.12 shows that M_U/M_y and M_U/M_{crD} values decreased when n_D increased, particularly those with high slenderness values.
- (ii) The elastic and elastic-plastic distortional post-buckling behaviors of SCA and SCB beams with the same geometry and yield stress were clearly distinct in stiffness and strength. In particular, unlike SCB beams, non-stocky SCA beams exhibited practically no elastic-plastic strength reserve.

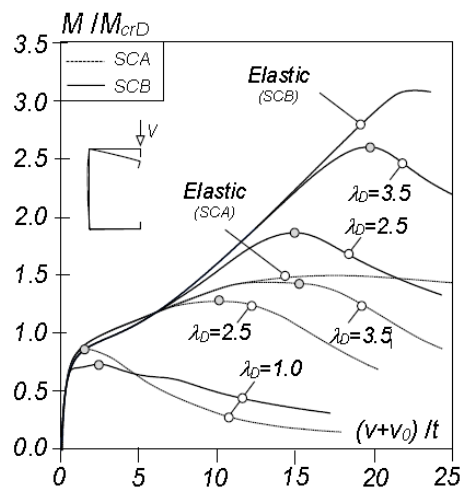


Figure 2.10 - Elastic and elastic-plastic post-buckling equilibrium paths M/M_{crD} vs. $(v+v_0)/t$ for beams with identical C cross-section dimensions and distinct boundary conditions (MARTINS *et al.*, 2016)

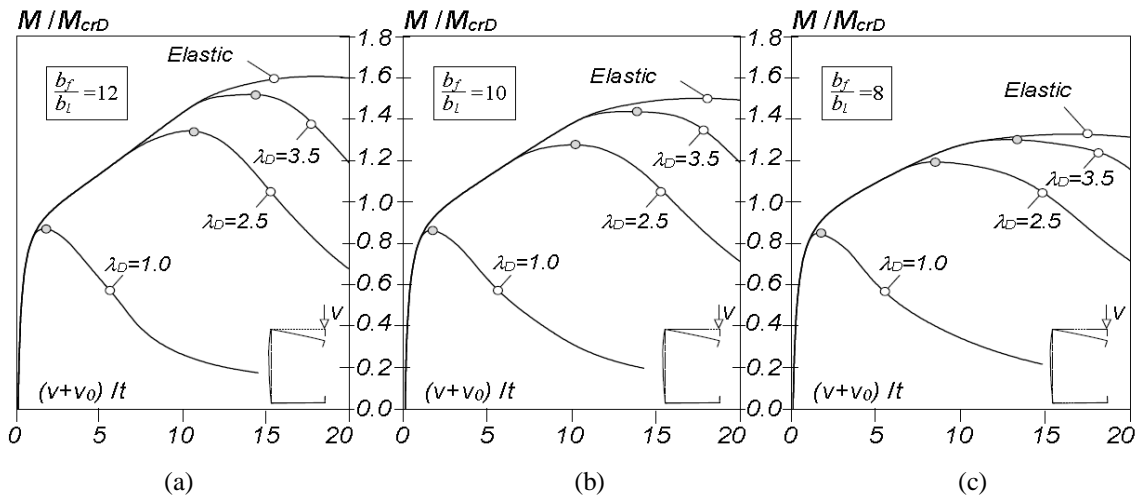


Figure 2.11 - M/M_{crD} vs. $(v+v_0)/t$ equilibrium paths for C+SCA beams with b_f/b_l ratios equal to (a) 12, (b) 10 and (c) 8 (MARTINS *et al.*, 2016)

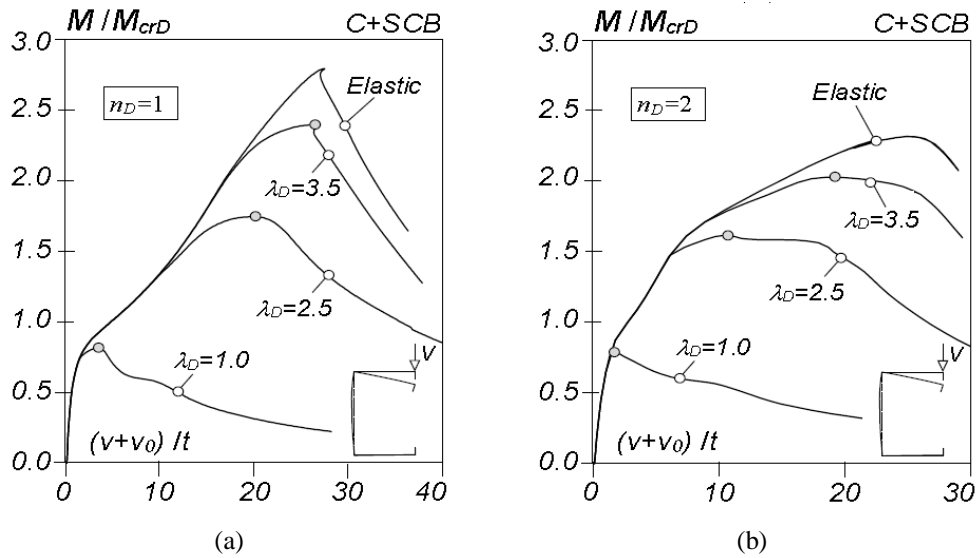


Figure 2.12 - M/M_{crD} vs. $(v+v_0)/t$ equilibrium paths for C+SCB beams with n_D equal to (a) 1 and (b) 2 (MARTINS *et al.*, 2016)

2.5 Design methods for cold formed shapes

The main current design methods employed for CFS members are described in this section, namely the Effective Width Method (EWM), the Effective Section Method (ESM) and the Direct Strength Method (DSM). All these methods involve elastic strength, since they assume that the ultimate condition is reached when the yield stress is reached anywhere in the member. Their differences and advantages are discussed hereafter.

2.5.1 Effective Width Method (EWM)

The EWM is an empirical approach presented in AISI (2012) which the key idea is that the local plate buckling drives to a reduction in the effectiveness of the plates that comprise the cross-section. The method needs the elastic buckling stress of an element and the material yielding stress as inputs to get the effective width of a cross-section element. For beams, the method works as follows: a beam strength curve is employed to consider lateral-torsional buckling. Hence, to account for the interaction of the lateral-torsional buckling with other modes, the gross section modulus is reduced to an effective section modulus by executing a cross-section individually component reduction through Winter's effective width formula. This reduction in the components aims to comprise the local buckling effects (SCHAFER, 2006).

The calculations of the property sections are iterative. Thus, for simpler cross-sections this approach proves to be adequate. Nevertheless, for more optimized cross-sections (*i.e.*; with intermediate stiffeners), the estimation of the elastic buckling stress and the effective properties might income in a complex task. Besides the EWM does not include specific distortional buckling predictions and the interaction between flange and web in local buckling is neglected (YU & SCHAFER, 2005).

2.5.2 Effective Section Method (ESM)

The ESM, included in ABNT (2010), is a direct method employed for design of CFS members under local and local-global buckling modes interaction. The approach proposed by the ESM is similar to the DSM prescription since it is based on the actual buckling behavior of the CFS member whole cross-section. The implementation of the ESM includes three steps: (i) computation of the global buckling effect – taken with the help of appropriate buckling curves, (ii) computation of the local buckling effect including the interaction with global buckling – computed by Winter-type formulation which comprises a reduction of the flexural modulus and (iii) ultimate strength calculation (BATISTA, 2010).

According to BATISTA (2010), the ESM presents practical tables and equations that allow designers to directly access the elastic critical buckling loads for CFS members and to identify if the section is sensitive or not to distortional buckling effects. The

advantages of this method rely on a simpler approach than the EWM with reliability similar to the DSM results.

2.5.3 Direct Strength Method (DSM)

The DSM is the alternative approach addressed in AISI (2012) and, as well as the EWM, is an empirical method. The method was developed in the later 1990s, aiming to cover EWM limitations and it was incorporated to AISI in 2004 as the Appendix 1. The DSM consists in expressions to estimate the strength as a function of elastic buckling for a local-plate mode, similar to the effective width but it is applicable for distortional and global modes too. Different from the EWM, the DSM is based in the entire member behavior instead of a cross-section component. The inputs for the DSM are the elastic buckling loads and the material yielding, the former might be easily obtained through numerical procedures, such as the finite element method (FEM), finite strip method (FSM), and generalized beam theory (GBT). This possibility of integration with numerical methods in the design must be highlighted.

In comparison with the EWM, DSM has the advantages of the sections properties employed are from the gross cross-sections and no iterations or effective width calculations are required. Thus, the characteristics of the DSM leads to flexibility in cross-section geometry, therefore facilitating the task of optimizing CFS member's sections. Besides the DSM has an explicit formulation to take distortional buckling in account for design and includes interaction of cross-sections components. The formulation employed in AISI (2012) concerning the DSM applied for beam distortional buckling design is the same described in SCHAFFER & PEKÖZ (1998) and is presented in Equation 2.5, where M_{nD} comprises the nominal ultimate distortional bending moment, M_y is the yielding moment, M_{crD} is the critical distortional bending moment and λ_D is the distortional slenderness.

$$M_{nD} = \left\{ \begin{array}{ll} M_y & \text{for } \lambda_D \leq 0.673 \\ M_y \left[1 - 0.22(M_{crD}/M_y)^{0.5} \right] (M_{crD}/M_y) & \text{for } \lambda_D > 0.673 \end{array} \right\} \quad (\text{Eq. 2.5})$$

The DSM is calibrated to cover only pre-qualified sections, thus, the AISI (2012) addresses a list with the geometrical and material limitations. This list is reproduced in Figure 2.13. This pre-qualification is certainly a limitation for the method, but it is intrinsic to empirical methods.

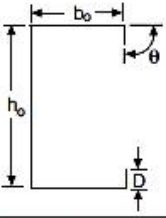
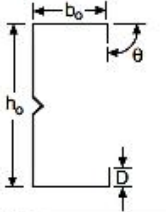
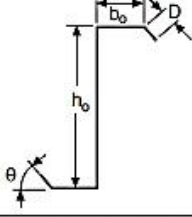
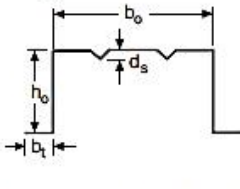
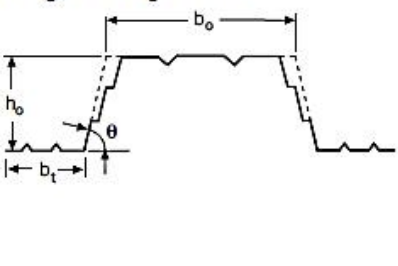
<p>C-Sections</p> 	$h_o/t < 321$ $b_o/t < 75$ $0 < D/t < 34$ $1.5 < h_o/b_o < 17.0$ $0 < D/b_o < 0.70$ $44 \text{ deg} < \theta < 90 \text{ deg}$ $E/F_y > 421$ [$F_y < 70 \text{ ksi (483 MPa or 4920 kg/cm}^2\text{)}$]
<p>Lipped C-Sections with Web Stiffener</p> 	$h_o/t < 358$ $b_o/t < 58$ $14 < D/t < 17$ $5.5 < h_o/b_o < 11.7$ $0.27 < D/b_o < 0.56$ $\theta = 90 \text{ deg}$ $E/F_y > 578$ [$F_y < 51 \text{ ksi (352 MPa or 3590 kg/cm}^2\text{)}$]
<p>Z-Sections</p> 	$h_o/t < 183$ $b_o/t < 71$ $10 < D/t < 16$ $2.5 < h_o/b_o < 4.1$ $0.15 < D/b_o < 0.34$ $36 \text{ deg} < \theta < 90 \text{ deg}$ $E/F_y > 440$ [$F_y < 67 \text{ ksi (462 MPa or 4710 kg/cm}^2\text{)}$]
<p>Hats (Decks) with stiffened flange in compression</p> 	$h_o/t < 97$ $b_o/t < 467$ $0 < d_s/t < 26$ (depth of stiffener) $0.14 < h_o/b_o < 0.87$ $0.88 < b_o/b_t < 5.4$ $0 < n \leq 4$ (number of compression flange stiffeners) $E/F_y > 492$ [$F_y < 60 \text{ ksi (414 MPa or 4220 kg/cm}^2\text{)}$]
<p>Trapezoids (Decks) with stiffened flange in compression</p> 	$h_o/t < 203$ $b_o/t < 231$ $0.42 < (h_o/\sin\theta)/b_o < 1.91$ $1.10 < b_o/b_t < 3.38$ $0 < n_c \leq 2$ (number of compression flange stiffeners) $0 < n_w \leq 2$ (number of web stiffener/folds) $0 < n_t \leq 2$ (number of tension flange stiffeners) $52 \text{ deg} < \theta < 84 \text{ deg}$ (angle between web and horizontal plane) $E/F_y > 310$ [$F_y < 95 \text{ ksi (655 MPa or 6680 kg/cm}^2\text{)}$]

Figure 2.13 - DSM pre-qualified sections limitations (AISI, 2012)

YU & SCHAFER (2005) reported in their work that the DSM predictions for distortional failures had good agreement with the results of distortional buckling tests, since they presented conservative errors of 1% in average (against 10 – 15% unconservative for the EWM). Figure 2.14 illustrates the experimental results obtained in their work in comparison with the respective DSM curves. Though, the authors also observed that the distortional buckling data showed greater deviation with the increase of the slenderness $(M_y/M_{cr})^{0.5}$.

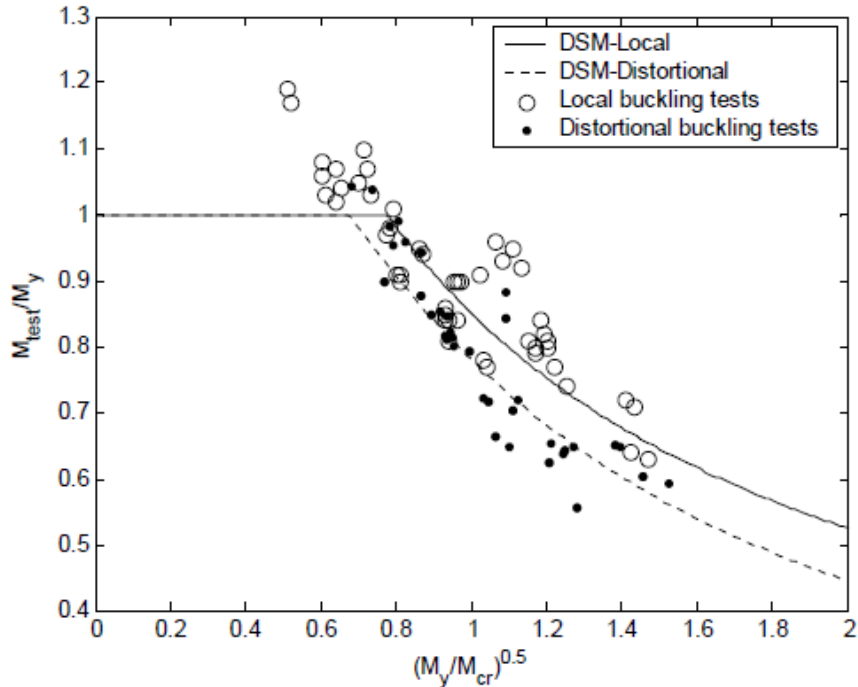


Figure 2.14 - Direct Strength Method predictions versus experimental results (YU & SCHAFER, 2005)

Similar results were obtained by LANDESMANN & CAMOTIM (2015). The numerical ultimate moment ratios obtained in their work were compared with the DSM estimates, SCHAFER (1997) and YU & SCHAFER (2006) experimental results – they are displayed in Figure 2.15. Figure 2.15 also illustrates the ratios $M_{u,20}/M_{n,D,20}$ obtained in their work against $\lambda_{D,20}$ – where $M_{n,D,20}$ is the DSM nominal ultimate bending for room temperature. The latter provide pictorial representations of the accuracy and safety of the DSM distortional ultimate moment estimates – the averages, standard deviations and maximum/minimum values of $M_{u,20}/M_{n,D,20}$ are also given. Through the observation of these figures, they inferred that:

- (i) Concerning the numerical ultimate moments obtained by LANDESMANN & CAMOTIM (2015), the DSM estimates were (ii₁) mostly safe and accurate in the low-to-moderate slenderness range ($\lambda_{D,20} \leq 1.25$) and (ii₂) clearly unsafe in the moderate-to-

high slenderness range ($\lambda_{D,20} > 1.25$) – the overestimation grew with $\lambda_{D,20}$ and was particularly severe for the most slender F beams.

- (ii) The DSM design curve provided accurate and mostly safe predictions of the numerical and experimental distortional failure moments reported by YU & SCHAFFER (2006) since these moments were part of those used to develop/calibrate this design curve. The results of YU & SCHAFFER (2006) concerned beams (ii₁) formed by back-to-back lipped channel and Z-section profiles (similar to the P-beams) and (ii₂) exhibiting solely small-to-moderate distortional slenderness (0.59 to 1.53).
- (iii) Concerning the F-beam failure moments obtained by SCHAFFER (1997), the DSM curve predictions were (iii₁) mostly underestimations in the low-to-moderate slenderness range ($\lambda_{D,20} \leq 1.5$) and (i₂) clear overestimations in the moderate-to-high slenderness range ($\lambda_{D,20} > 1.25$) – since the $M_{u,20}/M_{n,D,20}$ values were shown to be almost perfectly aligned along the elastic buckling strength curve.

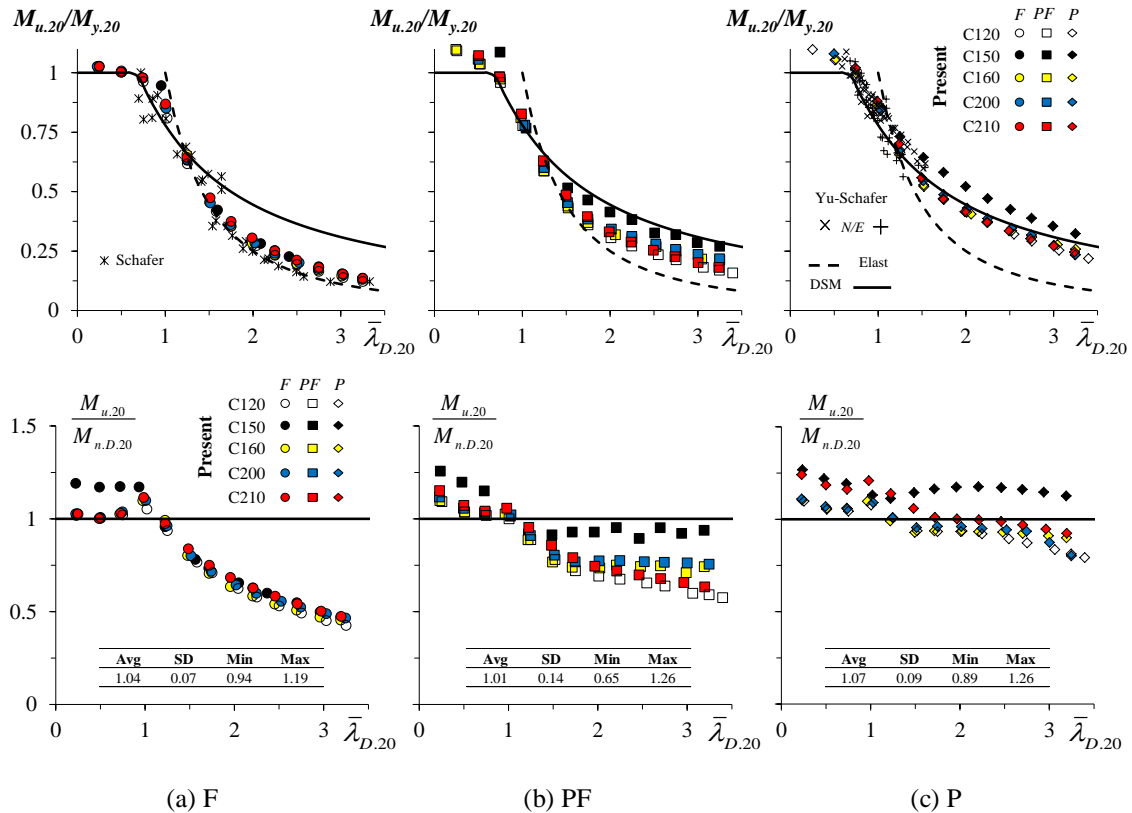


Figure 2.15 - Plots of the (a) F, (b) PF and (c) P beams ultimate bending moment ratios (a) $M_{u,20}/M_{y,20}$ against their DSM estimates and (b) $M_{u,20}/M_{n,D,20}$ against the distortional slenderness $\lambda_{D,20}$ (LANDESMANN & CAMOTIM, 2015)

Later on, MARTINS *et al.* (2016) confirmed the results obtained in LANDESMANN & CAMOTIM (2015) regarding the DSM distortional curve applied for beams. These authors addressed that the currently codified DSM distortional design curve was unable to predict adequately the failure moments of the simply supported beams analyzed in their work because it provided excessively unsafe estimates for the moderate-to-high slender beams. Therefore, they proposed two DSM-based distortional design curves to estimate the failure moments of simply supported cold-formed steel beams under uniform (i) major-axis bending (C and H_M beams), (ii) skew bending (Z beams) and (iii) minor-axis bending (H_m beams) in SCA and SCB end support conditions. The comparison between the numerical results, the current DSM curve and the proposed ones can be seen in Figure 2.16.

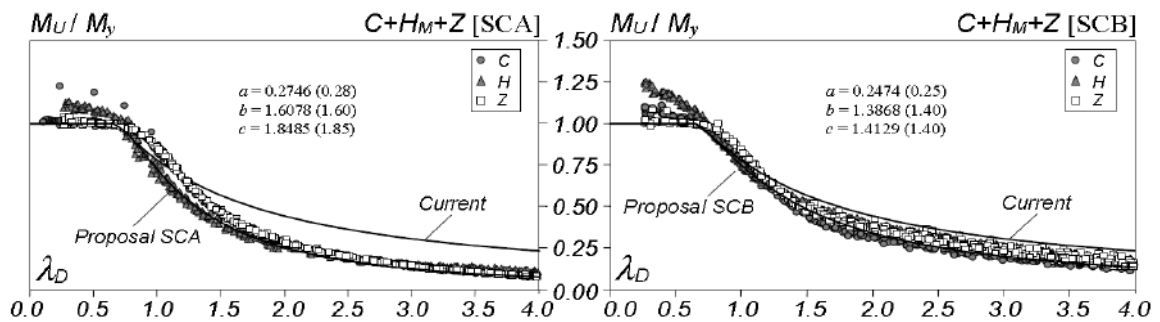


Figure 2.16 – M_U/M_y vs. λ_D plots of the C, H_M, Z beams with (a) SCA and (b) SCB support conditions, and current and proposed DSM beam distortional design curves (MARTINS *et al.*, 2016)

3 Beam Selection and Buckling Behavior

The method adopted for the beam geometry selection procedure and buckling analysis developed in this work is shown in this chapter. For the PLC, SLC, S45 and S90 beams are presented the cross-section dimensions, length related to the critical bending moment and the modal participation of the main buckling modes are discussed. Besides the curves showing the relation between critical bending moments and beam lengths are illustrated.

3.1 Beam geometry selection and buckling analysis

For the purpose of this work, the selected beams (i) were simply supported with respect to major-axis bending, (ii) had their end cross-section torsional rotations prevented and (iii) differed in the end cross-section warping (this designation covers here (i) differential longitudinal displacements and (ii) wall/local displacements and rotations) and minor-axis flexural rotation restraints. Two different end support conditions were considered, namely (i) free warping and rotations, termed here “F” and (ii) prevented warping and rotations, termed here “P”.

Once the end support conditions were determined, the selection of the beam cross-section dimensions and lengths could be performed. The method for the beam selection included sequences of “trial-and-error” buckling analysis for the single-span PLC, SLC, S45 and S90 beams and was carried out mostly through the code GBTUL (BEBIANO *et al.* 2010a,b), but also through ANSYS (2009) SFE analyzes. Basically, the beams to be selected should fulfill the specified conditions:

- (i) They should buckle in “pure” distortional modes and exhibit distortional collapse: the influence of the local and global modes should be avoided. Therefore, to achieve this purpose, it was necessary to ensure that the critical buckling load was clearly distortional and its value should be at maximum half of the lowest local and global bifurcation loads values.
- (ii) Their cross-section dimensions should provide different wall width proportions, such as web-to-flange width ratio, which is desirable to evaluate the influence of proportions on the beams distortional post-critical loads.

- (iii) Their cross-sections should be as much as possible commonly used in practice.
- (iv) Beams cross-sections should remain the same for the two types of end support conditions, only the length, must vary: this means to facilitate the parametric study to be developed in this work.
- (v) Their length, which is related to the distortional critical buckling load, should be the one with a single half-wave distortional buckling mode.

It is important to outline the meaning of “distortional” and “local” buckling before continuing with the beam selection method explanation. Both kinds of buckling imply in-plane transverse displacements, but while “local” displacements occur when a profile wall rotates about the cross-section fixed corners, located at the profile fold line – similar to a simply supported isolated plate rotating about its supports, “distortional buckling” occurs when these walls not only rotate but the corners also translate, causing a cross-section distortion regarding its original shape.

Local, distortional and global modes could be perfectly distinguished in GBT-based results for buckling and each individual mode might have a participation in the final buckling mode shape. Typically distortional modes for the beam cross-sections analyzed in this work are shown in Figure 3.1, the same is repeated for local modes in Figure 3.2. Therefore, to pick a “pure” distortional mode in GBTUL, it was necessary to verify if the distortional modes were the ones with the main contribution to the buckling mode shape with a little or no participation of local modes.

As stated by GARCIA (2015), some SLC cross-section distortional modes resemble local modes, since the flange or web stiffeners are unable to avoid the in-plane transverse displacements of the mid-points. For the SLC beams analyzed, all the distortional deformation modes of order higher than 6 correspond to this description, thus, they were considered as local for the purpose of this work.

Comparing PLC, SLC, S45 and S90 GBT deformation modes, based on Figure 3.1 and Figure 3.2, it is possible to infer that:

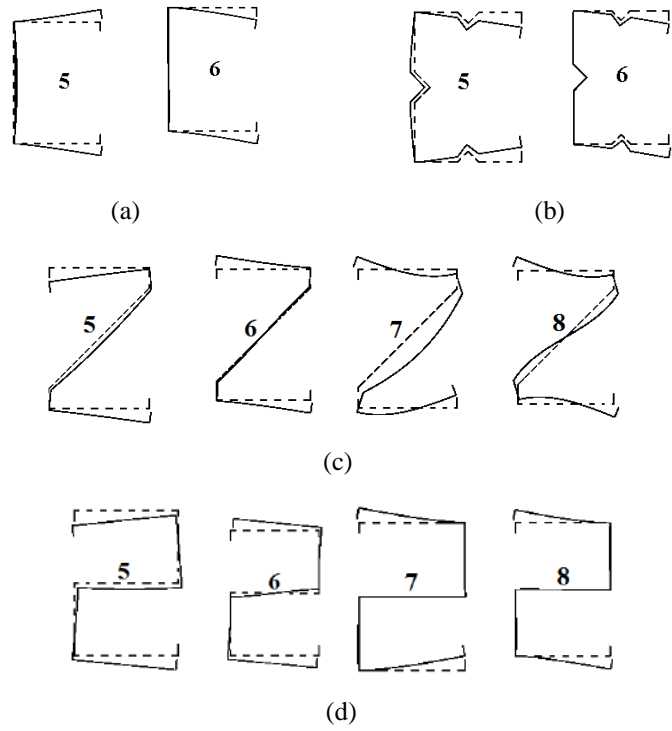


Figure 3.1 - Distortional modes found in (a) PLC, (b) SLC, (c) S45 and (d) S90 cross-sections

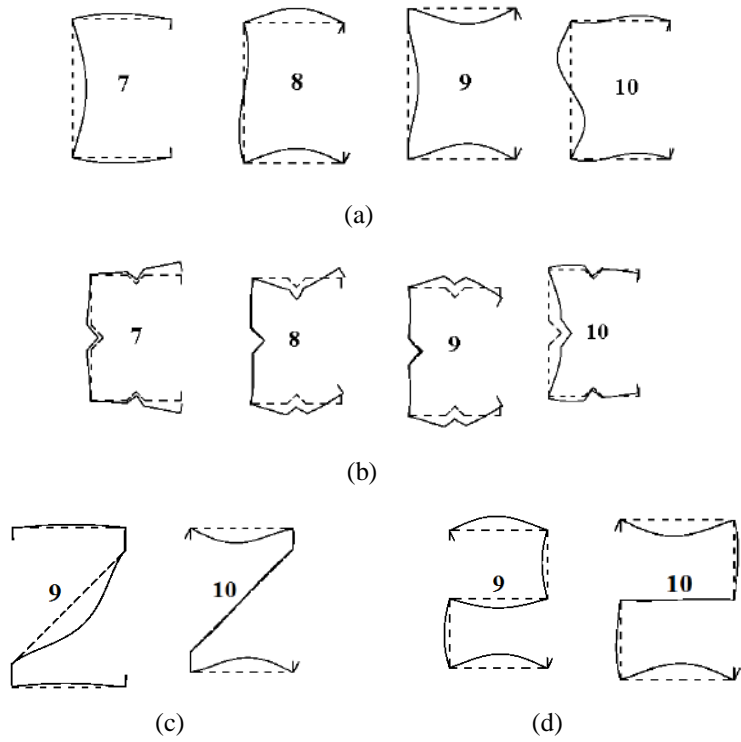


Figure 3.2 – Examples of local modes found in (a) PLC, (b) SLC, (c) S45 and (d) S90 cross-sections

- (i) For the “S” type beams, namely S45 and S90, the number of distortional deformation modes is higher than in the lipped channel cross-sections (PLC and SLC), fact that might be attributed to the additional number of walls. The same behavior is extended to the local modes, which are not the scope of this work.
- (ii) As expected, the S45 cross-section deformation modes are strongly similar to the respective S90. The same is verified between the PLC and SLC beams.
- (iii) The “S” type beams distortional deformation modes seem to occur in complementary pairs and the difference between them relies on the web behavior: meanwhile in modes **5** and **7** the web deflects in a half-wave shape, the modes **6** and **8** present a complete wave. The flange and lips keep their deformation shapes between the complementary pairs.

Considering the exposed above, 20 beams cross-section dimensions compose the scope of this work. The dimensions are shown in Figure 3.3, Table 3.1 and Table 3.2. One notices that (i) the web-to-flange width ratio (b_w/b_f) ranges from 1.15 to 1.60, (ii) the web-to-thickness ratio (b_w/t) varies from 37.5 to 56 and (iii) the web-to-lip ratio (b_w/b_l) extends from 12 to 15. Also for the 5 SLC beams (i) the web intermediate stiffener width-to-depth ratio (b_{w1}/b_{w2}) is 2.0, (ii) the flange intermediate stiffener width-to-depth ratio (b_{f1}/b_{f2}) is 2.0, (iii) the web-to-stiffener width ratio (b_w/b_{w1}) is 5.0 and (iv) the flange-to-stiffener width ratio (b_f/b_{f1}) is 5.0.

It is worth noting that the 2 PLC beams, namely the PLC-120 and PLC-150, shown in Table 3.1, were added aiming a validation to this work since they were previously analyzed and discussed by LANDESMANN & CAMOTIM (2015). The beams selected in this work are not within the geometric limitations prescribed in the AISI (2012) for the application of the DSM.

For all beams analyzed in this work, Table 3.3 provides (i) the length associated with critical distortional buckling (L_D), (ii) corresponding critical (distortional) buckling bending moment (M_{crD}) – obtained by means of GBTUL buckling analysis including all deformation modes, and (iii) their ratios with respect to the lowest local (M_{bL}) and global (M_{bG}) bifurcation bending moments – also obtained by means of GBTUL buckling analysis, but only local and global deformation modes were included, respectively. All the buckling/bifurcation moments were calculated for $E=210GPa$ (elastic modulus) and $\nu=0.3$ (Poisson’s ratio).

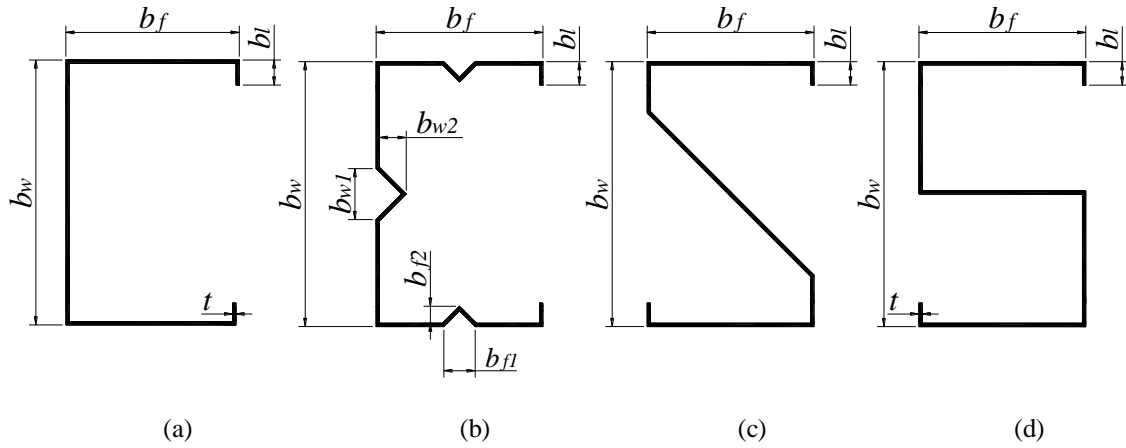


Figure 3.3 - Cross-section of (a) PLC, (b) SLC, (c) S45 and (d) S90 beams

Table 3.1 - Selected PLC, S45 and S90 beams cross-section dimensions, area and middle horizontal axis elastic modulus

Cross-section	b_w (mm)	b_f (mm)	b_l (mm)	t (mm)	A (cm ²)	S (cm ³)
PLC-075	75	65	5	2.0	4.3	12.3
PLC-090	90	75	6.25	1.8	4.5	15.5
PLC-120	120	75	10	3.0	8.7	37.2
PLC-140	140	100	10	2.5	9.0	46.2
PLC-150	150	120	10	3.5	14.4	80.7
S45-075	75	65	5	2.0	4.8	13.2
S45-090	90	75	6.25	1.8	5.1	16.5
S45-120	120	75	10	3.0	9.6	38.7
S45-140	140	100	10	2.5	10.0	48.6
S45-150	150	120	10	3.5	16.1	85.8
S90-075	75	65	5	2.0	5.6	13.0
S90-090	90	75	6.25	1.8	5.9	16.3
S90-120	120	75	10	3.0	10.9	38.2
S90-140	140	100	10	2.5	11.5	47.9
S90-150	150	120	10	3.5	18.6	84.6

Table 3.2 - Selected SLC beams cross-section dimensions, area and major-axis elastic modulus

Cross-section	b_w (mm)	b_f (mm)	b_l (mm)	t (mm)	b_{w1} (mm)	b_{w2} (mm)	b_{f1} (mm)	b_{f2} (mm)	A (cm ²)	S (cm ³)
SLC-075	75	65	5	2.0	15.0	7.5	13.0	6.5	4.6	12.6
SLC-090	90	75	6.25	1.8	18.0	9.0	15.0	7.5	4.9	15.9
SLC-120	120	75	10	3.0	24.0	12.0	15.0	7.5	9.4	38.6
SLC-140	140	100	10	2.5	28.0	14.0	20.0	10.0	9.0	56.5
SLC-150	150	120	10	3.5	30.0	15.0	24.0	12.0	15.5	83.3

Only for the SLC beams, M_{bL} corresponds to bifurcation bending moments obtained by means of GBTUL buckling analysis including deformation modes beyond the 6, which means that only the global and “truly distortional” modes were excluded.

Table 3.3 - Selected beam lengths, critical buckling moments and bifurcation-to-critical moment ratios

Beam	F beams				P beams			
	L_D (cm)	M_{crD} (kNcm)	$\frac{M_{bL}}{M_{crD}}$	$\frac{M_{bG}}{M_{crD}}$	L_D (cm)	M_{crD} (kNcm)	$\frac{M_{bL}}{M_{crD}}$	$\frac{M_{bG}}{M_{crD}}$
PLC-075	20	301.8	4.2	128.6	30.0	432.9	3.0	90.2
PLC-090	30	283.2	3.2	103.8	45.0	405.7	2.3	72.9
PLC-120	30	1798.3	3.3	44.5	50.0	2580.7	2.3	25.3
PLC-140	45	996.9	2.8	73.0	70.0	1439.0	2.0	47.4
PLC-150	40	1911.4	3.7	116.1	70.0	2693.7	2.7	61.0
SLC-075	25	386.3	9.6	63.3	40.0	568.0	7.1	38.1
SLC-090	35	359.2	10.7	59.2	55.0	539.1	7.4	36.2
SLC-120	35	1972.6	13.6	29.5	55.0	2889.2	10.0	18.4
SLC-140	50	1194.0	10.1	48.7	85.0	1781.0	6.9	25.6
SLC-150	50	2399.2	18.4	58.4	85.0	3521.7	13.6	31.2
S45-075	25	226.6	7.4	130.0	35.0	318.8	5.4	106.8
S45-090	35	210.9	4.8	123.8	50.0	301.5	3.5	96.2
S45-120	40	1310.5	4.5	46.4	60.0	1920.7	3.1	31.9
S45-140	50	725.5	4.0	105.7	80.0	1075.1	2.7	63.1
S45-150	40	1426.4	5.4	192.6	75.0	1995.3	4.0	88.8
S90-075	20.0	292.5	4.2	292.1	30.0	421.2	3.0	204.3
S90-090	25.0	280.3	3.1	330.1	40.0	408.5	2.2	200.5
S90-120	30.0	1744.9	3.3	95.4	50.0	2530.6	2.3	53.7
S90-140	40.0	982.0	2.8	201.7	65.0	1437.0	1.9	118.3
S90-150	40.0	1983.5	3.5	242.7	65.0	2659.6	2.7	156.7

It might be extracted from the information stated in Table 3.3 that all beams first “non-distortional” bifurcation bending moments are significantly above M_{crD} and correspond to local modes (or considered local modes, in case of SLC beams).

The buckling analysis performed on GBTUL also produced the curves M_{cr} vs. L (with L in logarithmic scale) to allow the comparison between different beams. These curves are shown in Figure 3.4 for PLC, SLC, S45 and S90-075 beams, as an example, where the length value (L_D) and the corresponding distortional critical buckling mode shape are illustrated. One notices that both beams exhibit similar single half-wave buckling mode shape comparing the “P” and “F” conditions.

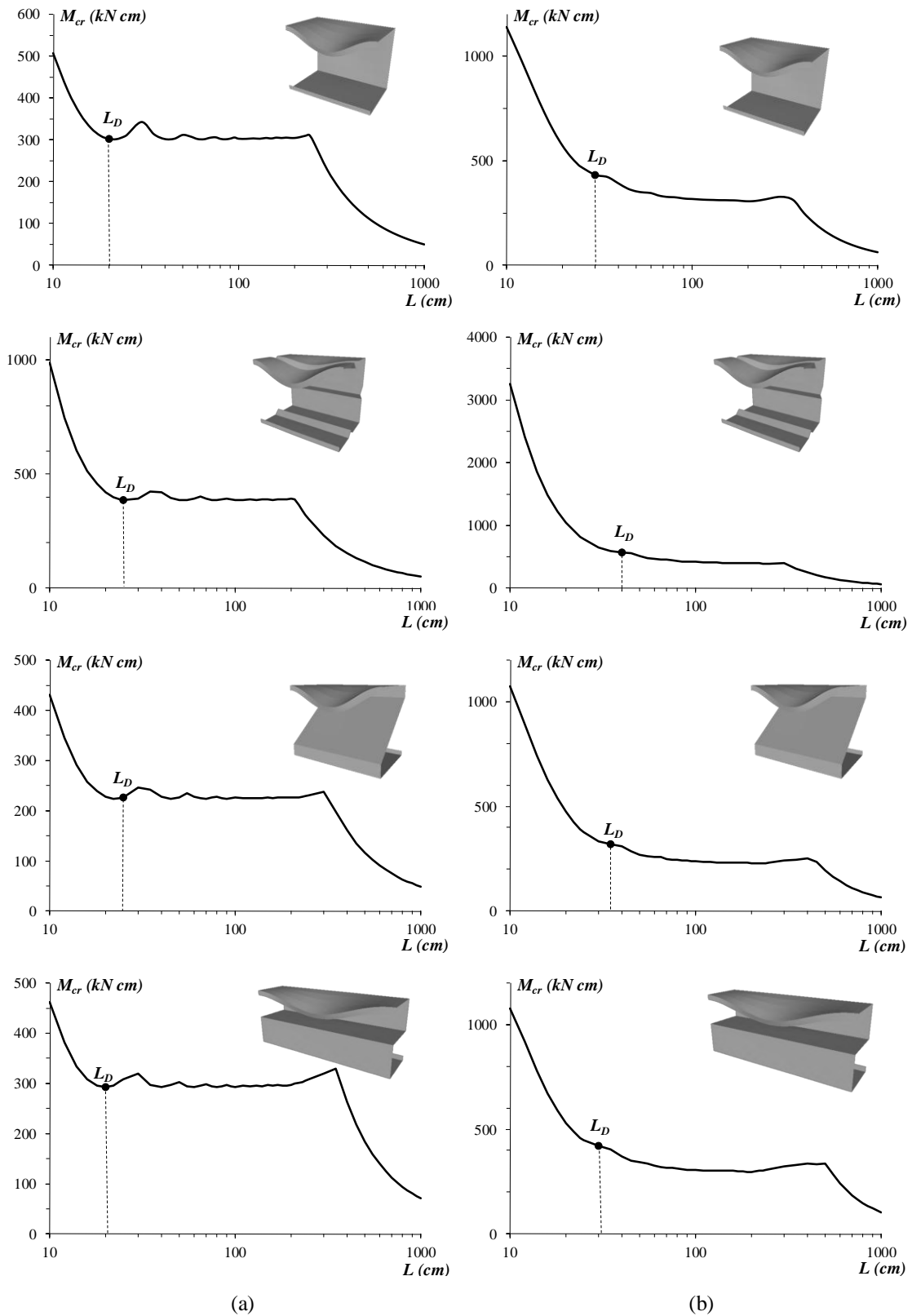


Figure 3.4 - Curves M_{cr} vs. L concerning 075 (a) F and (b) P beams, indicating the selected lengths (L_D) and showing the corresponding distortional buckling mode shapes (Note: the vertical scales are different)

The beams buckling shapes achieved in the present work are not “purely” distortional, they usually correspond to a composition of individual modes and they exhibit small contributions from local deformation modes. Table 3.4 provides, for all beams with length L_D , the GBT modal participation (p), presented in percentage, for the main modes of each type of beam. According to Table 3.4, for the beams analyzed main local deformation modes are **7** to **10** for PLC/SLC and modes **9** to **10** for S45/S90 and they have some influence in the mid-span buckling shapes found. The results presented in Table 3.4 confirm that all the beams analyzed in this work buckle in critical distortional modes, since the contributions from these are higher than the local deformation modes. The mid-span buckling shapes of the PLC/SLC/S45/S90-140 F beams and their respective modal participation are shown in Figure 3.5. All the other beams show similar buckled mid-span cross-section shape and deformation modes participation values.

Regarding the results of modal participation and buckled mid-span cross-section shape, they lead to the following conclusions:

- (i) A predominant participation from a combination of deformation modes **5** and **6** ($p_5 + p_6$) is identified in all beams, except the S90 ones – where modes **7** and **8** are dominant.
- (ii) The contribution of all distortional deformation modes together ranges from 84.26% to 97.49% for F beams and P beams, respectively.
- (iii) There are also small contributions from local deformation modes – namely p_7 to p_{10} for PLC and SLC beams and p_9 to p_{10} for S45 and S90 beams. While the former varies in the ranges of 4.94% - 15.08% for F beams and 7.55% - 18.87% for P beams, the latter amounts to 2.18% - 9.79% for F beams and 3.78% - 13.84% for P beams.
- (iv) One notices that S45 beams exhibit the smallest participation of local modes with an average of 2.91% / 4.59% for F/P beams. While 7.13% / 10.33% , 8.64% / 13.03% and 11.25% / 10.17% are the average participations of local modes for S90, PLC and SLC F/P beams respectively.
- (v) The maximum participation of the other deformation modes corresponds to 3.70% in the S90-075 F beam and the minimum is 0.2% related to PLC P beams. Therefore, these buckling modes (p_{other} – order higher than **10**) are considered irrelevant for the analyzed beams behavior.

Table 3.4 – Length and GBT modal decomposition of beams critical buckling modes

	Beam	GBT Buckling Modes						
		p_5	p_6	p_7	p_8	p_9	p_{10}	Others
Free	PLC-075	47.6%	42.1%	2.7%	4.7%	2.2%	4.7%	0.2%
	PLC-090	50.0%	42.6%	2.2%	3.3%	1.4%	3.3%	0.1%
	PLC-120	51.3%	43.4%	0.8%	2.2%	1.5%	0.4%	0.1%
	PLC-140	51.8%	43.5%	1.2%	2.0%	1.1%	2.0%	0.1%
	PLC-150	50.3%	44.3%	1.4%	2.4%	1.2%	2.4%	0.1%
	SLC-075	44.2%	46.0%	7.6%	0.4%	0.3%	0.2%	0.7%
	SLC-090	44.8%	46.2%	7.5%	0.1%	0.3%	0.1%	0.5%
	SLC-120	39.2%	45.0%	12.1%	1.4%	1.2%	0.2%	0.3%
	SLC-140	39.7%	46.2%	12.0%	0.7%	0.7%	0.0%	0.4%
	SLC-150	42.4%	46.7%	9.6%	0.1%	0.4%	0.1%	0.5%
	S45-075	51.2%	45.2%	0.0%	0.2%	1.6%	1.2%	0.2%
	S45-090	51.8%	44.4%	0.0%	0.2%	1.3%	1.4%	0.9%
	S45-120	51.2%	43.3%	1.6%	1.4%	0.6%	0.9%	0.6%
	S45-140	51.5%	44.7%	0.7%	0.5%	0.7%	1.1%	0.8%
	S45-150	49.7%	46.2%	0.1%	0.2%	1.3%	1.5%	0.9%
	S90-075	6.5%	4.8%	38.9%	39.7%	3.4%	4.1%	2.4%
	S90-090	5.6%	4.1%	39.9%	40.6%	3.4%	4.0%	2.2%
	S90-120	10.7%	7.9%	37.5%	38.7%	1.4%	2.0%	1.6%
	S90-140	7.1%	5.2%	40.7%	41.5%	1.7%	2.2%	1.4%
	S90-150	7.0%	5.1%	40.4%	41.2%	2.1%	2.6%	1.5%
Prevented	PLC-075	46.1%	39.7%	3.9%	5.9%	3.1%	5.9%	0.4%
	PLC-090	47.8%	39.2%	4.1%	5.3%	2.5%	5.3%	0.2%
	PLC-120	51.3%	40.2%	1.8%	3.0%	2.1%	0.5%	0.2%
	PLC-140	50.8%	40.3%	2.6%	3.4%	2.0%	3.4%	0.2%
	PLC-150	51.1%	41.3%	2.1%	3.1%	1.6%	3.1%	0.2%
	SLC-075	45.2%	44.2%	6.6%	0.9%	0.1%	0.2%	0.9%
	SLC-090	45.9%	44.6%	6.7%	0.4%	0.1%	0.1%	0.8%
	SLC-120	40.9%	43.4%	11.0%	1.5%	1.3%	0.3%	0.5%
	SLC-140	43.0%	44.0%	10.3%	0.6%	0.6%	0.0%	0.6%
	SLC-150	45.3%	44.6%	8.0%	0.3%	0.1%	0.1%	0.7%
	S45-075	50.3%	43.3%	0.0%	0.3%	2.6%	2.0%	0.6%
	S45-090	50.6%	42.1%	0.1%	0.2%	2.2%	2.6%	1.5%
	S45-120	50.6%	40.9%	1.9%	1.7%	0.8%	1.6%	1.4%
	S45-140	51.8%	42.1%	0.8%	0.6%	0.9%	1.8%	1.5%
	S45-150	52.0%	43.4%	0.1%	0.1%	1.3%	1.6%	1.1%
	S90-075	5.9%	4.3%	37.2%	37.9%	4.7%	5.7%	3.7%
	S90-090	5.7%	4.2%	37.5%	38.2%	4.8%	5.7%	3.3%
	S90-120	12.3%	9.1%	34.3%	35.5%	2.2%	3.0%	2.6%
	S90-140	7.8%	5.8%	38.2%	38.9%	2.9%	3.6%	2.4%
	S90-150	7.4%	5.4%	39.1%	39.8%	2.6%	3.2%	2.1%

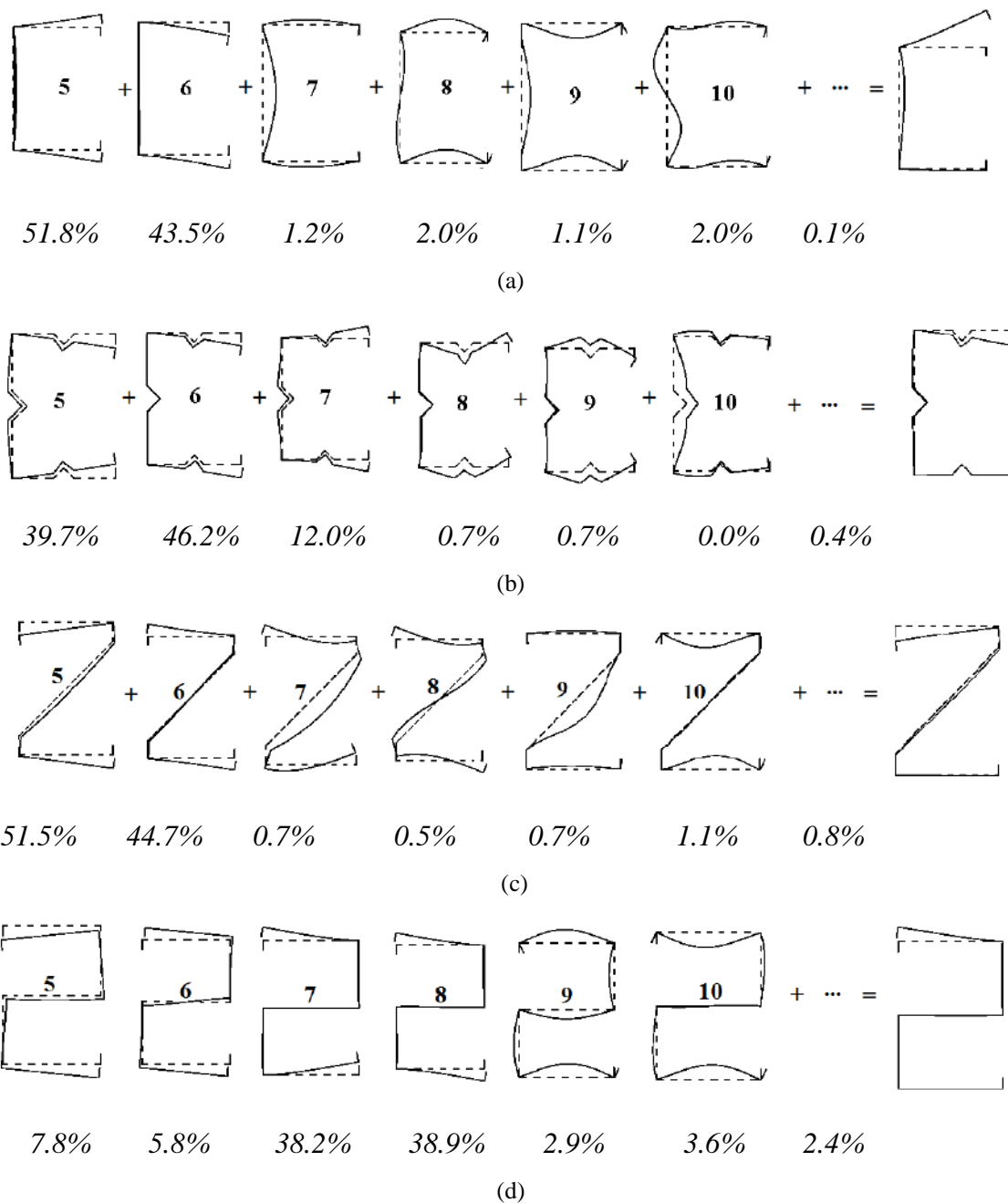


Figure 3.5 - Buckled mid-span cross-section and thee modal participation for (a) PLC, (b) SLC, (c) S45 and (d) S90-140 F beams

Intending to establish a correlation between the modal participation and the width ratios of the elements, graphics in Figure 3.6 and Figure 3.7 are shown, where the participation of distortional (p_{dist}), local (p_{local}) and other (p_{other}) deformation modes are shown. The observation of the results from Figure 3.6 and Figure 3.7 leads to the conclusion that the ratios analyzed are not related to any modal participation, neither for distortional modes nor local modes. Other modes participation also presents no relation with the geometric ratios analyzed.

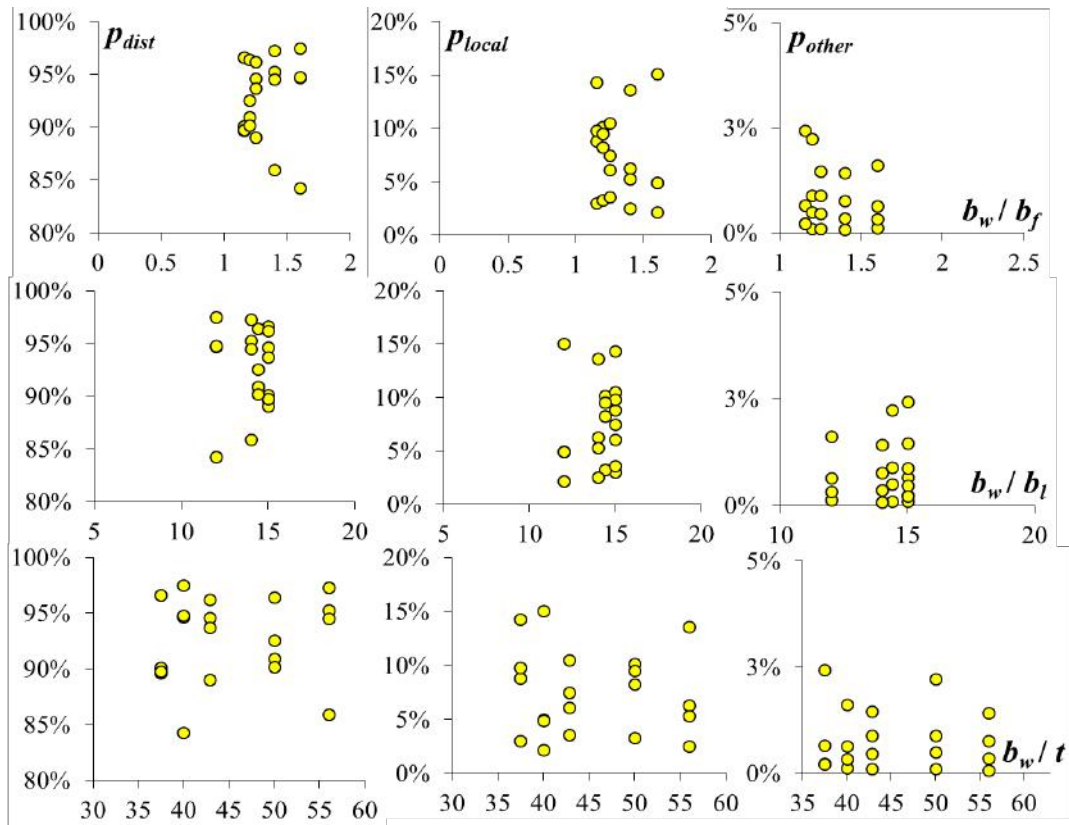


Figure 3.6 - Variation of p_{dist} , p_{local} and p_{other} with b_w/b_f , b_w/b_l and b_w/t ratios

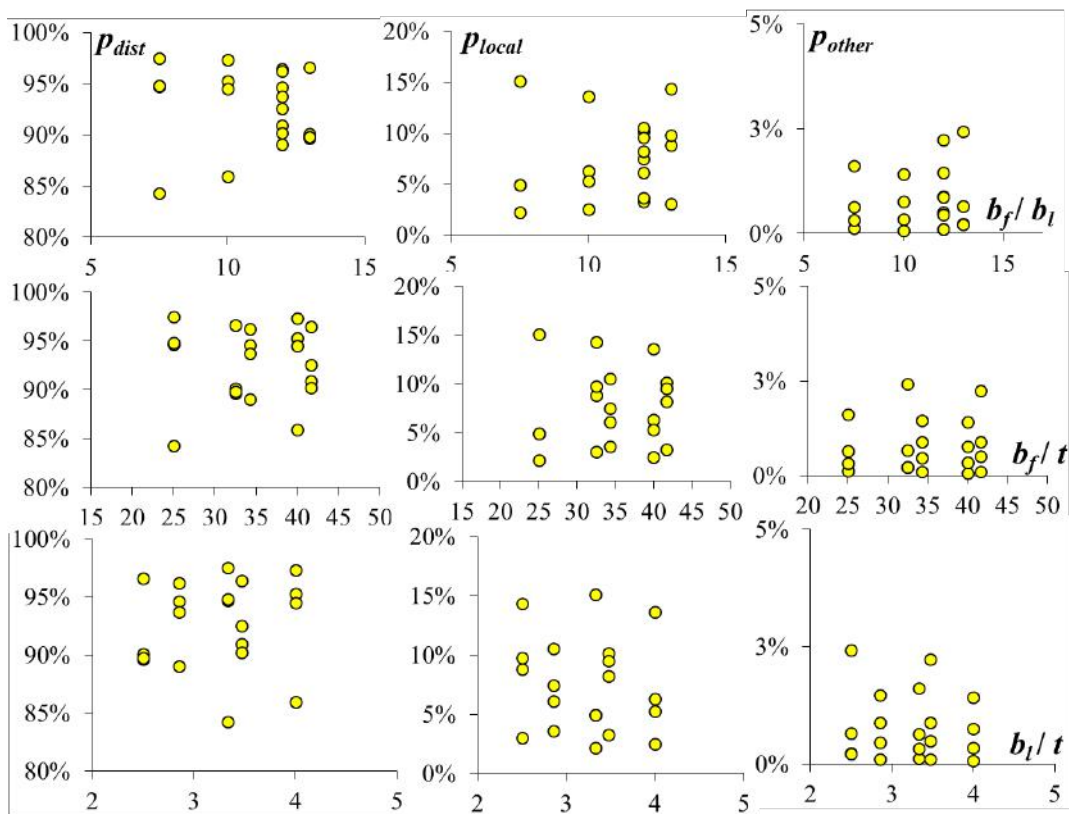


Figure 3.7 - Variation of p_{dist} , p_{local} and p_{other} with b_f/b_l , b_f/t and b_l/t ratios

4 Post-buckling, Ultimate Strength and DSM

The results and methods employed in the SFE analyzes carried out with ANSYS are presented and discussed in this chapter. The adopted model for this investigation is discussed on section 4.1. The results for the elastic post-buckling behavior of the PLC, SLC, S45 and S90 sections are illustrated on section 4.2, while the inelastic post-buckling is discussed on section 4.3. The results obtained for the analyzed sections is finally compared with the DSM estimates for ultimate strength on section 4.4.

4.1 Finite Element Analysis (FEA)

SFE analysis was used to obtain the beam distortional post-buckling equilibrium paths and ultimate strength values for the selected beams. The geometrically and materially non-linear analysis was performed through the code ANSYS (2009). The finite elements used for the beams analysis were *SHELL181*, which is an ANSYS nomenclature for a 4-node shear deformable thin-shell elements with six degrees of freedom per node and full integration. After several mesh tests, a satisfactory accuracy was reached for a $5\text{mm} \times 5\text{mm}$ mesh, illustrated in Figure 4.1.

The material behavior was simulated as either perfectly elastic or elastic-perfectly plastic (*Prandtl-Reuss* model: *von Mises* yield criterion and associated flow rule), with an elastic modulus $E = 210\text{ GPa}$, a Poisson's ratio $\nu = 0.3$ and a number of yield stresses f_y (see Appendix A and B). A larger part of the yield stresses treated in this work are unconventionally high and this was necessary so the study can cover a wide extension of slenderness. Strain-hardening, residual stresses and rounded corner effects were not included in this work.

Two types of models were designed aiming the simulation of the beam end support conditions studied in this work: F and P beams. For the F beams, the nodes of the end cross-section are simply restricted in X and Y direction, as illustrated in Figure 4.2(a) and, for the P beams, was attached a rigid plate to the end cross-sections to avoid the occurrence of warping and local/global displacements and rotations – see Figure 4.2(b). In both end support conditions, the rigid-body axial translation is free at end sections due to the load application.

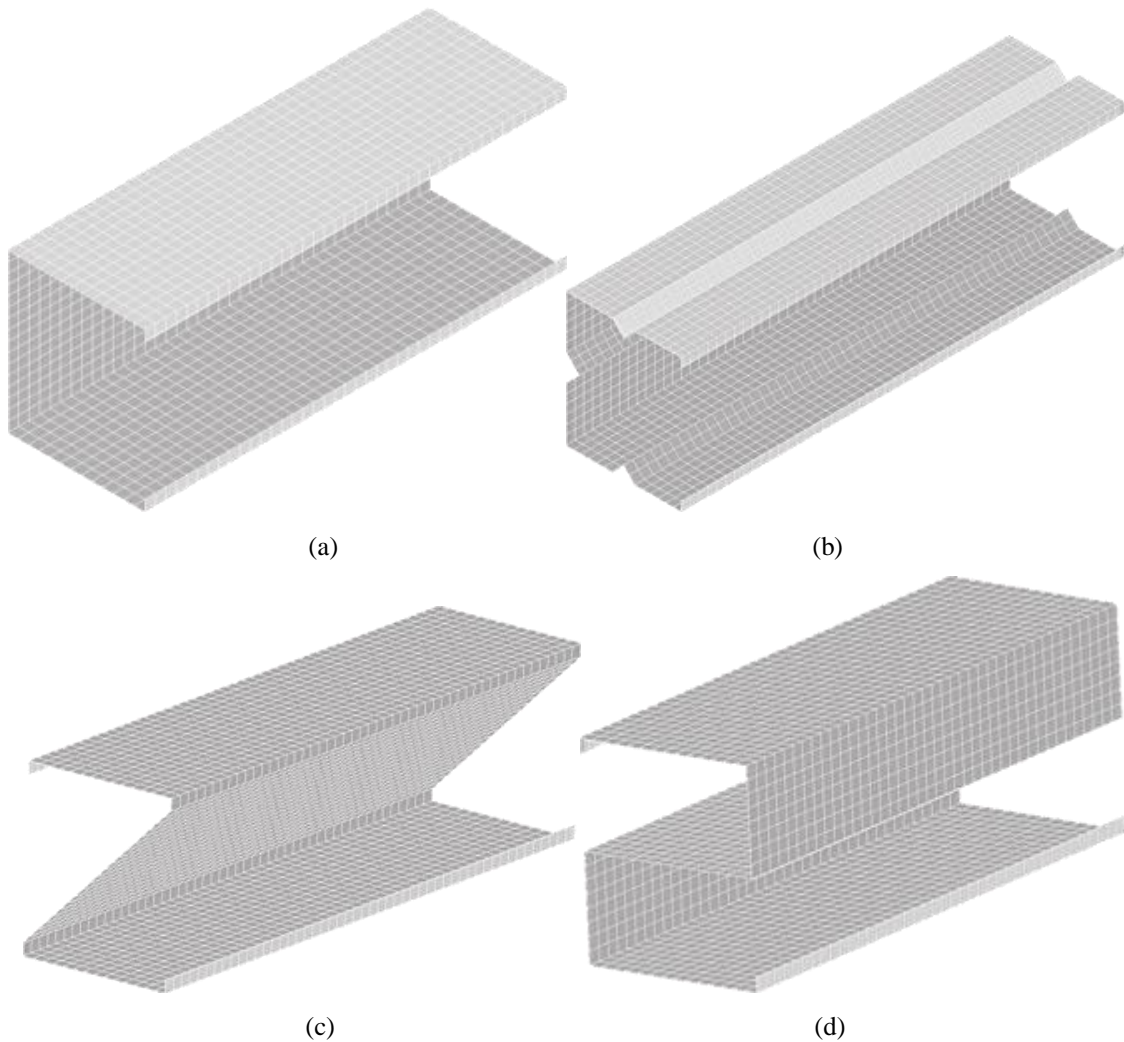


Figure 4.1 - (a) PLC, (b) SLC, (c) S45 and (d) S90-075 beam shape with mesh

The applied load comprised a uniform bending moment, which was simulated through the application of sets of concentrated forces acting on the nodes of both end cross-sections, in the case of F beams – see Figure 4.2(a) – and for P beams, two concentrated moments acting on the rigid end-plates as illustrated in Figure 4.2(b). In both end support conditions, the load was applied on the end cross-sections centroid. The load application was increased in small increments, by means of the ANSYS automatic load stepping procedure. The model was inputted with initial imperfections with small amplitudes (10% of the wall thickness t) corresponding to the typical distortional buckling shape.

The critical-mode initial geometrical imperfections in the beams were automatically included employing a procedure as follows:

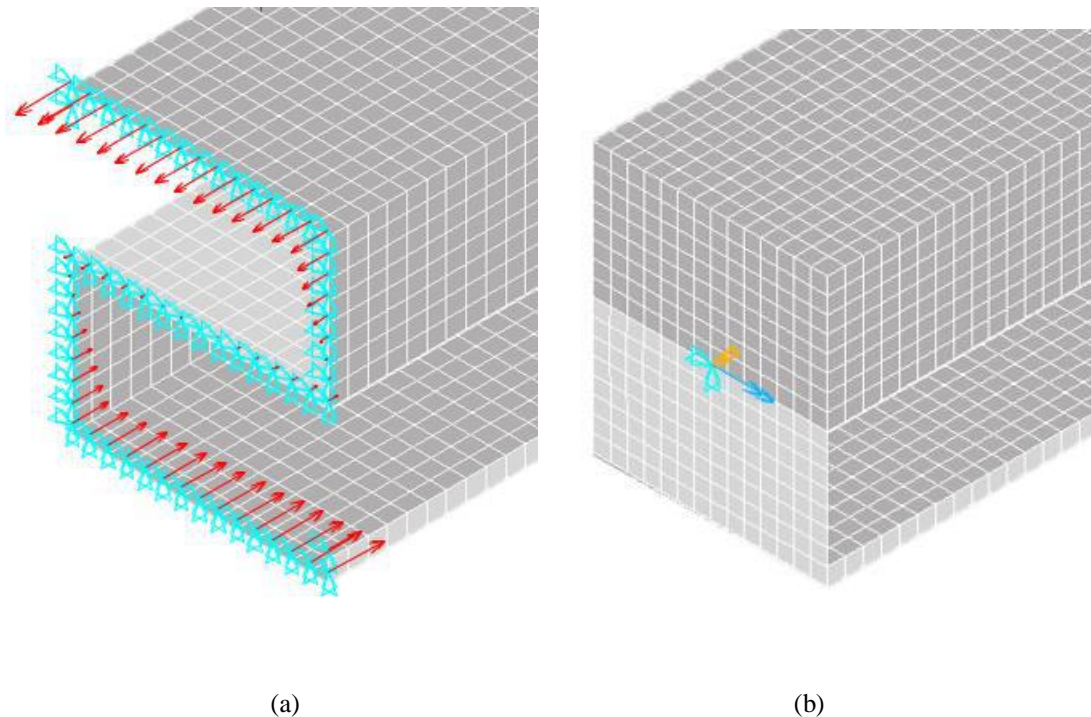


Figure 4.2 - End support conditions and applied bending moment details at S90-075 (a) F and (b) P beam finite element model end cross-section

- (i) ANSYS buckling analysis: the main result of this analysis is the critical buckling mode shape from which was extracted the maximum displacement value. The maximum displacement value always occurs in the mid-span cross-section near the compressed flange due to the fact that all selected beams buckle with one half wave.
- (ii) The same SFE mesh was kept in the model to perform the subsequent post-buckling analysis.
- (iii) The model geometry was updated applying a scale factor of $0.1 t$ in the absolute maximum displacement value, obtained in buckling analysis, so the final maximum transversal displacements along the flange-lip longitudinal would correspond to $0.1 t$.
- (iv) ANSYS non-linear analyzes: the buckling analysis output was employed as the input of the post-buckling analyzes.

Two types of non-linear analysis were performed in this work: the elastic post-buckling analysis – employed to assess the inward or outward flange-lip motions, thus, to investigate the lower post-buckling strength condition and the elastic-plastic post-buckling analysis – carried out to obtain the beams distortional post-buckling behavior and ultimate strength.

For the non-linear analyzes an incremental-iterative technique that combines *Newton-Raphson's* method with an arc-length control strategy was employed. In some analysis, the stabilization control strategy substituted the arc-length, aiming a faster convergence.

Therefore, the ANSYS SFE model described in this section was used to carry out the parametric study presented hereafter. It is worth noting that the model described in this section was previously validated by LANDESMANN & CAMOTIM (2015).

4.2 Elastic post-buckling behavior

As stated in PROLA & CAMOTIM (2002), LANDESMANN & CAMOTIM (2015) and MARTINS *et al.* (2016) the inward compressed flange-lip motion commonly leads to lower post-buckling strengths for CFS beam sections. Therefore, the elastic post-buckling analyzes were carried out in this work to check if the same is verified for the PLC, SLC, S45 and S90 selected beams by testing the two possible types of compressed flange-lip motions: inward and outward. Since this work deals with odd numbers of half-waves in the distortional critical buckling shape, the discussion of which flange-lip motion is the most detrimental is valid.

Both initial imperfections were applied in the elastic analysis – outward and inward – and the results are presented through the equilibrium paths in Figure 4.3(a)-(b) for 075 F and P beams, respectively. The elastic equilibrium paths correspond to the applied moments normalized by the distortional critical one (M/M_{crD}) versus the maximum absolute transversal displacement along the flange-lip longitudinal edges normalized by the wall thickness ($|\delta|/t$). It was observed that the outward flange-lip motions shape led to significantly higher post-buckling strengths, for all sections and for both end support conditions. Thus, the inward initial imperfections results were selected to conduct this work.

For comparison purposes, all the elastic post-buckling equilibrium paths with inward initial imperfections for the PLC, SLC, S45 and S90 F and P beams were plotted in Figure 4.4 and it is possible observe that:

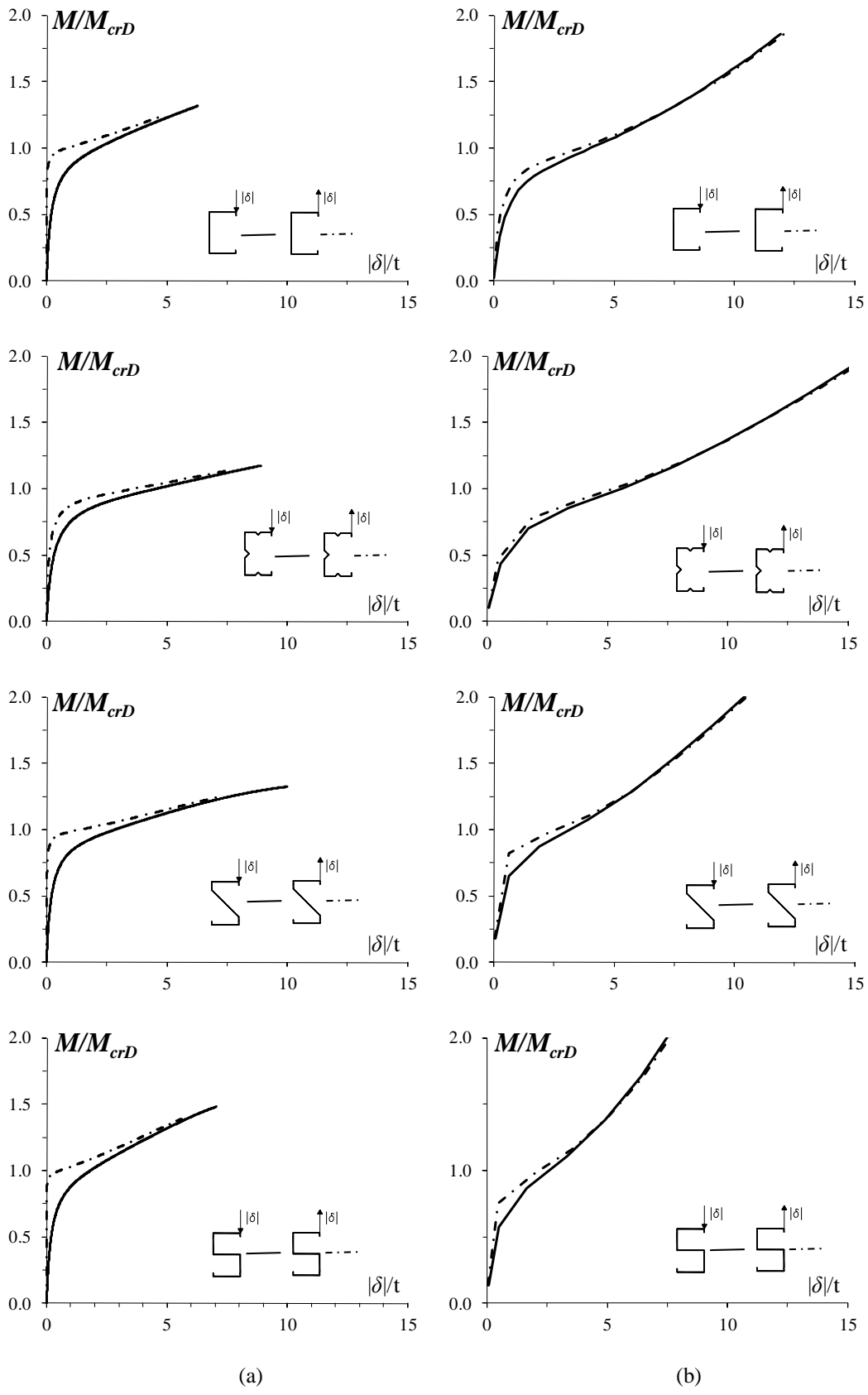


Figure 4.3 - Elastic equilibrium paths M/M_{crD} vs. $|\delta|/t$ of the (a) F and (b) P 075 beams

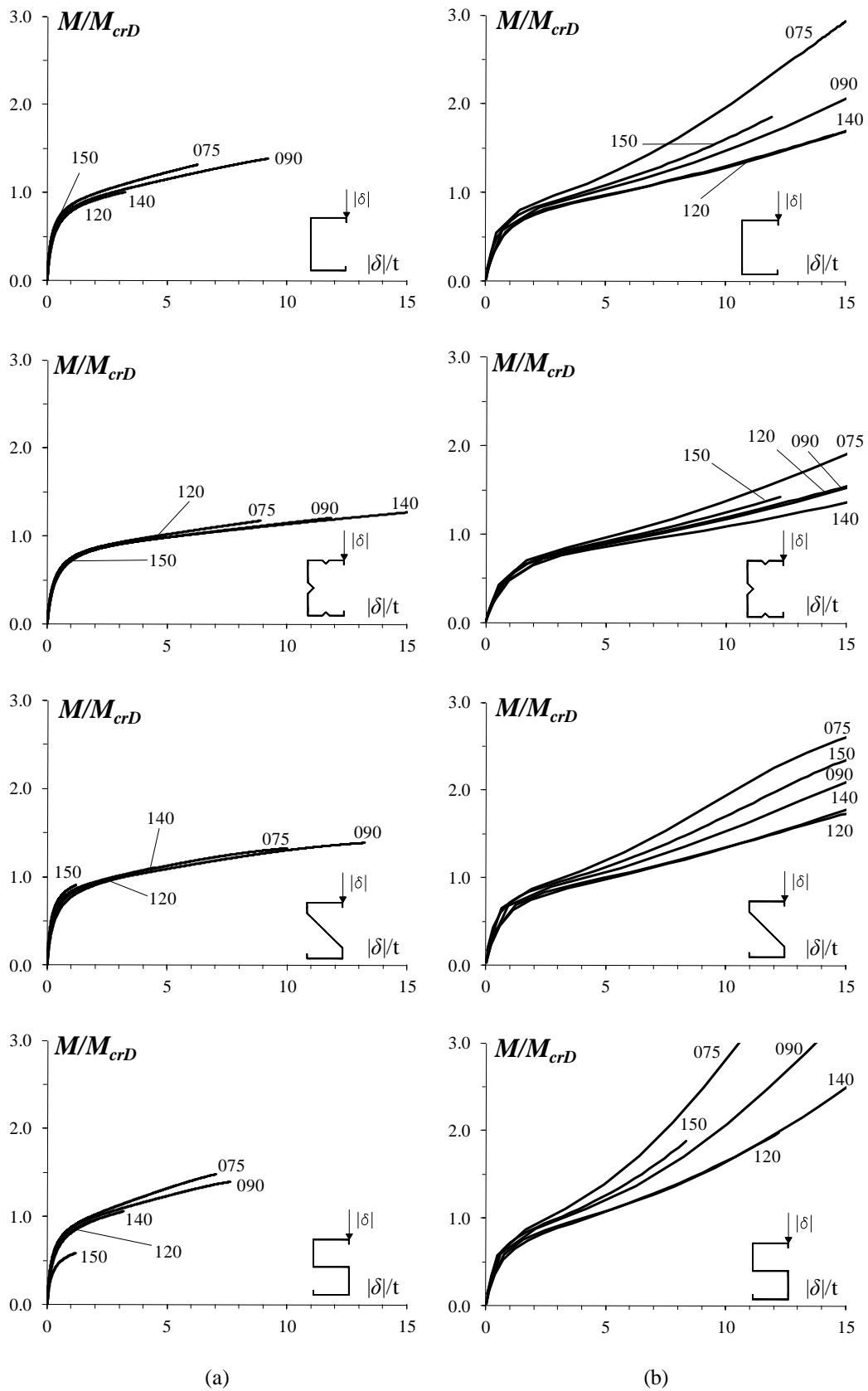


Figure 4.4 - Elastic equilibrium paths M/M_{crD} vs. $|\delta|/t$ of the (a) F and (b) P PLC, SLC, S45 and S90 beams

- (i) The stiffness and strength of the P beams are higher in comparison with F beams for all sections. This fact is confirmed by a difference between the F and P beams equilibrium paths: while the F beam curve presents a convexity, related to a stiffness degradation driving to elastic limit points, the P beam curve exhibits a concavity, which is attributed to the increase of the stiffness near the beam ends constrained, which seems to avoid the elastic limit point.
- (ii) Unlike MARTINS *et al.* (2016), an inversely proportional influence of the geometrical parameter b_w/b_f is remarkable on both F and P beams. While the 120 beams, which retain the highest ratio b_w/b_f (equal to 1.6) exhibit the lowest strength, the 075 beams, with b_w/b_f equal to 1.15, exhibit the highest.
- (iii) The strength seems to have also a relation inversely proportional with the dimension b_l , since the ratios b_w/b_l and b_f/b_l are the lowest for 120 beams (12 and 7.5, respectively) and the 075 beams have the highest ratios (15 and 13, respectively).
- (iv) No direct correspondence with the thickness was found in the studied beams.
- (v) These results confirm that the end support conditions and cross-section dimensions affect the beam elastic distortional post-buckling behavior. Although the limited sample (40 beams studied), it is expected some influence of these factors on the ultimate strength and, therefore, on design methods predictions.

4.3 Elastic-plastic post-buckling behavior and ultimate strength

The same ANSYS finite element model described on section 4.1 was applied to develop a parametric study with the purpose of assessing the elastic-plastic post-buckling and ultimate strength of analyzed beams. Therefore, the results presented in this section concern to 40 beams, including (i) the 5 geometries pointed on Table 3.1 and Table 3.2, (ii) the 2 end support conditions applied in this work (F and P), (iii) web-to-flange width ratios ranging from 1.15 to 1.60, (iv) web-to-lip width ratios varying from 12 to 15 and (v) 14 distortional slenderness values (λ_D varying between 0.25 and 3.5 with 0.25 intervals) – reminding that $\lambda_D = [M_y/M_{crD}]^{0.5}$ and $M_y = S \cdot f_y$, where S is the middle horizontal axis elastic modulus (shown on Table 3.1 and Table 3.2). All beams were modeled with inward initial imperfections (according to the discussion on section 4.2).

Figure 4.5 reproduces the S45-075 F and P beams mid-span cross-section deformed configurations in the proximity of failure for $\lambda_D = 1.5$ (which corresponds to f_y

= 387 and 545 MPa, respectively for F and P beams), where the distortional behavior of the beam failure modes is visible. All 40 beams analyzed exhibit failure modes characterized by inward flange-lip motions.

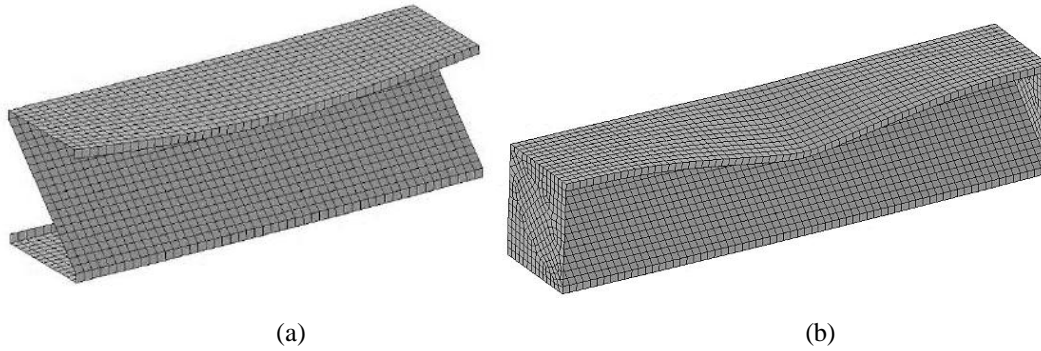


Figure 4.5 – Distortional failure modes of S45-075 (a) F and (b) P beams and (c) the common corresponding mid-span cross-section deformed configuration

The Figure 4.6 illustrates the non-linear and elastic plastic equilibrium paths M/M_{crD} versus $|\delta|/t$ and the corresponding ultimate moments M_u (represented by white circles) for the F and P beams, with $\lambda_D = 1.0, 1.5$ and 2.0 . Figure 4.7 displays the ratios M_u/M_{crD} versus λ_D for F and P beams based on the ultimate moments pointed on Figure 4.6. Appendix A and B show the results obtained for all PLC, SLC, S45 and S90 beams concerning (i) the distortional slenderness λ_D , (ii) the respective yielding stress f_y , (iii) the $(|\delta|/t)_{lim}$ value obtained through ANSYS analyzes, (iv) the yielding bending moment M_y , (v) the ultimate bending moment M_u , (vi) the ultimate bending moment obtained through DSM predictions M_{nD} and (vii) the bending moment ratios M_u/M_y , M_{nD}/M_u and M_u/M_{crD} . Through the results displayed in Figure 4.6, Figure 4.7 and Appendix A-B, it is possible to infer that:

- (i) The ultimate moment M_u and respective $(|\delta|/t)_{lim}$ values increase as the slenderness increases, for all the analyzed beams and for both end support conditions. This behavior is also evidenced by the Figure 4.7: regarding the ones with ratio $M_u/M_{crD} \leq 1$, what means that they fail below the critical bending moment, they present a little elastic-plastic strength reserve and a small ductility preceding the failure. In this range, the curves for F and P beams have almost the same behavior. On the other hand, for ratios $M_u/M_{crD} > 1$ the behavior is completely different: F beams practically collapse right after the onset of yielding, while the P beams present a pronounced elastic-plastic strength reserve, which is attributed to the increase of the stiffness near the beam ends constrained - the same discussion on section 4.2 applies here.

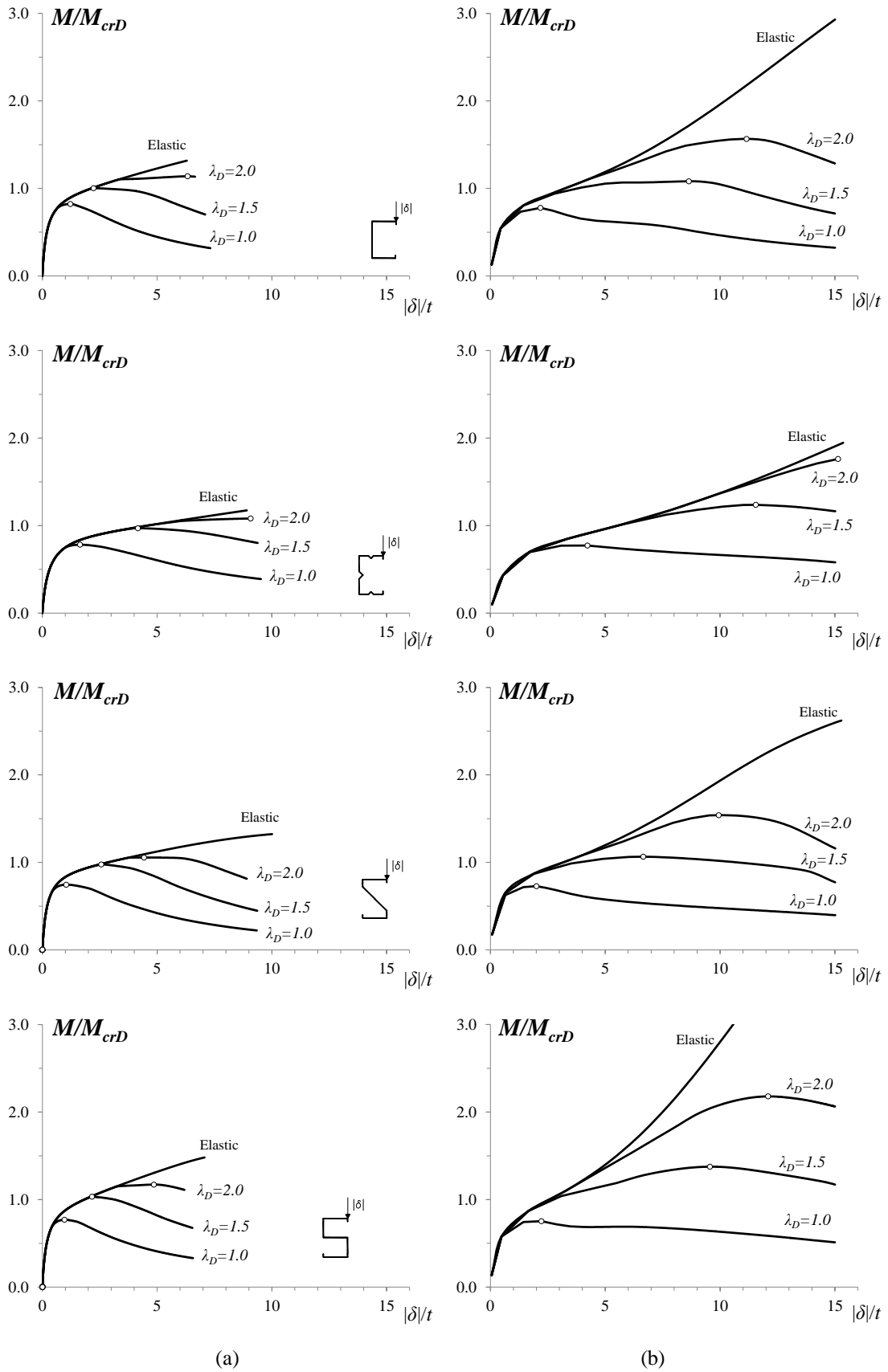


Figure 4.6 - Elastic-plastic equilibrium paths M/M_{crD} vs. $|\delta|/t$ of the (a) F and (b) P 075 beams

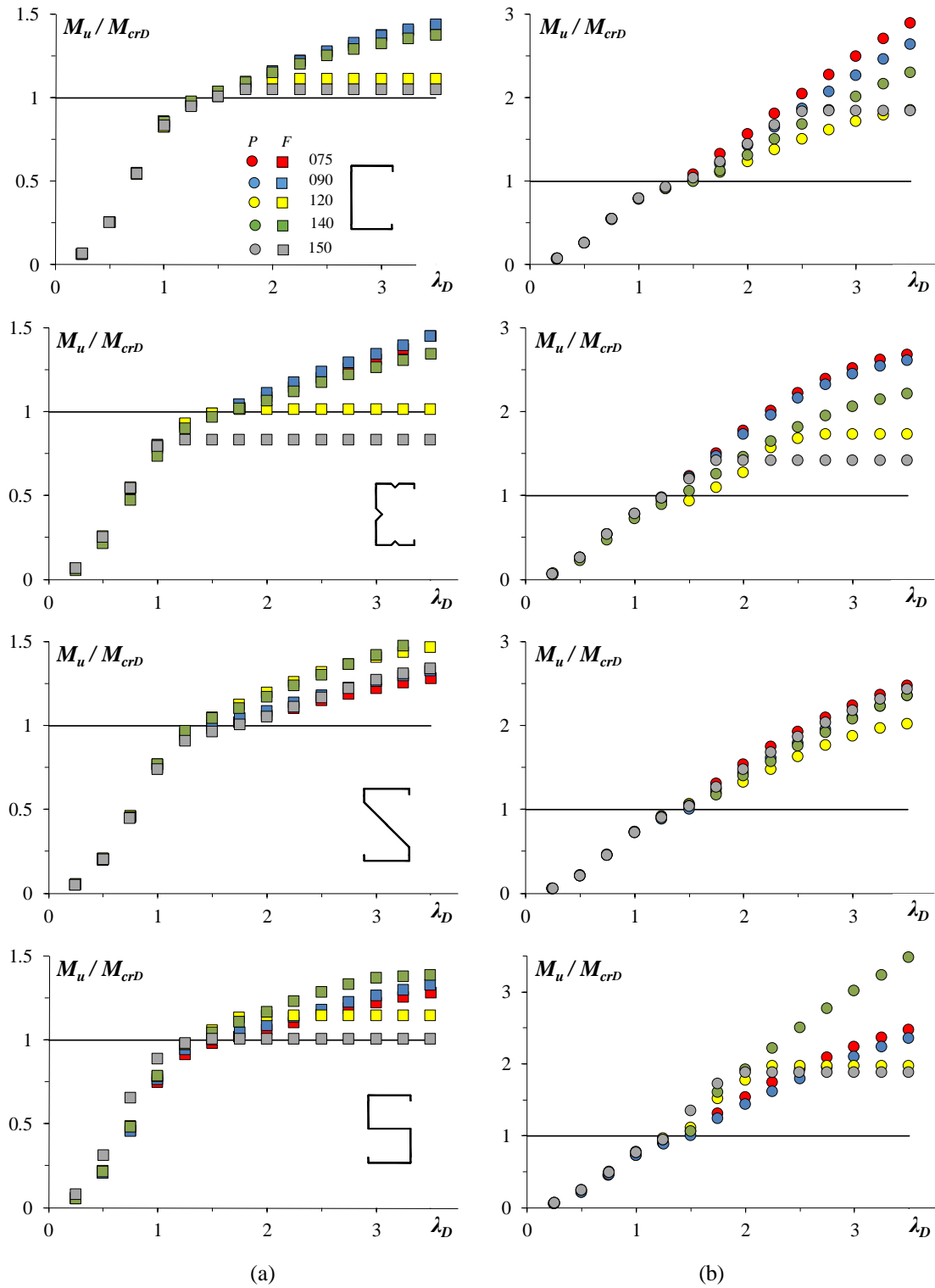


Figure 4.7 - Plots of the (a) F and (c) P beams ultimate bending moment ratios M_u/M_{crD} against the distortional slenderness λ_D

- (ii) It is worth noting that, as observed on section 4.2, the largest post-critical strength reserve is detected on the 075 beams, especially for the P ones, on which the strength increases regularly with the slenderness λ_D . The opposite phenomenon occurs with the 150 beams.

The ultimate bending moment M_u , the ratios M_u/M_y versus λ_D are plotted in Figure 4.8. These plots prompt the following remarks:

- (i) The slenderer beams ($\lambda_D \geq 1.25$) follow the trend of the elastic buckling strength curve (I/λ_D^2), specially the F ones.
- (ii) The P beams present some vertical dispersion in comparison to the curve (I/λ_D^2) – their ratios lie considerably above this curve. This happens because of the distortional post-critical strength reserve, which are pronounced in the P beams as discussed before. Naturally, the 075 P beams are the ones that exhibited the highest dispersion. It is worth noting that the dispersion increases with the slenderness λ_D .

Figure 4.9 illustrates the S45-075 F and P beam with $\lambda_D = 1.0$ (with the corresponding $f_y = 172$ and 242 MPa) elastic and elastic-plastic equilibrium paths and the progression of their deformed configurations and respective von Mises stress (f_{VM}) contours – before, at and beyond the peak load. The sets of diagrams correspond to the equilibrium states marked on the respective equilibrium path. It shall be considered that (i) the deformed configurations are magnified by 3 times scale, and (ii) the point named state II refers to the beam failure. The plots in Figure 4.9 leads to the following observations:

- (i) The yielding initiates at the compressed lip free edge mid-span area – as shown in state I.
- (ii) The occurrence of the collapse for both beams is associated to the complete yielding of the web-flange corner at mid-span, inducing the creation of a “distortional plastic hinge” – depicted in state II, which implies that the plasticity has already propagated over the compressed lip mid-span zone.
- (iii) The compressed flange yielding occurs regularly over the descendent branch of the equilibrium path – shown in state III and IV. However, the spread of plasticity rate, after the onset of yielding, is much higher in the F beams than in their P counterparts. Moreover, the stress diagrams IV indicate the occurrence of elastic unloading in the mid-span compressed flange regions of the F (mostly) and P beams.
- (iv) Similar behavior is observed and reported in LANDESMANN & CAMOTIM (2015).

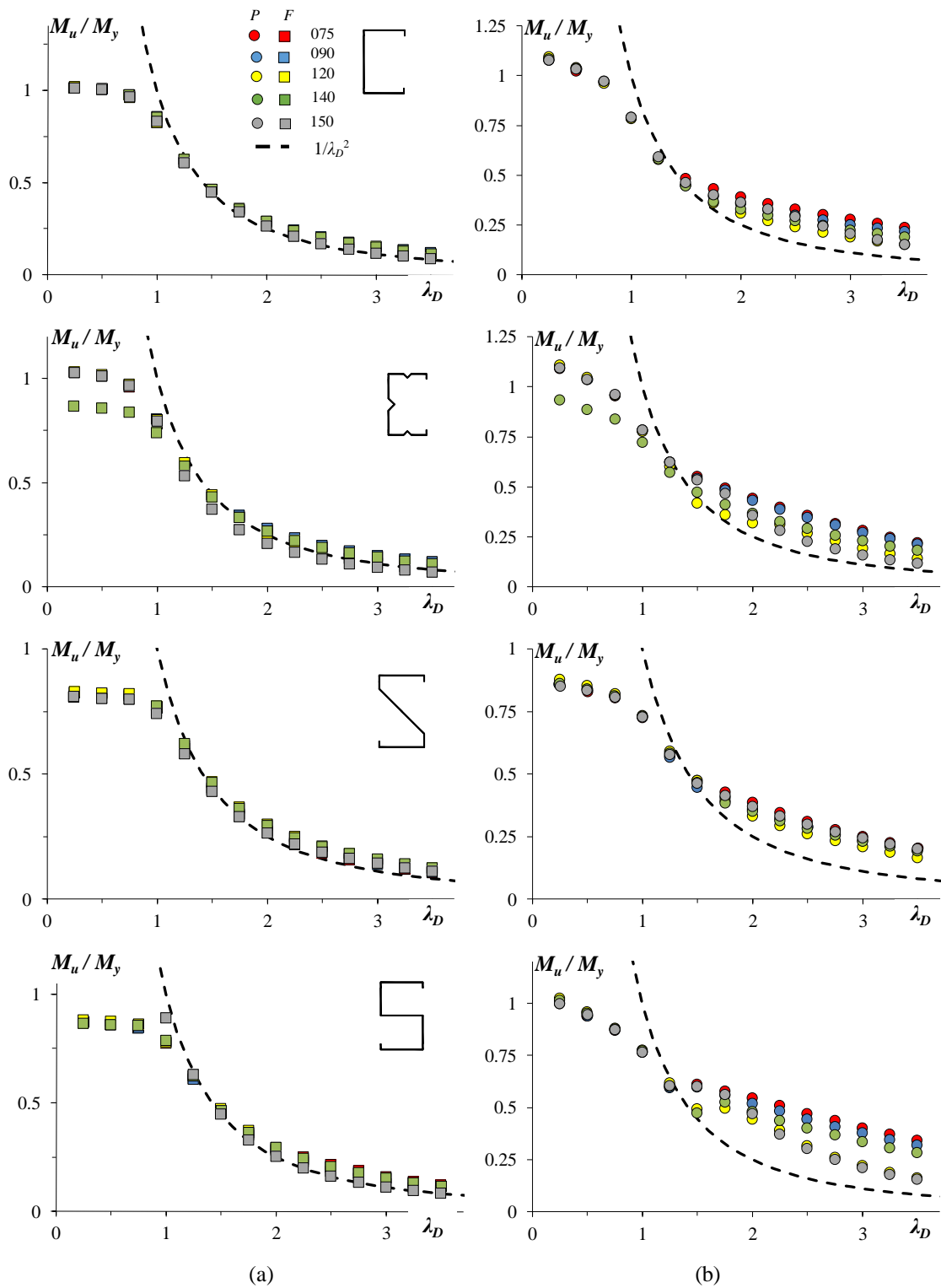


Figure 4.8 - Plots of the (a) F and (c) P beams M_u/M_y against the distortional slenderness λ_D

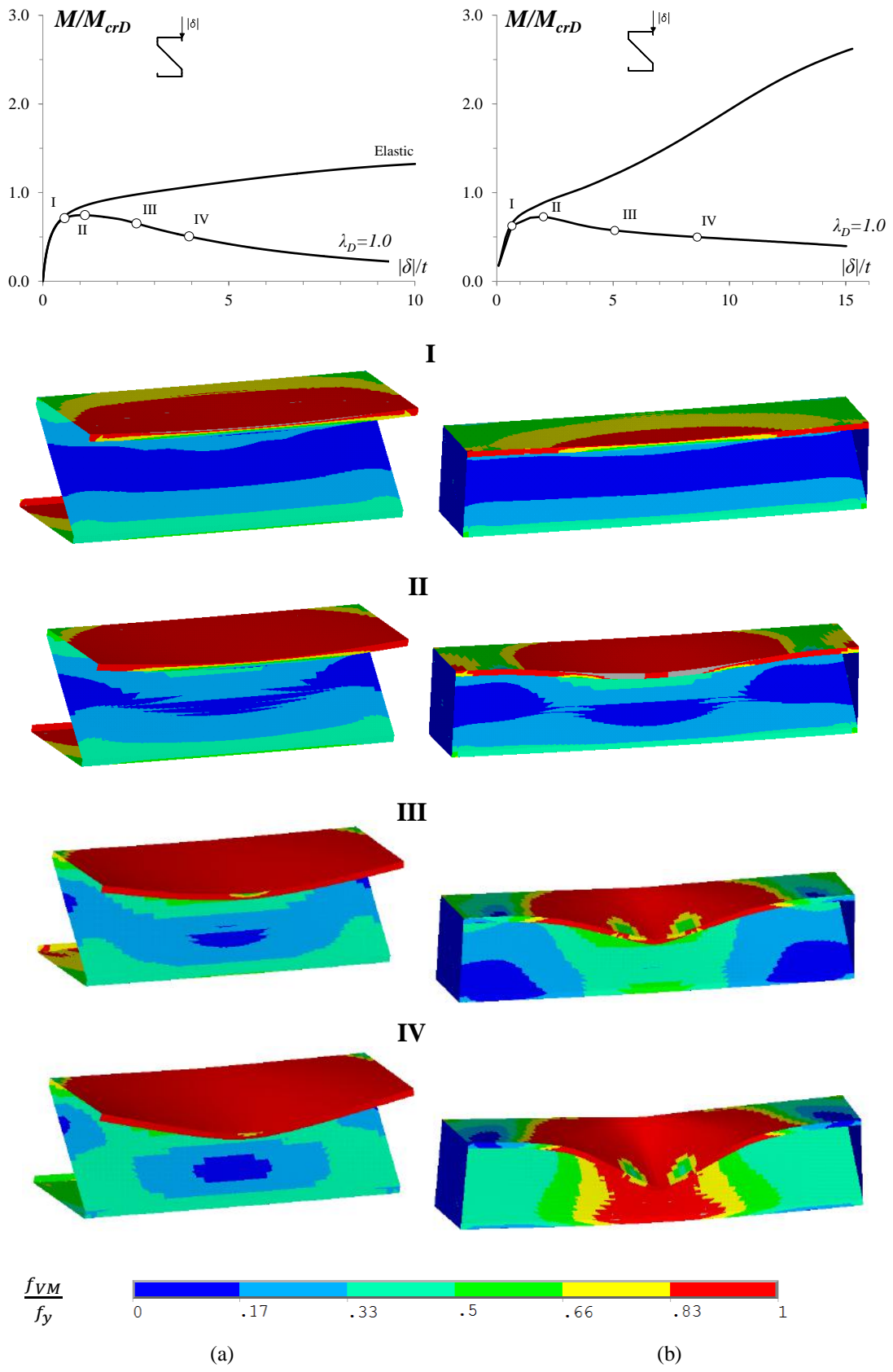


Figure 4.9 - S45-075 (a) F and (b) P beam elastic and elastic-plastic equilibrium paths, deformed configurations (including the collapse mechanisms) and von Mises stress contours ($\lambda_D=1.0$)

4.4 Direct Strength Method

This section is dedicated to discuss the application of DSM predictions in the design of cold formed profiles buckling in distortional mode, specifically beam members. Figure 4.10 illustrates the DSM curve for distortional buckling (see Equation 2.5) and the ratios M_u/M_y (the same exhibited on Figure 4.8) versus the slenderness λ_D , to allow the comparison between the estimates of ultimate bending moment. Figure 4.11 shows the relation between the numerical ultimate bending moments (M_u), obtained through the parametric study discussed on section 4.3, and the nominal ultimate bending moment (M_{nD}), provided by the DSM curve for distortional buckling – which enable the assessment of the accuracy and safety of the DSM predictions for the analyzed beams. Table 4.1 exhibits the averages, standard deviations and maximum/minimum values of M_{nD}/M_u , which were calculated to guide the assessment. The observation of the results presented in Figure 4.10, Figure 4.11 and Table 4.1 make possible to conclude that:

- (i) The behavior of the beams can be clearly distinguished in low-to-moderate slenderness (*i.e.*; $\lambda_D < 1.25$) and moderate-to-high slenderness (*i.e.*; $\lambda_D \geq 1.25$) and there is a significant difference in the behavior of F and P beams, as suggested on section 4.2;
- (ii) In the low-to-moderate slenderness region, the numerical results for the PLC and SLC F beams are well aligned with the DSM estimations. However, for S45 and S90 F beams, in the same region, the DSM overestimates the ultimate bending moments considerably. While for the P beams, in the same region, the DSM curve underestimates the ultimate bending for the PLC and SLC and overestimates for the “S” type beams.
- (iii) In the moderate-to-high slenderness region, the PLC, SLC, S45 and S90 F beams practically follow the trend of the elastic buckling strength curve ($1/\lambda_D^2$), thus, the DSM is clearly overestimating these ultimate moments. For the PLC, SLC and S45 P beams, in the same region, there is an overestimation, while for the S90 P beams there is mostly underestimation, by the DSM curve.

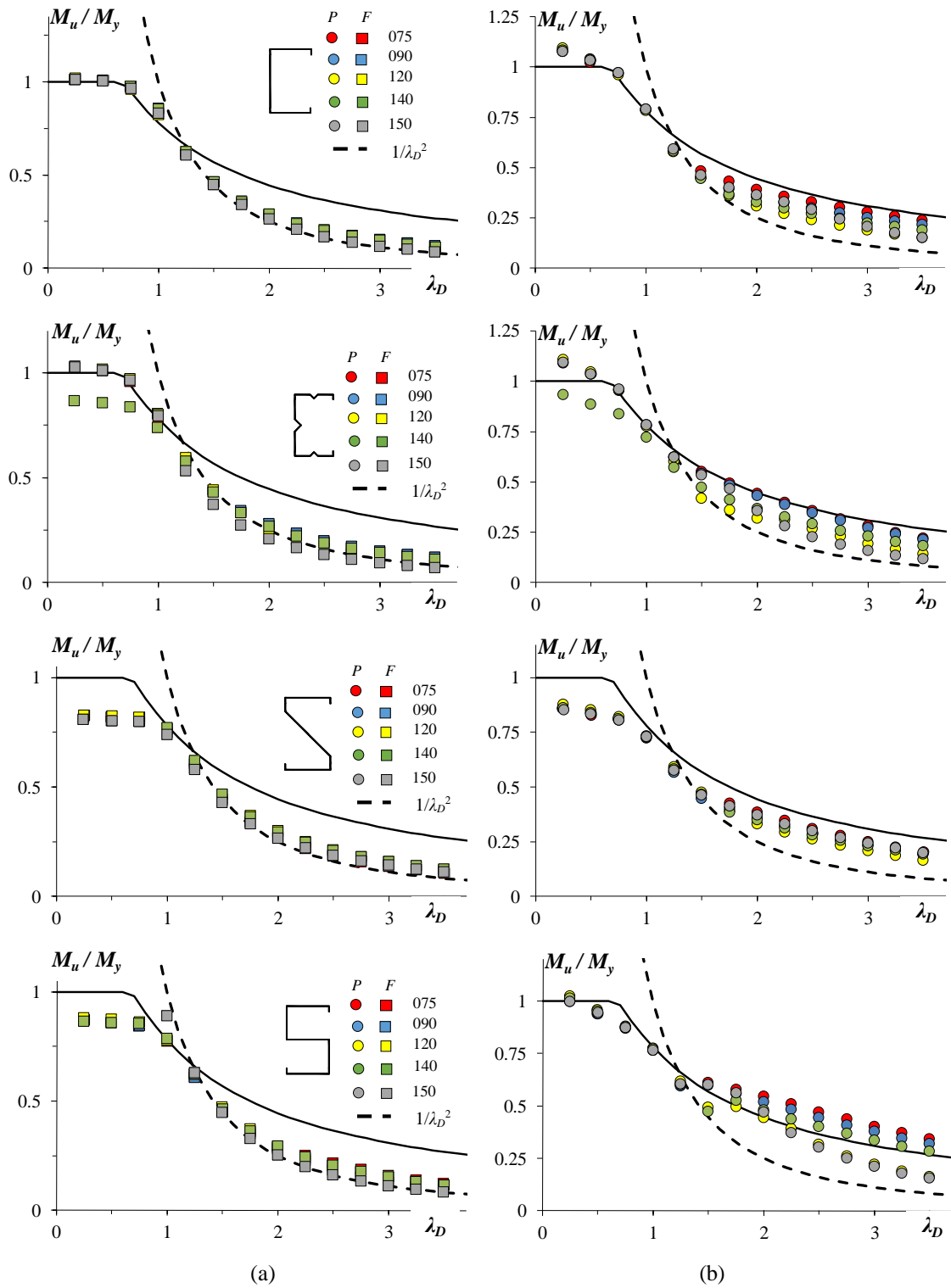


Figure 4.10 - Comparison between the numerical and experimental M_u/M_{nD} values and their DSM estimates for the (a) F and (b) P beams

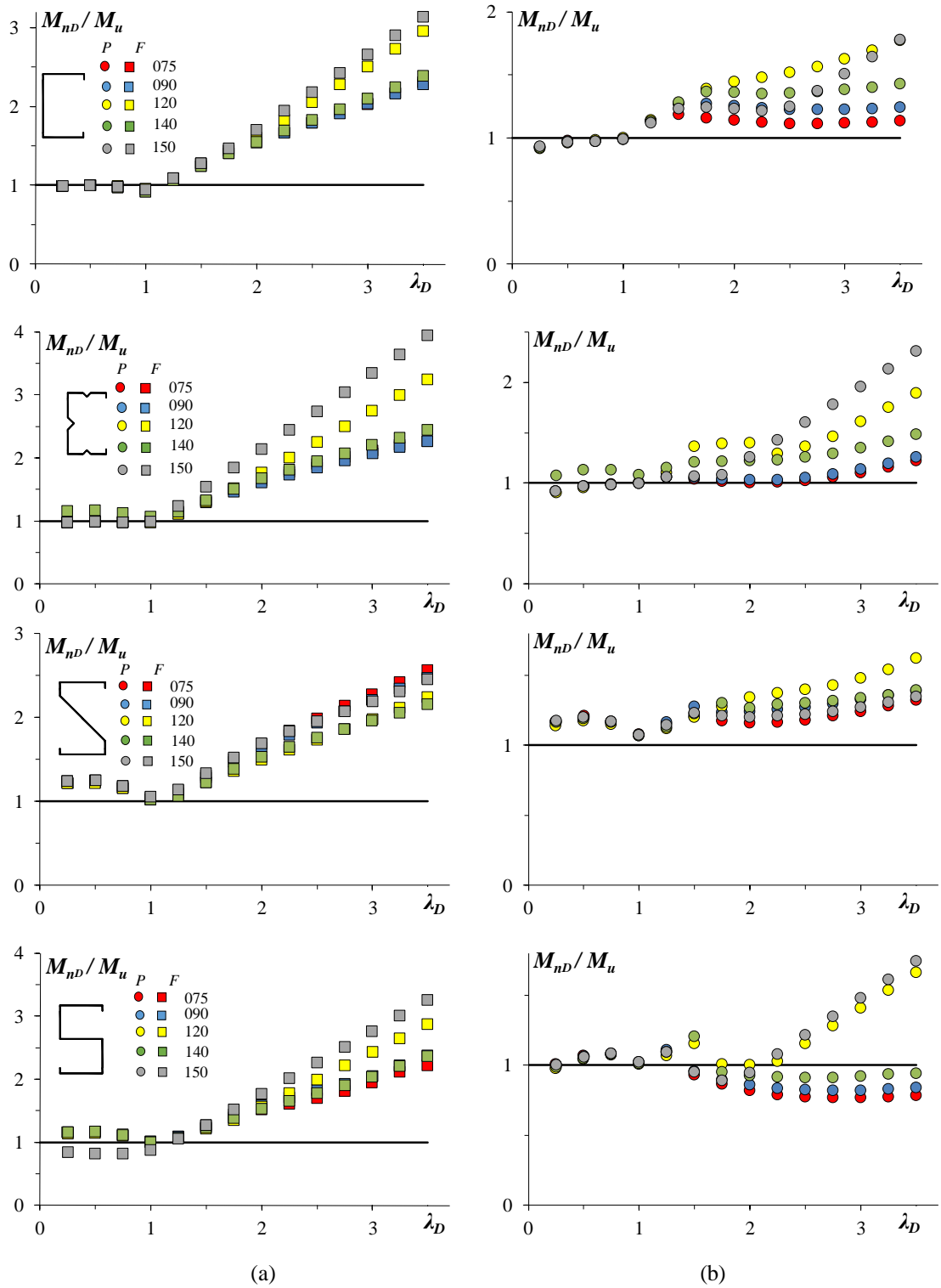


Figure 4.11 – M_{nD}/M_u plots for the (a) F and (b) P beams

Table 4.1 - Statistical parameters for the ratios M_{nD}/M_u sample

Slenderness	Statistical Parameters	PLC		SLC		S45		S90	
		F	P	F	P	F	P	F	P
Whole range	Average	1.60	1.21	1.73	1.21	1.60	1.24	1.61	1.03
	Standard Deviation	0.60	0.22	0.72	0.29	0.45	0.11	0.58	0.21
	Maximum	3.14	1.78	3.94	2.31	2.56	1.62	3.26	1.74
	Minimum	0.91	0.91	0.97	0.90	1.01	1.07	0.81	0.77
Low-to-moderate	Average	0.99	1.00	1.04	1.01	1.15	1.15	1.05	1.05
	Standard Deviation	0.05	0.07	0.08	0.07	0.08	0.04	0.11	0.04
	Maximum	1.09	1.14	1.24	1.15	1.25	1.21	1.17	1.11
	Minimum	0.91	0.91	0.97	0.90	1.01	1.07	0.81	0.98
Moderate-to-high	Average	1.93	1.33	2.12	1.32	1.85	1.29	1.92	1.02
	Standard Deviation	0.49	0.18	0.63	0.31	0.37	0.10	0.50	0.26
	Maximum	3.14	1.78	3.94	2.31	2.56	1.62	3.26	1.74
	Minimum	1.24	1.11	1.29	1.01	1.22	1.16	1.21	0.77

- (iv) An overall view of the DSM curve for distortional buckling predictions is that they are safe and accurate for PLC and SLC in the region of low-to-moderate slenderness for both end support conditions. However, the nominal DSM ultimate bending moments results are extremely unsafe for almost all the analyzed beams in the region of moderate-to-high slenderness, except the S90 P ones – due their higher post-buckling strength.
- (v) The observation of the statistical parameters enhances the DSM curve behavior above mentioned. The average values for PLC, SLC, S45 and S90 beams ratios M_{nD}/M_u are substantially lower for the low-to-moderate slenderness range and higher for the moderate-to-high than the same values considering the whole range, indicating that the DSM predictions best fit occurs in the low-to-moderate slenderness range for both end support conditions. Besides, the average and standard deviation for the F beams are also higher than the P ones, confirming that the DSM predictions are less accurate for the former end support condition.
- (vi) The results obtained in this study evidence that the DSM distortional curve predictions for ultimate bending moments lead to an overestimation of the analyzed beam types strength, especially in the moderate-to-high slenderness region.

5 Concluding Remarks

LANDESMANN & CAMOTIM (2015) addressed a SFE investigation concerning cold formed steel PLC beams and they found that the cross-section dimensions and end support conditions had a significant influence on the post-buckling behavior and ultimate bending moments of these beams. They also revealed that DSM distortional strength curve applied to beams provided unsafe nominal ultimate bending moments in the moderate-to-high slenderness range (*i.e.*; $\lambda_D \geq 1.25$) in comparison with the numerical results obtained. These findings motivated the development of this work, that aimed to extend their investigation and apply it to other section types like SLC, S45 and S90 – specially the last two, that were not considered in the DSM validation studies.

Thus, the investigation reported in this work involved cold formed steel beams (i) concerning 4 different cross-sections types (namely, PLC, SLC, S45 and S90), (ii) submitted to bending moments acting around the middle horizontal center axis of their ends cross-sections, (iii) comprising 2 simply supported end support conditions – differing only about the warping and minor-axis flexural rotations constraint – and (iv) buckling in “pure” distortional modes. Based on this principle, it was necessary to conduct a geometry selection through GBTUL to find beams with dimensions that would lead to failure in “pure” distortional buckling modes at the same time that would provide different geometrical ratios, enabling to assess the influence of the cross-section geometry in the beams distortional behavior. The selection resulted in an amount of 40 beams and among them were 4 beams previously analyzed by LANDESMANN & CAMOTIM (2015) (namely, PLC-120 and PLC-150 F and P beams), aiming a validation. These beams were submitted to successive SFE analyzes carried out in ANSYS: (i) the first was the linear buckling analysis, in order to validate GBTUL critical moments, (ii) then the geometrically and materially non-linear elastic post-buckling analyzes, intending to seek for the most detrimental strength results among the compressed flange inward or outward motion condition and finally (iii) the elastic-plastic analyzes, focus of this work, that came out with the numerical ultimate bending moments of the selected beams and enabled the proper comparison with the nominal ultimate bending moments, provided by the DSM distortional curve. The numerical results obtained through these analyzes, which comprised equilibrium paths, failure loads and deformed configurations were discussed in this work and led to the following concluding remarks:

- (i) As expected, the cross-section dimensions really influenced the distortional post-buckling response and the ultimate moment of the cold formed PLC, SLC, S45 and S90 simply supported beams. The direct proportion of the ratios b_w/b_l and b_f/b_l and the inverse proportion of the ratio b_w/b_f with greater distortional strength were clearly demonstrated in the elastic and elastic-plastic analyzes results (*i.e.*; equilibrium paths and M_u/M_y versus λ_D plots).
- (ii) The end support conditions were determinant in the beams post-buckling behavior. While the F beams practically followed the trend of the elastic buckling strength curve ($1/\lambda_D^2$) in the M_u/M_y versus λ_D plots, the P beams presented a significant vertical dispersion. This dispersion is attributed to the pronounced elastic-plastic strength reserve caused by its end cross-sections constraints, clearly shown in the elastic and elastic-plastic equilibrium paths. As the strength reserve increases with the distortional slenderness λ_D , the dispersion also increases.
- (iii) Concerning the DSM distortional strength curve, it was verified a good agreement between its results and the PLC and SLC beams numerical ultimate bending moments in the low-to-moderate slenderness range. This was expected due to the fact that these section types are part of the data basis from where the DSM was created.
- (iv) However, in the moderate-to-high slenderness range, DSM distortional strength curve offered mostly unsafe predictions. The majority of the analyzed beams in this range had their ultimate bending moments overestimated, even the PLC and SLC beams, for both end support conditions (worst for F beams). This behavior was expected and it was observed even in beams that were part of the DSM curve data basis – *i.e.*; YU & SCHAFER (2005, 2006) results.
- (v) The DSM predictions for the “S” type beams were inaccurate in the whole range of distortional slenderness. These cold formed section types are not mentioned in the AISI (2012) specifications and they are not part of the DSM sections data basis. Thus, it would be necessary to conduct a larger investigation on the behavior of the ultimate bending moments for the “S” type beams to proceed a calibration in the DSM distortional strength curve so that it could be applicable to them.

The conclusions obtained in this work are basically aligned with the ones found in LANDESMANN & CAMOTIM (2015), with the addition of the SLC, S45 and S90 post-buckling distortional responses, which reinforced the need of recalibrating the DSM distortional strength curve for the moderate-to-high slenderness range. And this work is also responsible for bringing up the need of adjust the same distortional curve to comprise the “S” type beams post-buckling responses.

5.1 Suggestions for future works

The issues raised in this work are relevant and contributed to the objective of providing more accurate ultimate bending moment predictions for CFS beams failing in distortional modes, despite its limited scope. Thus, new numerical investigations and/or experimental tests with larger samples of the analyzed sections types would certainly contribute to the validation of what was reported here. Therefore, it would be interesting adding to the scope beams with different cross-section dimensions – exploring the influence of the geometrical ratios b_w/b_l , b_{fl}/b_l and b_w/b_f – and different end support and load conditions than the ones which were described in this work.

In the special case of the “S” type beams, it would be not only interesting as necessary to extend the investigation to a larger data basis in order to contribute to the DSM distortional strength curve as a design tool for this type of CFS.

6 Bibliography

ABNT, 2010. *Brazilian Standard on Design of Cold-Formed Steel Structures* (NBR 14762:2010), Brazilian Standards Association, Rio de Janeiro, RJ. (Portuguese)

AISI, 2012. *North American Specification for the Design of Cold-Formed Steel Structural Members* (NAS), American Iron and Steel Institute, Washington DC.

ANSYS, 2009. Reference Manual, *Swanson Analysis Systems (SAS)*, version 12.0.1

BATISTA, E. M., 2010. “Effective section method: A general direct method for the design of steel cold-formed members under local–global buckling interaction”, *Thin-Walled Structures*, v.48, pp.345-356.

BAZANT, Z. P., CEDOLIN, L., 2010. *Stability of Structures - Elastic, Inelastic, Fracture and Damage Theories*, World Scientific Publishing Co. Pte. Ltd., Singapore.

BEBIANO, R., PINA, P., SILVESTRE, N., CAMOTIM, D., 2010a. *GBTUL 1.0 β – Buckling and Vibration Analysis of Thin-Walled Members – GBT Theoretical Background*, DECivil/IST, Technical University of Lisbon. (<http://www.civil.ist.utl.pt/gbt>)

BEBIANO, R., PINA, P., SILVESTRE, N., CAMOTIM, D., 2010b. *GBTUL 1.0 β – Buckling and Vibration Analysis of Thin-Walled Members - User Manual*, DECivil/IST, Technical University of Lisbon. (<http://www.civil.ist.utl.pt/gbt>)

CHEN, W. F., LUI, E. M., 1987. *Structural Stability – Theory and Implementation*, Elsevier, New York.

CHODRAUI, G. M. B., *Flambagem por distorção da seção transversal em perfis de aço formado a frio submetidos à compressão centrada e à flexão*. Dissertação de M.Sc., USP, São Carlos, SP, Brasil, 2003.

CHODRAUI, G. M. B., NETO, J. M., GONÇALVES, R. M., MALITE, M., 2006. “Distortional Buckling of Cold-Formed Steel Members”. *Journal of Structural Engineering*, v.132(4), pp. 636-639.

GALAMBOS, T. V., SUROVEK, A. E., 2008. *Structural Stability of Steel: Concepts and Applications for Structural Engineers*, John Wiley & Sons, New York.

GARCIA, R. A. S., *Behaviour and DSM design of cold-formed steel web/flange stiffened lipped channel columns experiencing distortional failure*. Dissertação de M.Sc., COPPE/UFRJ, Rio de Janeiro, RJ, Brasil, 2015.

HANCOCK, G.J., KWON, Y.B., BERNARD, E.S., 1994. “Strength design curves for thin-walled sections undergoing distortional buckling”, *Journal of Constructional Steel Research*, v.31, pp. 169-186.

HANCOCK, G.J., ROGERS, C. A., SCHUSTER, R. M., 1996. “Comparison of the Distortional Buckling Method for Flexural Members with Tests”, *Thirteenth International Specialty Conference on Cold-Formed Steel Structures*. St. Louis, Missouri, October 17-18.

LANDESMANN, A., CAMOTIM, D., 2015. “Distortional failure and DSM design of cold-formed steel lipped channel beams under elevated temperatures”, *Thin-Walled Structures*, v.98, pp.75-93.

MADULIAT, S., BAMBACH, M. R., ZHAO, X. L., 2011. “Inelastic behavior and design of cold-formed channel sections in bending”, *Thin-Walled Structures*, v.51, pp.158-166.

MARTINS, A. D., LANDESMANN, A., CAMOTIM, D., DINIS, P. B., 2016. “Distortional Failure of Cold-Formed Steel Beams under Uniform Bending: Behavior, Strength and DSM Design”, *Proceedings of the Annual Stability Conference Structural Stability Research Council*. Orlando, Florida, April 12-15.

METALSHOP – Sistemas de armazenagem e sistemas construtivos. <http://www.metalshop.com.br/>. Accessed on December 31, 2015.

PROLA, L. C., CAMOTIM, D., 2002. “On the distortional post-buckling behavior of cold-formed lipped channel steel beams”, *Advances in Steel Structures*, v.1, pp. 331-339.

ROGERS, C.A., SCHUSTER, R.M., 1997. “Flange/Web Distortional Buckling of Cold-Formed Steel Sections in Bending”, *Thin-Walled Structures*, v.27(1), pp. 13-29.

SCHAFFER, B.W., *Cold-Formed Steel Behavior and Design: Analytical and Numerical Modeling of Elements and Members with Longitudinal Stiffeners*. Ph.D. Dissertation, Cornell University, Ithaca, USA, 1997.

SCHAFFER, B.W., 2006. “Review: The Direct Strength Method of cold-formed steel member design”. *International Colloquium on Stability and Ductility of Steel Structures*. Lisbon, Portugal.

SCHAFFER, B.W., PEKÖZ, T., 1998. “Direct strength prediction of cold-formed steel members using numerical elastic buckling solutions”, *Fourteenth International Specialty Conference on Cold-Formed Steel Structures*. St. Louis, Missouri, October 15-16.

SIMITSES, G.J., HODGES, D. H., 2006. *Fundamentals of Structural Stability*, Elsevier/ Butterworth-Heinemann, Burlington/Oxford.

YU, C., SCHAFFER, B.W., 2005. *Distortional Buckling of Cold-formed Steel Members in Bending*. The American Iron and Steel Institute (AISI) Final report, January 2005. http://www.ce.jhu.edu/bschafer/dist_beams/AISI%20DB%20Report.pdf. Accessed on December 23, 2015.

YU, C., SCHAFFER, B.W., 2006. “Distortional Buckling of Cold-Formed Steel Members”. *Journal of Structural Engineering*, v.132(4), pp. 515-528.

YU, W., LABOUBE, R. A., 2010. *Cold-formed steel design*, 4th Edition, John Wiley & Sons, New York.

APPENDIX A

Data concerning F beams

Tables A1 to A8 show the results obtained for all PLC, SLC, S45 and S90 F beams concerning (i) the distortional slenderness λ_D , (ii) the respective yielding stress f_y , (iii) the $(|\delta|/t)_{lim}$ value obtained through ANSYS analyzes, (iv) the yielding bending moment M_y , (v) the ultimate bending moment M_u , (vi) the ultimate bending moment obtained through DSM predictions M_{nD} and (vii) the bending moment ratios M_u/M_y , M_{nD}/M_u and M_u/M_{crD} .

Table A1. Numerical ultimate loads and DSM data/estimates concerning the PLC-075/090/120 F beams analyzed

PLC	λ_D	f_y (MPa)	$(\delta /t)_{lim}$	M_y (kN cm)	M_u (kN cm)	M_{nD} (kN cm)	$\frac{M_u}{M_y}$	$\frac{M_{nD}}{M_u}$	$\frac{M_u}{M_{crD}}$
075	0.25	15	0.20	18.42	18.69	18.42	1.01	0.99	0.06
	0.50	61	0.31	74.92	75.17	74.92	1.00	1.00	0.25
	0.75	138	0.79	169.49	163.67	159.77	0.97	0.98	0.54
	1.00	246	1.27	302.14	248.75	235.56	0.82	0.95	0.82
	1.25	384	2.23	471.63	286.75	310.87	0.61	1.08	0.95
	1.50	553	3.97	679.19	302.88	386.33	0.45	1.28	1.00
	1.75	752	5.25	923.61	320.34	461.54	0.35	1.44	1.06
	2.00	983	6.59	1207.32	343.89	537.21	0.28	1.56	1.14
	2.25	1244	7.71	1527.88	368.47	612.62	0.24	1.66	1.22
	2.50	1536	7.89	1886.51	383.73	688.12	0.20	1.79	1.27
	2.75	1858	7.78	2281.99	395.27	763.44	0.17	1.93	1.31
	3.00	2211	9.67	2715.55	414.13	838.85	0.15	2.03	1.37
	3.25	2595	10.15	3187.17	421.69	914.31	0.13	2.17	1.40
	3.50	3010	11.08	3696.88	429.09	989.82	0.12	2.31	1.42
090	0.25	11	0.14	17.01	17.22	17.01	1.01	0.99	0.06
	0.50	46	0.19	71.12	71.53	71.12	1.01	0.99	0.25
	0.75	103	0.83	159.24	155.31	150.06	0.98	0.97	0.55
	1.00	183	1.95	282.92	242.09	220.76	0.86	0.91	0.85
	1.25	286	3.09	442.16	275.15	291.57	0.62	1.06	0.97
	1.50	412	4.12	636.96	292.97	362.43	0.46	1.24	1.03
	1.75	561	5.37	867.32	309.59	433.31	0.36	1.40	1.09
	2.00	733	6.95	1133.23	327.67	504.22	0.29	1.54	1.16
	2.25	927	8.17	1433.16	344.66	574.79	0.24	1.67	1.22
	2.50	1145	9.38	1770.19	361.12	645.75	0.20	1.79	1.28
	2.75	1385	11.52	2141.23	375.35	716.43	0.18	1.91	1.33
	3.00	1649	11.58	2549.38	387.59	787.42	0.15	2.03	1.37
	3.25	1935	13.65	2991.54	398.09	858.16	0.13	2.16	1.41
	3.50	2244	13.13	3469.26	407.15	928.93	0.12	2.28	1.44
120	0.25	30	0.23	111.72	113.85	111.72	1.02	0.98	0.06
	0.50	121	0.32	450.60	453.64	450.60	1.01	0.99	0.25
	0.75	272	0.93	1012.91	971.90	954.01	0.96	0.98	0.54
	1.00	483	1.64	1798.67	1477.65	1402.84	0.82	0.95	0.82
	1.25	755	3.12	2811.58	1710.70	1852.92	0.61	1.08	0.95
	1.50	1086	4.03	4044.21	1819.80	2301.14	0.45	1.26	1.01
	1.75	1479	5.17	5507.72	1914.70	2751.49	0.35	1.44	1.06
	2.00	1932	5.77	7194.67	1997.60	3201.30	0.28	1.60	1.11
	2.25	2445	4.82	9105.06	1997.60	3650.76	0.22	1.83	1.11
	2.50	3018	4.82	11238.89	1997.60	4099.98	0.18	2.05	1.11
	2.75	3652	4.82	13599.87	1997.60	4549.68	0.15	2.28	1.11
	3.00	4346	4.82	16184.29	1997.60	4999.14	0.12	2.50	1.11
	3.25	5101	4.82	18995.88	1997.60	5448.98	0.11	2.73	1.11
	3.50	5915	4.82	22027.17	1997.60	5898.06	0.09	2.95	1.11

Table A2. Numerical ultimate loads and DSM data/estimates concerning the PLC-140/150 F beams analyzed

PLC	λ_D	f_y (MPa)	$(\delta /t)_{lim}$	M_y (kN cm)	M_u (kN cm)	M_{nD} (kN cm)	$\frac{M_u}{M_y}$	$\frac{M_{nD}}{M_u}$	$\frac{M_u}{M_{crD}}$
140	0.25	13	0.07	60.05	60.77	60.05	1.01	0.99	0.06
	0.50	54	0.20	249.45	250.52	249.45	1.00	1.00	0.25
	0.75	121	0.75	558.95	544.30	527.15	0.97	0.97	0.55
	1.00	216	2.06	997.80	851.60	778.03	0.85	0.91	0.85
	1.25	337	3.58	1556.76	971.30	1026.44	0.62	1.06	0.97
	1.50	486	5.48	2245.06	1033.00	1276.70	0.46	1.24	1.04
	1.75	661	5.54	3053.46	1087.60	1525.37	0.36	1.40	1.09
	2.00	863	7.71	3986.59	1145.45	1774.21	0.29	1.55	1.15
	2.25	1092	8.87	5044.45	1197.35	2023.16	0.24	1.69	1.20
	2.50	1349	9.75	6231.65	1245.15	2273.11	0.20	1.83	1.25
	2.75	1632	11.08	7538.95	1285.60	2522.11	0.17	1.96	1.29
	3.00	1942	11.66	8970.98	1319.75	2771.17	0.15	2.10	1.32
	3.25	2279	13.25	10527.74	1347.60	3020.27	0.13	2.24	1.35
3.50	2644	14.43	12213.84	1368.15	3270.06	0.11	2.39	1.37	
150	0.25	15	0.08	121.08	122.60	121.08	1.01	0.99	0.06
	0.50	59	0.26	476.24	478.46	476.24	1.00	1.00	0.25
	0.75	133	0.47	1073.56	1034.95	1011.98	0.96	0.98	0.54
	1.00	237	1.38	1913.03	1591.15	1491.71	0.83	0.94	0.83
	1.25	370	2.28	2986.59	1806.80	1968.76	0.60	1.09	0.95
	1.50	533	3.39	4302.31	1919.45	2447.16	0.45	1.27	1.00
	1.75	725	3.28	5852.10	1997.60	2924.01	0.34	1.46	1.05
	2.00	947	2.89	7644.06	1997.60	3401.92	0.26	1.70	1.05
	2.25	1199	2.89	9678.17	1997.60	3880.54	0.21	1.94	1.05
	2.50	1480	2.89	11946.36	1997.60	4358.04	0.17	2.18	1.05
	2.75	1791	2.89	14456.71	1997.60	4836.19	0.14	2.42	1.05
	3.00	2131	2.89	17201.15	1997.60	5313.48	0.12	2.66	1.05
	3.25	2501	2.89	20187.74	1997.60	5791.36	0.10	2.90	1.05
3.50	2901	2.89	23416.49	1997.60	6269.69	0.09	3.14	1.05	

Table A3. Numerical ultimate loads and DSM data/estimates concerning the SLC-075/090/120 F beams analyzed

SLC	λ_D	f_y (MPa)	$(\delta /t)_{lim}$	M_y (kN cm)	M_u (kN cm)	M_{nD} (kN cm)	$\frac{M_u}{M_y}$	$\frac{M_{nD}}{M_u}$	$\frac{M_u}{M_{crD}}$
075	0.25	19	0.00	24.03	24.75	24.03	1.03	0.97	0.06
	0.50	76	0.31	96.11	97.00	96.11	1.01	0.99	0.25
	0.75	172	1.06	217.50	208.15	204.89	0.96	0.98	0.54
	1.00	306	2.30	386.95	302.26	301.65	0.78	1.00	0.78
	1.25	477	3.45	603.19	351.50	397.75	0.58	1.13	0.91
	1.50	687	4.77	868.75	374.83	494.35	0.43	1.32	0.97
	1.75	936	6.99	1183.63	395.59	591.23	0.33	1.49	1.02
	2.00	1222	9.76	1545.29	419.09	687.67	0.27	1.64	1.08
	2.25	1547	12.08	1956.27	442.50	784.37	0.23	1.77	1.15
	2.50	1909	15.43	2414.04	464.60	880.74	0.19	1.90	1.20
	2.75	2310	15.90	2921.13	485.59	977.34	0.17	2.01	1.26
	3.00	2750	17.91	3477.54	507.05	1074.11	0.15	2.12	1.31
	3.25	3227	20.15	4080.73	530.90	1170.62	0.13	2.20	1.37
3.50	3743	21.41	4733.24	559.70	1267.28	0.12	2.26	1.45	
090	0.25	14	0.02	22.31	22.91	22.31	1.03	0.97	0.06
	0.50	56	0.27	89.23	90.23	89.23	1.01	0.99	0.25
	0.75	127	1.22	202.36	196.08	190.58	0.97	0.97	0.55
	1.00	225	2.49	358.51	288.16	279.82	0.80	0.97	0.80
	1.25	352	4.86	560.87	333.09	369.81	0.59	1.11	0.93
	1.50	507	7.86	807.85	355.60	459.64	0.44	1.29	0.99
	1.75	690	10.56	1099.44	375.60	549.38	0.34	1.46	1.05
	2.00	902	13.10	1437.23	399.48	639.46	0.28	1.60	1.11
	2.25	1141	15.61	1818.05	422.60	729.06	0.23	1.73	1.18
	2.50	1409	19.37	2245.08	444.13	818.96	0.20	1.84	1.24
	2.75	1705	21.19	2716.72	464.10	908.79	0.17	1.96	1.29
	3.00	2029	23.86	3232.98	482.61	998.57	0.15	2.07	1.34
	3.25	2381	25.41	3793.85	501.35	1088.30	0.13	2.17	1.40
3.50	2761	27.78	4399.34	521.50	1178.00	0.12	2.26	1.45	
120	0.25	32	0.00	123.47	127.34	123.47	1.03	0.97	0.06
	0.50	128	0.26	493.90	502.10	493.90	1.02	0.98	0.25
	0.75	288	0.98	1111.27	1079.50	1046.60	0.97	0.97	0.55
	1.00	511	2.09	1971.73	1578.65	1538.19	0.80	0.97	0.80
	1.25	799	4.05	3082.99	1830.65	2032.10	0.59	1.11	0.93
	1.50	1150	5.81	4437.35	1949.25	2524.59	0.44	1.30	0.99
	1.75	1566	5.02	6042.51	1997.60	3018.48	0.33	1.51	1.01
	2.00	2045	4.98	7890.76	1997.60	3511.32	0.25	1.76	1.01
	2.25	2588	4.98	9985.96	1997.60	4004.30	0.20	2.00	1.01
	2.50	3195	4.98	12328.11	1997.60	4497.40	0.16	2.25	1.01
	2.75	3866	4.98	14917.21	1997.60	4990.57	0.13	2.50	1.01
	3.00	4601	4.98	17753.26	1997.60	5483.80	0.11	2.75	1.01
	3.25	5400	4.98	20836.25	1997.60	5977.08	0.10	2.99	1.01
3.50	6263	4.98	24166.19	1997.60	6470.39	0.08	3.24	1.01	

Table A4. Numerical ultimate loads and DSM data/estimates concerning the SLC-140/150 F beams analyzed

SLC	λ_D	f_y (MPa)	$(\delta /t)_{lim}$	M_y (kN cm)	M_u (kN cm)	M_{nD} (kN cm)	$\frac{M_u}{M_y}$	$\frac{M_{nD}}{M_u}$	$\frac{M_u}{M_{crD}}$
140	0.25	13	0.02	73.46	63.72	73.46	0.87	1.15	0.05
	0.50	53	0.20	299.48	256.92	299.48	0.86	1.17	0.22
	0.75	119	0.78	672.41	563.05	633.35	0.84	1.12	0.47
	1.00	211	2.36	1192.26	878.70	930.46	0.74	1.06	0.74
	1.25	330	3.67	1864.67	1076.10	1229.46	0.58	1.14	0.90
	1.50	475	6.18	2684.00	1154.65	1527.51	0.43	1.32	0.97
	1.75	647	8.12	3655.89	1213.70	1826.64	0.33	1.51	1.02
	2.00	845	11.77	4774.69	1272.70	2125.03	0.27	1.67	1.07
	2.25	1070	14.71	6046.06	1338.35	2424.18	0.22	1.81	1.12
	2.50	1321	16.88	7464.34	1400.65	2722.74	0.19	1.94	1.17
	2.75	1598	20.30	9029.54	1458.10	3020.86	0.16	2.07	1.22
	3.00	1902	22.09	10747.30	1510.20	3319.60	0.14	2.20	1.26
	3.25	2232	24.23	12611.97	1558.60	3617.94	0.12	2.32	1.31
	3.50	2589	25.98	14629.21	1607.00	3916.78	0.11	2.44	1.35
150	0.25	18	0.00	149.91	154.09	149.91	1.03	0.97	0.06
	0.50	72	0.26	599.63	606.75	599.63	1.01	0.99	0.25
	0.75	162	0.94	1349.18	1303.20	1271.33	0.97	0.98	0.54
	1.00	288	2.02	2398.54	1902.90	1871.06	0.79	0.98	0.79
	1.25	450	1.63	3747.72	1997.60	2470.78	0.53	1.24	0.83
	1.50	648	1.63	5396.71	1997.60	3070.50	0.37	1.54	0.83
	1.75	882	1.63	7345.53	1997.60	3670.23	0.27	1.84	0.83
	2.00	1152	1.63	9594.16	1997.60	4269.95	0.21	2.14	0.83
	2.25	1458	1.63	12142.61	1997.60	4869.67	0.16	2.44	0.83
	2.50	1801	1.63	14999.20	1997.60	5471.06	0.13	2.74	0.83
	2.75	2179	1.63	18147.29	1997.60	6070.63	0.11	3.04	0.83
	3.00	2593	1.63	21595.19	1997.60	6670.23	0.09	3.34	0.83
	3.25	3043	1.63	25342.91	1997.60	7269.84	0.08	3.64	0.83
	3.50	3529	1.63	29390.44	1997.60	7869.47	0.07	3.94	0.83

Table A5. Numerical ultimate loads and DSM data/estimates concerning the S45-075/090/120 F beams analyzed

S45	λ_D	f_y (MPa)	$(\delta /t)_{lim}$	M_y (kN cm)	M_u (kN cm)	M_{nD} (kN cm)	$\frac{M_u}{M_y}$	$\frac{M_{nD}}{M_u}$	$\frac{M_u}{M_{crD}}$
075	0.25	11	0.01	14.48	11.95	14.48	0.83	1.21	0.05
	0.50	43	0.07	56.62	46.52	56.62	0.82	1.22	0.21
	0.75	97	0.37	127.72	104.48	120.27	0.82	1.15	0.46
	1.00	172	1.30	226.47	169.40	176.69	0.75	1.04	0.75
	1.25	269	2.14	354.18	206.66	233.46	0.58	1.13	0.91
	1.50	387	3.34	509.55	222.25	289.96	0.44	1.30	0.98
	1.75	527	4.03	693.88	230.85	346.69	0.33	1.50	1.02
	2.00	689	5.88	907.18	240.18	403.57	0.26	1.68	1.06
	2.25	871	5.80	1146.81	249.59	459.95	0.22	1.84	1.10
	2.50	1076	8.06	1416.72	260.10	516.77	0.18	1.99	1.15
	2.75	1302	8.96	1714.29	269.09	573.45	0.16	2.13	1.19
	3.00	1549	9.15	2039.50	277.27	630.00	0.14	2.27	1.22
	3.25	1818	10.37	2393.68	284.59	686.68	0.12	2.41	1.26
	3.50	2109	10.75	2776.83	290.65	743.44	0.10	2.56	1.28
090	0.25	8	0.01	13.19	10.84	13.19	0.82	1.22	0.05
	0.50	32	0.06	52.77	43.07	52.77	0.82	1.23	0.20
	0.75	72	0.28	118.74	96.31	111.85	0.81	1.16	0.46
	1.00	128	1.57	211.09	161.17	164.61	0.76	1.02	0.76
	1.25	200	3.19	329.82	198.69	217.36	0.60	1.09	0.94
	1.50	288	3.88	474.94	210.84	270.12	0.44	1.28	1.00
	1.75	392	5.68	646.45	219.81	322.87	0.34	1.47	1.04
	2.00	512	7.19	844.34	229.35	375.63	0.27	1.64	1.09
	2.25	648	8.57	1068.62	239.46	428.38	0.22	1.79	1.14
	2.50	799	9.25	1317.64	249.18	480.80	0.19	1.93	1.18
	2.75	967	10.76	1594.69	258.27	533.59	0.16	2.07	1.22
	3.00	1151	12.00	1898.12	266.31	586.37	0.14	2.20	1.26
	3.25	1351	12.78	2227.94	273.83	639.14	0.12	2.33	1.30
	3.50	1567	14.82	2584.15	280.27	691.92	0.11	2.47	1.33
120	0.25	21	0.01	81.27	67.27	81.27	0.83	1.21	0.05
	0.50	85	0.08	328.96	270.72	328.96	0.82	1.22	0.21
	0.75	190	0.33	735.32	602.20	693.34	0.82	1.15	0.46
	1.00	339	1.57	1311.96	1006.50	1022.92	0.77	1.02	0.77
	1.25	529	3.19	2047.28	1252.90	1349.66	0.61	1.08	0.96
	1.50	762	4.98	2949.01	1376.25	1677.57	0.47	1.22	1.05
	1.75	1037	6.24	4013.29	1474.20	2005.03	0.37	1.36	1.12
	2.00	1354	7.43	5240.10	1567.10	2332.22	0.30	1.49	1.20
	2.25	1714	8.86	6633.34	1650.35	2660.08	0.25	1.61	1.26
	2.50	2116	10.02	8189.11	1726.10	2987.64	0.21	1.73	1.32
	2.75	2561	11.21	9911.31	1790.40	3315.68	0.18	1.85	1.37
	3.00	3048	11.95	11796.04	1844.10	3643.45	0.16	1.98	1.41
	3.25	3577	13.00	13843.32	1885.95	3970.99	0.14	2.11	1.44
	3.50	4148	13.73	16053.14	1923.15	4298.37	0.12	2.24	1.47

Table A6. Numerical ultimate loads and DSM data/estimates concerning the S45-140/150 F beams analyzed

S45	λ_D	f_y (MPa)	$(\delta /t)_{lim}$	M_y (kN cm)	M_u (kN cm)	M_{nD} (kN cm)	$\frac{M_u}{M_y}$	$\frac{M_{nD}}{M_u}$	$\frac{M_u}{M_{crD}}$
140	0.25	9	0.01	43.72	35.32	43.72	0.81	1.24	0.05
	0.50	37	0.06	179.75	144.18	179.75	0.80	1.25	0.20
	0.75	84	0.25	408.08	326.29	384.50	0.80	1.18	0.45
	1.00	149	1.67	723.86	557.05	565.06	0.77	1.01	0.77
	1.25	233	2.88	1131.94	702.35	746.58	0.62	1.06	0.97
	1.50	336	4.40	1632.32	758.20	928.60	0.46	1.22	1.05
	1.75	457	6.10	2220.15	801.55	1109.50	0.36	1.38	1.10
	2.00	597	7.67	2900.28	848.55	1290.93	0.29	1.52	1.17
	2.25	756	9.04	3672.72	898.10	1472.70	0.24	1.64	1.24
	2.50	933	10.26	4532.61	945.00	1653.74	0.21	1.75	1.30
	2.75	1129	11.31	5484.79	989.60	1835.14	0.18	1.85	1.36
	3.00	1344	12.97	6529.28	1031.45	2016.80	0.16	1.96	1.42
	3.25	1577	13.72	7661.22	1070.35	2197.92	0.14	2.05	1.48
	3.50	1829	14.84	8885.46	1103.80	2379.30	0.12	2.16	1.52
150	0.25	10	0.01	85.83	69.40	85.83	0.81	1.24	0.05
	0.50	42	0.05	360.48	288.84	360.48	0.80	1.25	0.20
	0.75	93	0.22	798.21	637.20	753.23	0.80	1.18	0.45
	1.00	166	0.89	1424.77	1054.50	1111.78	0.74	1.05	0.74
	1.25	260	1.64	2231.56	1293.85	1470.33	0.58	1.14	0.91
	1.50	374	2.97	3210.02	1376.05	1826.01	0.43	1.33	0.96
	1.75	509	3.05	4368.72	1437.25	2182.51	0.33	1.52	1.01
	2.00	665	5.45	5707.66	1503.90	2539.53	0.26	1.69	1.05
	2.25	841	6.67	7218.25	1584.10	2894.97	0.22	1.83	1.11
	2.50	1039	7.52	8917.67	1666.65	3252.76	0.19	1.95	1.17
	2.75	1257	8.76	10788.76	1744.75	3609.12	0.16	2.07	1.22
	3.00	1496	9.96	12840.08	1816.65	3965.84	0.14	2.18	1.27
	3.25	1755	11.18	15063.06	1871.95	4321.52	0.12	2.31	1.31
	3.50	2036	11.04	17474.87	1913.60	4678.84	0.11	2.45	1.34

Table A7. Numerical ultimate loads and DSM data/estimates concerning the S90-075/090/120 F beams analyzed

S90	λ_D	f_y (MPa)	$(\delta /t)_{lim}$	M_y (kN cm)	M_u (kN cm)	M_{nD} (kN cm)	$\frac{M_u}{M_y}$	$\frac{M_{nD}}{M_u}$	$\frac{M_u}{M_{crD}}$
075	0.25	14	0.05	18.22	15.82	18.22	0.87	1.15	0.05
	0.50	56	0.09	72.90	62.63	72.90	0.86	1.16	0.21
	0.75	126	0.53	164.02	138.32	154.68	0.84	1.12	0.47
	1.00	225	1.02	292.89	226.23	228.33	0.77	1.01	0.77
	1.25	351	1.76	456.91	278.72	301.21	0.61	1.08	0.95
	1.50	505	2.79	657.38	303.85	374.13	0.46	1.23	1.04
	1.75	688	4.11	895.60	321.13	447.44	0.36	1.39	1.10
	2.00	899	4.97	1170.26	343.17	520.68	0.29	1.52	1.17
	2.25	1137	6.05	1480.07	368.86	593.58	0.25	1.61	1.26
	2.50	1404	7.28	1827.64	393.05	666.76	0.22	1.70	1.34
	2.75	1699	7.45	2211.65	409.59	739.90	0.19	1.81	1.40
	3.00	2022	7.54	2632.11	418.84	813.03	0.16	1.94	1.43
	3.25	2373	7.02	3089.02	420.34	886.13	0.14	2.11	1.44
	3.50	2752	8.45	3582.38	432.49	959.22	0.12	2.22	1.48
090	0.25	11	0.06	17.90	15.56	17.90	0.87	1.15	0.06
	0.50	43	0.10	69.95	60.07	69.95	0.86	1.16	0.21
	0.75	97	0.76	157.80	133.65	148.65	0.85	1.11	0.48
	1.00	172	1.52	279.82	216.94	218.39	0.78	1.01	0.77
	1.25	269	1.97	437.62	265.30	288.57	0.61	1.09	0.95
	1.50	388	3.36	631.22	284.48	358.96	0.45	1.26	1.01
	1.75	528	3.88	858.98	299.49	429.01	0.35	1.43	1.07
	2.00	689	5.41	1120.90	314.71	498.85	0.28	1.59	1.12
	2.25	872	7.00	1418.61	333.27	568.91	0.23	1.71	1.19
	2.50	1077	7.93	1752.12	351.91	639.12	0.20	1.82	1.26
	2.75	1303	8.32	2119.79	369.59	709.15	0.17	1.92	1.32
	3.00	1551	7.96	2523.25	380.90	779.31	0.15	2.05	1.36
	3.25	1820	8.54	2960.87	383.95	849.33	0.13	2.21	1.37
	3.50	2111	7.87	3434.28	387.09	919.46	0.11	2.38	1.38
120	0.25	29	0.01	110.77	97.55	110.77	0.88	1.14	0.06
	0.50	114	0.05	435.42	381.15	435.42	0.88	1.14	0.22
	0.75	257	0.60	981.61	846.75	924.86	0.86	1.09	0.49
	1.00	457	1.48	1745.51	1362.15	1361.32	0.78	1.00	0.78
	1.25	714	2.60	2727.12	1698.25	1797.53	0.62	1.06	0.97
	1.50	1028	3.80	3926.44	1847.15	2233.60	0.47	1.21	1.06
	1.75	1399	4.96	5343.48	1976.75	2669.61	0.37	1.35	1.13
	2.00	1827	4.15	6978.22	1997.60	3105.56	0.29	1.55	1.14
	2.25	2313	4.15	8834.50	1997.60	3542.34	0.23	1.77	1.14
	2.50	2855	4.15	10904.66	1997.60	3978.16	0.18	1.99	1.14
	2.75	3455	4.15	13196.36	1997.60	4414.68	0.15	2.21	1.14
	3.00	4112	4.15	15705.77	1997.60	4851.08	0.13	2.43	1.14
	3.25	4825	4.15	18429.07	1997.60	5286.80	0.11	2.65	1.14
	3.50	5596	4.15	21373.91	1997.60	5723.09	0.09	2.86	1.14

Table A8. Numerical ultimate loads and DSM data/estimates concerning the S90-140/150 F beams analyzed

S90	λ_D	f_y (MPa)	$(\delta /t)_{lim}$	M_y (kN cm)	M_u (kN cm)	M_{nD} (kN cm)	$\frac{M_u}{M_y}$	$\frac{M_{nD}}{M_u}$	$\frac{M_u}{M_{crD}}$
140	0.25	13	0.00	62.23	53.76	62.23	0.86	1.16	0.05
	0.50	51	0.08	244.15	209.47	244.15	0.86	1.17	0.21
	0.75	115	0.85	550.54	470.82	519.23	0.86	1.10	0.48
	1.00	205	1.51	981.39	771.25	765.65	0.79	0.99	0.79
	1.25	321	2.72	1536.72	957.30	1012.39	0.62	1.06	0.97
	1.50	462	3.79	2211.72	1025.35	1257.70	0.46	1.23	1.04
	1.75	628	4.74	3006.41	1087.10	1502.18	0.36	1.38	1.11
	2.00	820	5.77	3925.57	1146.80	1747.34	0.29	1.52	1.17
	2.25	1038	6.69	4969.20	1207.60	1992.97	0.24	1.65	1.23
	2.50	1282	7.63	6137.29	1260.65	2238.91	0.21	1.78	1.28
	2.75	1551	8.47	7425.07	1308.00	2484.21	0.18	1.90	1.33
	3.00	1846	8.79	8837.32	1343.70	2729.83	0.15	2.03	1.37
	3.25	2167	8.84	10374.04	1352.60	2975.70	0.13	2.20	1.38
	3.50	2513	10.22	12030.44	1363.30	3221.08	0.11	2.36	1.39
150	0.25	15	0.01	126.94	152.63	126.94	1.20	0.83	0.08
	0.50	59	0.17	499.28	614.20	499.28	1.23	0.81	0.31
	0.75	132	0.83	1117.03	1297.10	1052.12	1.16	0.81	0.65
	1.00	234	1.88	1980.19	1763.30	1545.47	0.89	0.88	0.89
	1.25	366	3.19	3097.22	1945.40	2042.19	0.63	1.05	0.98
	1.50	527	2.75	4459.66	1997.60	2537.79	0.45	1.27	1.01
	1.75	718	2.75	6075.97	1997.60	3035.16	0.33	1.52	1.01
	2.00	938	2.75	7937.69	1997.60	3531.53	0.25	1.77	1.01
	2.25	1187	2.75	10044.82	1997.60	4027.22	0.20	2.02	1.01
	2.50	1465	2.75	12397.35	1997.60	4522.44	0.16	2.26	1.01
	2.75	1773	2.75	15003.76	1997.60	5018.86	0.13	2.51	1.01
	3.00	2109	2.75	17847.11	1997.60	5513.36	0.11	2.76	1.01
	3.25	2476	2.75	20952.80	1997.60	6010.28	0.10	3.01	1.01
	3.50	2871	2.75	24295.43	1997.60	6505.48	0.08	3.26	1.01

APPENDIX B

Data concerning P beams

Tables B1 to B8 show the results obtained for all PLC, SLC, S45 and S90 P beams concerning (i) the distortional slenderness λ_D , (ii) the respective yielding stress f_y , (iii) the $(|\delta|/t)_{lim}$ value obtained through ANSYS analyzes, (iv) the yielding bending moment M_y , (v) the ultimate bending moment M_u , (vi) the ultimate bending moment obtained through DSM predictions M_{nD} and (vii) the bending moment ratios M_u/M_y , M_{nD}/M_u and M_u/M_{crD} .

Table B1. Numerical ultimate loads and DSM data/estimates concerning the PLC-075/090/120 P beams analyzed

PLC	λ_D	f_y (MPa)	$(\delta /t)_{lim}$	M_y (kN cm)	M_u (kN cm)	M_{nD} (kN cm)	$\frac{M_u}{M_y}$	$\frac{M_{nD}}{M_u}$	$\frac{M_u}{M_{crD}}$
075	0.25	22	0.20	27.02	28.87	27.02	1.07	0.94	0.07
	0.50	88	0.53	108.08	111.28	108.08	1.03	0.97	0.26
	0.75	198	1.11	243.18	233.75	229.23	0.96	0.98	0.54
	1.00	352	2.18	432.33	337.13	337.38	0.78	1.00	0.78
	1.25	551	3.40	676.74	392.67	446.03	0.58	1.14	0.91
	1.50	793	8.64	973.96	468.44	554.11	0.48	1.18	1.08
	1.75	1080	9.94	1326.45	573.20	662.56	0.43	1.16	1.32
	2.00	1410	11.16	1731.76	677.90	770.62	0.39	1.14	1.57
	2.25	1784	12.22	2191.11	785.65	878.71	0.36	1.12	1.81
	2.50	2203	13.54	2705.72	889.55	987.06	0.33	1.11	2.05
	2.75	2666	14.50	3274.38	987.40	1095.37	0.30	1.11	2.28
	3.00	3172	15.01	3895.85	1079.85	1203.46	0.28	1.11	2.49
	3.25	3723	15.00	4572.58	1155.05	1311.74	0.25	1.14	2.67
	3.50	4318	15.00	5303.36	1211.40	1420.00	0.23	1.17	2.80
090	0.25	16	0.22	24.74	26.65	24.74	1.08	0.93	0.07
	0.50	66	0.62	102.04	105.14	102.04	1.03	0.97	0.26
	0.75	148	1.04	228.81	221.53	215.43	0.97	0.97	0.55
	1.00	262	2.78	405.06	318.91	316.13	0.79	0.99	0.79
	1.25	410	4.17	633.87	367.95	417.87	0.58	1.14	0.91
	1.50	590	5.79	912.15	407.54	519.09	0.45	1.27	1.00
	1.75	804	13.57	1243.00	489.13	620.90	0.39	1.27	1.21
	2.00	1050	15.04	1623.32	576.70	722.30	0.36	1.25	1.42
	2.25	1329	16.72	2054.66	667.20	823.78	0.32	1.23	1.64
	2.50	1640	18.28	2535.47	755.45	925.00	0.30	1.22	1.86
	2.75	1985	19.89	3068.84	838.85	1026.60	0.27	1.22	2.07
	3.00	2362	21.23	3651.69	918.70	1127.96	0.25	1.23	2.26
	3.25	2772	22.20	4285.56	997.60	1229.38	0.23	1.23	2.46
	3.50	3215	23.24	4970.44	1068.80	1330.84	0.22	1.25	2.63
120	0.25	43	1.05	160.13	175.28	160.13	1.09	0.91	0.07
	0.50	173	0.87	644.24	669.40	644.24	1.04	0.96	0.26
	0.75	390	1.52	1452.34	1392.30	1368.24	0.96	0.98	0.54
	1.00	693	3.53	2580.70	2017.65	2012.95	0.78	1.00	0.78
	1.25	1083	4.60	4033.04	2333.90	2658.41	0.58	1.14	0.90
	1.50	1559	6.50	5805.64	2600.00	3303.00	0.45	1.27	1.01
	1.75	2122	8.54	7902.23	2844.60	3948.15	0.36	1.39	1.10
	2.00	2772	11.35	10322.79	3178.05	4593.67	0.31	1.45	1.23
	2.25	3508	13.01	13063.62	3536.95	5238.59	0.27	1.48	1.37
	2.50	4331	14.58	16128.43	3871.95	5883.84	0.24	1.52	1.50
	2.75	5241	15.96	19517.23	4169.00	6529.33	0.21	1.57	1.62
	3.00	6237	16.71	23226.29	4412.00	7174.38	0.19	1.63	1.71
	3.25	7320	17.61	27259.33	4617.65	7819.66	0.17	1.69	1.79
	3.50	8489	18.60	31612.62	4774.25	8464.60	0.15	1.77	1.85

Table B2. Numerical ultimate loads and DSM data/estimates concerning the PLC-140/150 P beams analyzed

PLC	λ_D	f_y (MPa)	$(\delta /t)_{lim}$	M_y (kN cm)	M_u (kN cm)	M_{nD} (kN cm)	$\frac{M_u}{M_y}$	$\frac{M_{nD}}{M_u}$	$\frac{M_u}{M_{crD}}$
140	0.25	19	0.40	87.77	95.20	87.77	1.08	0.92	0.07
	0.50	78	0.77	360.32	372.78	360.32	1.03	0.97	0.26
	0.75	175	1.47	808.40	784.50	761.97	0.97	0.97	0.55
	1.00	311	3.46	1436.65	1136.60	1121.23	0.79	0.99	0.79
	1.25	487	5.09	2249.68	1311.00	1482.65	0.58	1.13	0.91
	1.50	701	6.25	3238.24	1434.45	1842.06	0.44	1.28	1.00
	1.75	954	15.37	4406.96	1609.60	2201.65	0.37	1.37	1.12
	2.00	1246	17.19	5755.84	1882.55	2561.35	0.33	1.36	1.31
	2.25	1577	18.82	7284.88	2160.35	2921.12	0.30	1.35	1.50
	2.50	1947	20.75	8994.08	2421.60	3280.94	0.27	1.35	1.68
	2.75	2356	22.21	10883.44	2665.45	3640.80	0.24	1.37	1.85
	3.00	2803	23.58	12948.34	2894.30	3999.92	0.22	1.38	2.01
	3.25	3290	24.50	15198.01	3108.20	4359.89	0.20	1.40	2.16
	3.50	3816	24.47	17627.85	3306.95	4719.87	0.19	1.43	2.30
150	0.25	21	0.32	169.51	182.35	169.51	1.08	0.93	0.07
	0.50	83	0.58	669.97	692.25	669.97	1.03	0.97	0.26
	0.75	188	1.10	1517.51	1471.50	1429.20	0.97	0.97	0.55
	1.00	334	2.55	2696.00	2129.00	2102.25	0.79	0.99	0.79
	1.25	521	3.86	4205.44	2482.00	2773.14	0.59	1.12	0.92
	1.50	751	5.80	6061.97	2795.65	3448.33	0.46	1.23	1.04
	1.75	1022	12.16	8249.45	3309.75	4121.38	0.40	1.25	1.23
	2.00	1335	13.55	10775.94	3890.35	4795.09	0.36	1.23	1.44
	2.25	1689	14.78	13633.38	4491.35	5467.46	0.33	1.22	1.67
	2.50	2086	13.88	16837.92	4924.55	6142.12	0.29	1.25	1.83
	2.75	2524	12.35	20373.39	4958.90	6815.51	0.24	1.37	1.84
	3.00	3003	12.02	24239.82	4958.90	7487.94	0.20	1.51	1.84
	3.25	3525	11.92	28453.33	4958.90	8162.12	0.17	1.65	1.84
	3.50	4088	11.83	32997.79	4958.90	8835.37	0.15	1.78	1.84

Table B3. Numerical ultimate loads and DSM data/estimates concerning the SLC-075/090/120 P beams analyzed

SLC	λ_D	f_y (MPa)	$(\delta /t)_{lim}$	M_y (kN cm)	M_u (kN cm)	M_{nD} (kN cm)	$\frac{M_u}{M_y}$	$\frac{M_{nD}}{M_u}$	$\frac{M_u}{M_{crD}}$
075	0.25	28	0.28	35.41	38.48	35.41	1.09	0.92	0.07
	0.50	112	0.68	141.63	146.75	141.63	1.04	0.97	0.26
	0.75	253	1.47	319.93	305.41	301.34	0.95	0.99	0.54
	1.00	449	4.23	567.79	438.40	442.95	0.77	1.01	0.77
	1.25	702	8.27	887.72	553.70	585.15	0.62	1.06	0.97
	1.50	1011	11.56	1278.47	702.70	727.22	0.55	1.03	1.24
	1.75	1376	13.66	1740.03	855.95	869.22	0.49	1.02	1.51
	2.00	1797	15.14	2272.41	1000.35	1011.18	0.44	1.01	1.76
	2.25	2274	15.05	2875.61	1053.85	1153.11	0.37	1.09	1.86
	2.50	2808	15.18	3550.88	1084.20	1295.27	0.31	1.19	1.91
	2.75	3397	15.36	4295.71	1105.60	1437.13	0.26	1.30	1.95
	3.00	4043	15.36	5112.61	1105.70	1579.20	0.22	1.43	1.95
	3.25	4745	15.36	6000.33	1105.70	1721.23	0.18	1.56	1.95
	3.50	5503	15.36	6958.87	1105.70	1863.24	0.16	1.69	1.95
090	0.25	21	0.34	33.46	36.55	33.46	1.09	0.92	0.07
	0.50	85	0.78	135.44	140.31	135.44	1.04	0.97	0.26
	0.75	190	1.71	302.74	290.18	285.38	0.96	0.98	0.54
	1.00	338	4.70	538.56	421.19	420.22	0.78	1.00	0.78
	1.25	529	8.96	842.90	523.20	555.48	0.62	1.06	0.97
	1.50	761	14.15	1212.57	653.50	689.89	0.54	1.06	1.21
	1.75	1036	17.06	1650.75	794.15	824.73	0.48	1.04	1.47
	2.00	1353	19.87	2155.85	932.15	959.43	0.43	1.03	1.73
	2.25	1713	22.27	2729.47	1059.00	1094.40	0.39	1.03	1.96
	2.50	2114	24.22	3368.42	1166.35	1228.92	0.35	1.05	2.16
	2.75	2558	25.92	4075.88	1253.40	1363.69	0.31	1.09	2.33
	3.00	3045	27.38	4851.86	1320.55	1498.64	0.27	1.13	2.45
	3.25	3573	28.63	5693.17	1371.45	1633.25	0.24	1.19	2.54
	3.50	4144	29.63	6602.99	1407.80	1768.05	0.21	1.26	2.61
120	0.25	47	0.89	181.35	200.67	181.35	1.11	0.90	0.07
	0.50	187	0.79	721.55	754.05	721.55	1.05	0.96	0.26
	0.75	421	1.85	1624.46	1553.80	1530.79	0.96	0.99	0.54
	1.00	749	4.20	2890.06	2243.15	2254.01	0.78	1.00	0.78
	1.25	1170	7.14	4514.52	2708.85	2975.93	0.60	1.10	0.94
	1.50	1685	7.14	6501.68	2708.85	3698.50	0.42	1.37	0.94
	1.75	2293	10.69	8847.69	3177.80	4420.33	0.36	1.39	1.10
	2.00	2995	13.20	11556.40	3675.75	5142.67	0.32	1.40	1.27
	2.25	3791	17.16	14627.82	4548.15	5865.34	0.31	1.29	1.57
	2.50	4680	18.65	18058.08	4845.70	6587.48	0.27	1.36	1.68
	2.75	5663	18.73	21851.05	5000.00	7309.93	0.23	1.46	1.73
	3.00	6739	18.28	26002.87	5000.00	8031.97	0.19	1.61	1.73
	3.25	7909	18.14	30517.39	5000.00	8754.29	0.16	1.75	1.73
	3.50	9172	18.14	35390.75	5000.00	9476.28	0.14	1.90	1.73

Table B4. Numerical ultimate loads and DSM data/estimates concerning the SLC-140/150 P beams analyzed

SLC	λ_D	f_y (MPa)	$(\delta /t)_{lim}$	M_y (kN cm)	M_u (kN cm)	M_{nD} (kN cm)	$\frac{M_u}{M_y}$	$\frac{M_{nD}}{M_u}$	$\frac{M_u}{M_{crD}}$
140	0.25	20	0.92	113.01	105.34	113.01	0.93	1.07	0.06
	0.50	79	0.77	446.39	394.92	446.39	0.88	1.13	0.22
	0.75	177	1.53	1000.14	835.75	942.81	0.84	1.13	0.47
	1.00	315	3.79	1779.92	1283.45	1388.63	0.72	1.08	0.72
	1.25	492	7.17	2780.06	1589.55	1833.31	0.57	1.15	0.89
	1.50	709	12.26	4006.22	1885.30	2279.31	0.47	1.21	1.06
	1.75	965	16.18	5452.76	2239.75	2724.46	0.41	1.22	1.26
	2.00	1261	19.31	7125.31	2600.20	3170.47	0.36	1.22	1.46
	2.25	1596	21.99	9018.24	2937.10	3615.82	0.33	1.23	1.65
	2.50	1970	24.23	11131.53	3231.60	4060.69	0.29	1.26	1.81
	2.75	2384	26.10	13470.85	3478.45	4506.25	0.26	1.30	1.95
	3.00	2837	27.78	16030.54	3675.00	4951.38	0.23	1.35	2.06
	3.25	3329	29.20	18810.59	3826.60	5396.18	0.20	1.41	2.15
	3.50	3861	30.39	21816.67	3940.90	5841.53	0.18	1.48	2.21
150	0.25	26	0.41	216.53	236.47	216.53	1.09	0.92	0.07
	0.50	106	0.66	882.80	915.20	882.80	1.04	0.96	0.26
	0.75	238	1.58	1982.13	1902.90	1867.28	0.96	0.98	0.54
	1.00	423	4.09	3522.86	2757.25	2747.50	0.78	1.00	0.78
	1.25	661	8.05	5504.98	3415.75	3628.27	0.62	1.06	0.97
	1.50	951	12.18	7920.18	4233.05	4506.54	0.53	1.06	1.20
	1.75	1295	13.56	10785.10	5000.00	5388.15	0.46	1.08	1.42
	2.00	1691	12.46	14083.09	5000.00	6267.68	0.36	1.25	1.42
	2.25	2141	12.26	17830.81	5000.00	7149.51	0.28	1.43	1.42
	2.50	2643	12.26	22011.60	5000.00	8029.64	0.23	1.61	1.42
	2.75	3198	12.26	26633.79	5000.00	8910.04	0.19	1.78	1.42
	3.00	3806	12.26	31697.37	5000.00	9790.63	0.16	1.96	1.42
	3.25	4466	12.26	37194.03	5000.00	10670.10	0.13	2.13	1.42
	3.50	5180	12.26	43140.41	5000.00	11551.07	0.12	2.31	1.42

Table B5. Numerical ultimate loads and DSM data/estimates concerning the S45-075/090/120 P beams analyzed

S45	λ_D	f_y (MPa)	$(\delta /t)_{lim}$	M_y (kN cm)	M_u (kN cm)	M_{nD} (kN cm)	$\frac{M_u}{M_y}$	$\frac{M_{nD}}{M_u}$	$\frac{M_u}{M_{crD}}$
075	0.25	15	0.20	19.75	16.69	19.75	0.85	1.18	0.05
	0.50	61	0.29	80.32	66.86	80.32	0.83	1.20	0.21
	0.75	136	0.89	179.07	144.06	168.78	0.80	1.17	0.45
	1.00	242	2.00	318.63	232.14	248.57	0.73	1.07	0.73
	1.25	378	3.04	497.70	282.56	328.18	0.57	1.16	0.89
	1.50	545	6.65	717.58	339.30	408.13	0.47	1.20	1.06
	1.75	741	8.79	975.64	416.03	487.54	0.43	1.17	1.31
	2.00	968	9.94	1274.53	490.73	567.26	0.39	1.16	1.54
	2.25	1226	10.90	1614.22	558.05	647.19	0.35	1.16	1.75
	2.50	1513	11.75	1992.10	616.10	726.74	0.31	1.18	1.93
	2.75	1831	12.56	2410.80	667.95	806.49	0.28	1.21	2.10
	3.00	2179	13.46	2869.00	713.45	886.17	0.25	1.24	2.24
	3.25	2557	14.20	3366.70	753.95	965.81	0.22	1.28	2.37
	3.50	2966	15.07	3905.21	789.85	1045.58	0.20	1.32	2.48
090	0.25	11	0.13	18.14	15.58	18.14	0.86	1.16	0.05
	0.50	46	0.53	75.86	63.54	75.86	0.84	1.19	0.21
	0.75	103	0.85	169.86	137.22	159.96	0.81	1.17	0.46
	1.00	183	2.35	301.79	219.37	235.30	0.73	1.07	0.73
	1.25	286	3.84	471.64	266.59	310.75	0.57	1.17	0.88
	1.50	411	5.59	677.78	302.35	385.70	0.45	1.28	1.00
	1.75	560	12.37	923.50	372.87	461.31	0.40	1.24	1.24
	2.00	731	13.49	1205.50	433.07	536.51	0.36	1.24	1.44
	2.25	925	13.96	1525.42	487.42	611.80	0.32	1.26	1.62
	2.50	1143	14.92	1884.93	540.15	687.49	0.29	1.27	1.79
	2.75	1382	15.93	2279.07	588.15	762.56	0.26	1.30	1.95
	3.00	1645	17.04	2712.78	631.85	838.00	0.23	1.33	2.10
	3.25	1931	18.08	3184.43	673.90	913.46	0.21	1.36	2.24
	3.50	2239	19.30	3692.35	711.85	988.71	0.19	1.39	2.36
120	0.25	31	0.85	119.97	105.36	119.97	0.88	1.14	0.05
	0.50	124	0.60	479.89	408.82	479.89	0.85	1.17	0.21
	0.75	279	1.37	1079.76	885.15	1017.54	0.82	1.15	0.46
	1.00	496	3.31	1919.57	1403.90	1497.57	0.73	1.07	0.73
	1.25	775	5.55	2999.32	1770.35	1977.61	0.59	1.12	0.92
	1.50	1117	7.30	4322.89	2048.05	2458.93	0.47	1.20	1.07
	1.75	1520	8.99	5882.54	2300.00	2938.77	0.39	1.28	1.20
	2.00	1985	11.05	7682.13	2549.40	3418.67	0.33	1.34	1.33
	2.25	2512	14.64	9721.67	2839.45	3898.59	0.29	1.37	1.48
	2.50	3102	16.36	12005.02	3138.40	4379.31	0.26	1.40	1.63
	2.75	3753	17.76	14524.45	3396.10	4859.20	0.23	1.43	1.77
	3.00	4467	18.79	17287.70	3611.20	5339.76	0.21	1.48	1.88
	3.25	5242	20.37	20287.02	3774.60	5819.64	0.19	1.54	1.97
	3.50	6080	21.85	23530.16	3885.55	6300.10	0.17	1.62	2.02

Table B6. Numerical ultimate loads and DSM data/estimates concerning the S45-140/150 P beams analyzed

S45	λ_D	f_y (MPa)	$(\delta /t)_{lim}$	M_y (kN cm)	M_u (kN cm)	M_{nD} (kN cm)	$\frac{M_u}{M_y}$	$\frac{M_{nD}}{M_u}$	$\frac{M_u}{M_{crD}}$
140	0.25	14	0.33	68.01	58.52	68.01	0.86	1.16	0.05
	0.50	55	0.68	267.20	224.33	267.20	0.84	1.19	0.21
	0.75	124	1.26	602.40	488.30	568.23	0.81	1.16	0.45
	1.00	221	3.35	1073.64	784.55	837.84	0.73	1.07	0.73
	1.25	346	5.30	1680.90	979.95	1107.76	0.58	1.13	0.91
	1.50	498	7.32	2419.33	1123.05	1376.22	0.46	1.23	1.04
	1.75	678	8.90	3293.79	1262.50	1645.24	0.38	1.30	1.17
	2.00	885	17.91	4299.42	1508.70	1913.40	0.35	1.27	1.40
	2.25	1120	18.53	5441.07	1691.20	2182.05	0.31	1.29	1.57
	2.50	1383	19.07	6718.75	1885.60	2451.06	0.28	1.30	1.75
	2.75	1674	19.83	8132.46	2065.00	2720.32	0.25	1.32	1.92
	3.00	1992	21.37	9677.33	2234.10	2988.96	0.23	1.34	2.08
	3.25	2337	23.11	11353.38	2397.75	3257.13	0.21	1.36	2.23
	3.50	2711	23.71	13170.30	2533.90	3526.31	0.19	1.39	2.36
150	0.25	15	0.38	128.74	109.59	128.74	0.85	1.17	0.05
	0.50	58	0.46	497.81	415.26	497.81	0.83	1.20	0.21
	0.75	131	0.95	1124.37	905.65	1058.85	0.81	1.17	0.45
	1.00	232	2.12	1991.24	1449.45	1554.31	0.73	1.07	0.73
	1.25	363	3.63	3115.61	1795.50	2054.35	0.58	1.14	0.90
	1.50	523	5.42	4488.88	2078.35	2553.81	0.46	1.23	1.04
	1.75	712	11.33	6111.05	2523.20	3052.95	0.41	1.21	1.26
	2.00	930	12.15	7982.13	2957.45	3551.88	0.37	1.20	1.48
	2.25	1177	12.34	10102.12	3354.70	4050.68	0.33	1.21	1.68
	2.50	1453	13.14	12471.01	3725.70	4549.38	0.30	1.22	1.87
	2.75	1758	14.05	15088.81	4062.10	5048.01	0.27	1.24	2.04
	3.00	2092	15.00	17955.51	4358.85	5546.59	0.24	1.27	2.18
	3.25	2456	15.94	21079.70	4624.20	6046.46	0.22	1.31	2.32
	3.50	2848	17.06	24444.21	4863.50	6544.87	0.20	1.35	2.44

Table B7. Numerical ultimate loads and DSM data/estimates concerning the S90-075/090/120 P beams analyzed

S90	λ_D	f_y (MPa)	$(\delta /t)_{lim}$	M_y (kN cm)	M_u (kN cm)	M_{nD} (kN cm)	$\frac{M_u}{M_y}$	$\frac{M_{nD}}{M_u}$	$\frac{M_u}{M_{crD}}$
075	0.25	20	0.30	26.03	25.63	26.03	0.98	1.02	0.06
	0.50	81	0.78	105.44	98.65	105.44	0.94	1.07	0.23
	0.75	182	1.03	236.92	205.82	223.23	0.87	1.08	0.49
	1.00	324	2.23	421.76	317.40	328.82	0.75	1.04	0.75
	1.25	506	7.88	658.68	425.14	434.06	0.65	1.02	1.01
	1.50	728	9.56	947.66	579.30	539.13	0.61	0.93	1.38
	1.75	991	10.98	1290.02	746.50	644.47	0.58	0.86	1.77
	2.00	1294	12.09	1684.45	917.85	749.66	0.54	0.82	2.18
	2.25	1638	13.00	2132.25	1086.80	855.03	0.51	0.79	2.58
	2.50	2022	13.58	2632.11	1247.95	960.27	0.47	0.77	2.96
	2.75	2447	14.13	3185.35	1396.95	1065.65	0.44	0.76	3.32
	3.00	2912	14.74	3790.66	1533.05	1170.93	0.40	0.76	3.64
	3.25	3418	15.00	4449.34	1650.05	1276.31	0.37	0.77	3.92
3.50	3964	15.01	5160.09	1737.75	1381.61	0.34	0.80	4.13	
090	0.25	16	0.37	26.03	26.02	26.03	1.00	1.00	0.06
	0.50	63	0.88	102.49	96.33	102.49	0.94	1.06	0.24
	0.75	141	1.41	229.39	200.40	216.24	0.87	1.08	0.49
	1.00	251	2.44	408.34	312.42	318.56	0.77	1.02	0.76
	1.25	392	3.58	637.73	379.08	420.54	0.59	1.11	0.93
	1.50	565	11.95	919.17	548.40	522.91	0.60	0.95	1.34
	1.75	769	13.44	1251.05	698.50	625.02	0.56	0.89	1.71
	2.00	1004	14.51	1633.36	847.15	726.99	0.52	0.86	2.07
	2.25	1271	15.35	2067.73	995.25	829.21	0.48	0.83	2.44
	2.50	1569	16.24	2552.53	1133.15	931.28	0.44	0.82	2.77
	2.75	1899	17.12	3089.39	1262.50	1033.55	0.41	0.82	3.09
	3.00	2260	17.92	3676.68	1383.45	1135.69	0.38	0.82	3.39
	3.25	2652	18.52	4314.41	1493.40	1237.73	0.35	0.83	3.66
3.50	3076	19.25	5004.19	1592.55	1339.92	0.32	0.84	3.90	
120	0.25	41	0.82	156.60	160.35	156.60	1.02	0.98	0.06
	0.50	166	1.48	634.04	608.35	634.04	0.96	1.04	0.24
	0.75	373	1.63	1424.67	1252.15	1342.02	0.88	1.07	0.49
	1.00	663	3.33	2532.33	1960.05	1974.72	0.77	1.01	0.77
	1.25	1035	4.82	3953.18	2439.90	2606.15	0.62	1.07	0.96
	1.50	1491	5.96	5694.87	2801.10	3239.49	0.49	1.16	1.11
	1.75	2029	14.05	7749.76	3840.50	3871.74	0.50	1.01	1.52
	2.00	2650	15.08	10121.67	4487.75	4504.26	0.44	1.00	1.77
	2.25	3354	15.26	12810.59	5000.00	5136.97	0.39	1.03	1.98
	2.50	4141	13.39	15816.54	5000.00	5769.80	0.32	1.15	1.98
	2.75	5010	12.62	19135.68	5000.00	6402.03	0.26	1.28	1.98
	3.00	5963	12.37	22775.66	5000.00	7035.08	0.22	1.41	1.98
	3.25	6998	12.25	26728.84	5000.00	7667.58	0.19	1.53	1.98
3.50	8116	12.23	30999.04	5000.00	8300.21	0.16	1.66	1.98	

Table B8. Numerical ultimate loads and DSM data/estimates concerning the S90-140/150 P beams analyzed

S90	λ_D	f_y (MPa)	$(\delta /t)_{lim}$	M_y (kN cm)	M_u (kN cm)	M_{nD} (kN cm)	$\frac{M_u}{M_y}$	$\frac{M_{nD}}{M_u}$	$\frac{M_u}{M_{crD}}$
140	0.25	19	1.35	90.96	92.25	90.96	1.01	0.99	0.06
	0.50	75	1.37	359.05	342.07	359.05	0.95	1.05	0.24
	0.75	169	2.01	809.05	708.70	762.10	0.88	1.08	0.49
	1.00	300	3.10	1436.18	1107.05	1120.45	0.77	1.01	0.77
	1.25	469	4.51	2245.23	1351.60	1480.07	0.60	1.10	0.94
	1.50	675	5.58	3231.41	1528.90	1838.74	0.47	1.20	1.06
	1.75	919	15.05	4399.51	2309.85	2198.23	0.53	0.95	1.61
	2.00	1201	16.33	5749.52	2758.25	2558.23	0.48	0.93	1.92
	2.25	1520	17.52	7276.67	3188.45	2917.51	0.44	0.92	2.22
	2.50	1876	18.70	8980.94	3600.40	3276.28	0.40	0.91	2.51
	2.75	2270	19.80	10867.13	3987.20	3635.56	0.37	0.91	2.77
	3.00	2702	20.77	12935.23	4336.90	3995.21	0.34	0.92	3.02
	3.25	3171	21.68	15180.47	4649.60	4354.42	0.31	0.94	3.24
	3.50	3677	22.59	17602.83	5000.00	4713.28	0.28	0.94	3.48
150	0.25	20	0.79	169.25	169.02	169.25	1.00	1.00	0.06
	0.50	79	1.14	668.53	631.90	668.53	0.95	1.06	0.24
	0.75	177	1.31	1497.84	1305.65	1410.79	0.87	1.08	0.49
	1.00	314	2.21	2657.18	2032.70	2073.27	0.76	1.02	0.76
	1.25	491	3.42	4155.02	2507.85	2739.14	0.60	1.09	0.94
	1.50	707	11.17	5982.89	3589.20	3403.88	0.60	0.95	1.35
	1.75	962	12.40	8140.79	4572.90	4067.97	0.56	0.89	1.72
	2.00	1257	10.28	10637.18	5000.00	4733.77	0.47	0.95	1.88
	2.25	1591	9.25	13463.61	5000.00	5398.84	0.37	1.08	1.88
	2.50	1964	8.68	16620.07	5000.00	6063.39	0.30	1.21	1.88
	2.75	2377	8.48	20115.02	5000.00	6729.10	0.25	1.35	1.88
	3.00	2829	8.40	23940.01	5000.00	7394.27	0.21	1.48	1.88
	3.25	3320	8.36	28095.03	5000.00	8059.03	0.18	1.61	1.88
	3.50	3850	8.36	32580.07	5000.00	8723.46	0.15	1.74	1.88